Universität Potsdam
Institut für Erd- und Umweltwissenschaften / Geoökologie
Hauptbetreuer: Prof. Sascha Oswald

Untersuchungen zur Mobilität künstlicher Kohlenstoff-Eisen-Komposite zum Einsatz in der Altlastensanierung

Investigations on mobility of carbon colloid supported nanoscale zero-valent iron (nZVI) for groundwater remediation

Publikationsbasierte Dissertation zur Erlangung des akademischen Grades „doctor rerum naturalium“ (Dr. rer. nat.) in der Wissenschaftsdisziplin Hydrogeologie, eingereicht bei der Mathematisch-Naturwissenschaftlichen Fakultät an der Universität Potsdam

Jan Busch
aus Viersen

im Januar 2015

Eingereicht: Januar 2015
Verteidigt: April 2015
Veröffentlicht: Mai 2015

Gutachter: S. E. Oswald, Universität Potsdam
Gutachter: R. Helmig, Universität Stuttgart
Gutachter: M. Ebert, Universität Kiel

Published online at the
Institutional Repository of the University of Potsdam:
URN urn:nbn:de:kobv:517-opus4-76873
http://nbn-resolving.de/urn:nbn:de:kobv:517-opus4-76873

Abstract

Injection of nanoscale zero-valent iron (nZVI) is an innovative technology for in situ installation of a permeable reactive barrier in the subsurface. Zero-valent iron (ZVI) is highly reactive with chlorinated hydrocarbons (CHCs) and renders them into less harmful substances. Application of nZVI instead of granular ZVI can increase rates of dechlorination of CHCs by orders of magnitude, due to its higher surface area. This approach is still difficult to apply due to fast agglomeration and sedimentation of colloidal suspensions of nZVI, which leads to very short transport distances. To overcome this issue of limited mobility, polyanionic stabilisers are added to increase surface charge and stability of suspensions. In field experiments maximum transport distances of a few metres were achieved. A new approach, which is investigated in this thesis, is enhanced mobility of nZVI by a more mobile carrier colloid. The investigated composite material consists of activated carbon, which is loaded with nZVI.

In this cumulative thesis, transport characteristics of carbon-colloid supported nZVI (c-nZVI) are investigated. Investigations started with column experiments in 40 cm columns filled with various porous media to investigate on physicochemical influences on transport characteristics. The experimental set-up was enlarged to a transport experiment in a 1.2-m-sized two-dimensional aquifer tank experiment, which was filled with granular porous media. Further, a field experiment was performed in a natural aquifer system with a targeted transport distance of 5.3 m. Parallel to these investigations, alternative methods for transport observations were investigated by using noninvasive tomographic methods. Experiments using synchrotron radiation and magnetic resonance (MRI) were performed to investigate in situ transport characteristics in a non-destructive way.

Results from column experiments show potentially high mobility under environmental relevant conditions. Addition of mono-and bivalent salts, e.g.

more than 0.5 mM/L $CaCl_2$, might decrease mobility. Changes in pH to values below 6 can inhibit mobility at all. Measurements of colloid size show changes in the mean particle size by a factor of ten. Measurements of zeta potential revealed an increase of –62 mV to –82 mV. Results from the 2D-aquifer test system suggest strong particle deposition in the first centimetres and only weak straining in the further travel path and no gravitational influence on particle transport. Straining at the beginning of the travel path in the porous medium was observed with tomographic investigations of transport. MRI experiments revealed similar results to the previous experiments, and observations using synchrotron radiation suggest straining of colloids at pore throats. The potential for high transport distances, which was suggested from laboratory experiments, was confirmed in the field experiment, where the transport distance of 5.3 m was reached by at least 10% of injected nZVI. Altogether, transport distances of the investigated carbon-colloid supported nZVI are higher than published results of traditional nZVI.

Zusammenfassung

Die Injektion nanoskaligen nullwertigen Eisens ist eine innovative Technik zur In-situ-Sanierung chlororganisch belasteter Standorte. Hierbei wird das nullwertige Eisen in den Untergrund injiziert und soll dort eine permeable reaktive Barriere aufbauen, in der chlororganische Schadstoffe zu weniger schädlichen Substanzen abgebaut werden sollen. Die Einbringung nanoskaliger Kolloide birgt gegenüber klassischen eisengefüllten permeablen reaktiven Barrieren den Vorteil einer durch die wesentlich größere Oberfläche vielfach schnelleren Reaktion und dadurch einer möglicherweise kürzeren Sanierungszeit. Noch ist die praktische Anwendung dieses Ansatzes durch schnelle Agglomeration und Sedimentation der Nanokolloide begrenzt. Durch Hinzufügen von polyanionischen Zusatzstoffen, welche die Oberflächenladung erhöhen und damit die Agglomeration und Sedimentation der Partikel verlangsamen, konnten bereits Transportreichweiten von wenigen Metern beobachtet werden. Ein weiterer Ansatz ist das Aufbringen von Nanoeisen auf ein mobiles Trägerkolloid.
In dieser kumulativen Dissertation werden die Transporteigenschaften von kohlenstoffkolloidunterstütztem Nanoeisen untersucht. Die Untersuchungen beginnen mit Versuchen in Laborsäulen, die mit verschiedenen porösen Medien gefüllt wurden. Hier wurde der Einfluss verschiedener physikochemischer Parameter (u.a. Salinität und pH-Wert) auf das Transportverhalten untersucht. Anschließend wurde der Versuchsaufbau auf einen 1,2 m langen 2D-Laboraquifer, der ebenfalls mit einem porösen Medium gefüllt wurde, vergrößert. Außerdem wurde ein Feldversuch in einem natürlichen Aquifer ein gerichtetes Fließfeld eingerichtet und darin der Transport über eine Distanz von 5,3 m untersucht. Parallel dazu wurde das Transportverhalten mit nichtinvasiven Methoden, hier Magnetresonanztomographie (MRT) und Synchrotronstrahlung, in laborskaliger Größe untersucht.
Die Ergebnisse der Säulenversuche deuten auf eine hohe Anwendbarkeit unter umweltrelevanten Bedingungen hin. Ein sehr niedriger pH-Wert oder eine

hohe Salinität (z. B. mehr als 5 mM/L $CaCl_2$) können die Anwendbarkeit jedoch einschränken. Zusätzlich wurde eine Änderung der durchschnittlichen Kolloidgröße um den Faktor einer Größenordnung und eine Änderung des Zetapotentials von –62 auf –80 mV beobachtet. Die Ergebnisse des Transportexperiments im 2D-Laboraquifer deuten auf eine Deposition der Kolloide auf den ersten Zentimetern der Fließstrecke hin, aber geringe Deposition im weiteren Verlauf des Transports. Dabei konnte kein direkter Einfluss der Gravitation festgestellt werden. Die Ergebnisse konnten mithilfe von MRT-Untersuchungen bestätigt werden. Die Beobachtung mittels Synchrotrontomographie deutet auf eine Deposition an Porenhälsen hin. Die vielversprechenden Ergebnisse der Laboruntersuchungen konnten in dem Feldversuch bestätigt werden, da hier mehr als 10% der zugegebenen nZVI eine Stecke von 5,3 m oder mehr im Aquifer passiert haben. In der Gesamtbetrachtung scheint der Einsatz dieses kolloidunterstützten nanoskaligem nullwertigen Eisens den gängigen Methoden der Eiseninjektion im Hinblick auf die erzielbare Transportreichweite überlegen zu sein.

Contents

1. Introduction **1**

1.1. Water resources and contamination 1
1.2. Dealing with contaminated sites 3
1.3. Classification of remediation technologies 3
1.4. *In situ* treatment of chlorinated compounds 4
1.4.1. Possible technologies for remediation of chlorinated compounds 4
1.4.2. Permeable reactive (iron) barriers 5
1.5. Introduction to nanotechnology and colloid transport 7
1.5.1. Introduction 7
1.5.2. Theoretical background of colloid mobility 9
1.6. Current state on research on nanoscale zero-valent iron (nZVI) . 15
1.6.1. Introduction 15
1.6.2. Reactivity 15
1.6.3. Production 16
1.6.4. Mobility 17
1.6.5. Limitations 20
1.6.6. Colloid enhanced mobility 21
1.7. Carbon-colloid supported nZVI (c-nZVI) 21
1.7.1. Introduction 21
1.7.2. Material production 21
1.7.3. Reactivity 22
1.7.4. Stability and mobility 22
1.8. Aim of this study 24

2. Transport of c-nZVI in saturated porous media **25**

2.0.1. Abstract 25
2.1. Introduction 26
2.2. Materials and Methods 28
2.3. Results and Discussion 31
2.3.1. Particle Characterization 31
2.3.2. Quality control and assurance of carbon analysis and column transport experiments 32
2.3.3. Electrostatic potential of c-nZVI suspensions 33
2.3.4. Stability of a c-nZVI suspension 33
2.3.5. Effect of a polyanionic stabilizer 36

2.3.6. Change of particle properties during transport in a column experiment . . . 37
2.3.7. Effect of porous media . . . 40
2.3.8. Effect of ionic strength . . . 42
2.3.9. Effect of pH . . . 43
2.3.10. General discussion and conclusion . . . 45
2.4. Acknowledgments . . . 46
2.5. Literature . . . 46

3. Investigations on mobility of c-nZVI in a laboratory 2D-aquifer test system 51
3.0.1. Abstract . . . 51
3.1. Introduction . . . 52
3.2. Materials and methods . . . 54
3.3. Results and Discussion . . . 57
3.3.1. Particle characterization . . . 57
3.3.2. Quality assessment and control of analytical data . . . 57
3.3.3. Sedimentation of Carbo-Iron Colloid suspension . . . 58
3.3.4. Column experiment . . . 59
3.3.5. 2D-aquifer experiment . . . 62
3.4. Conclusion . . . 69
3.5. Acknowledgments . . . 69
3.6. Literature . . . 70

4. A field investigation on the mobility of c-nZVI in groundwater 73
4.0.1. Abstract . . . 73
4.1. Introduction . . . 75
4.2. Materials and methods . . . 77
4.2.1. Site description . . . 77
4.2.2. Additional site characterization . . . 79
4.2.3. Tracer experiment . . . 79
4.2.4. Sediment samples . . . 80
4.2.5. Colloid transport experiment . . . 80
4.3. Results and discussion . . . 82
4.3.1. Tracer experiment . . . 82
4.3.2. Aquifer sampling . . . 83
4.3.3. Colloid transport experiment . . . 85
4.4. Conclusion . . . 91
4.4.1. CIC transport . . . 91
4.4.2. Methodology of injection . . . 92
4.4.3. Overall conclusions . . . 92
4.5. Acknowledgments . . . 93
4.6. Literature . . . 93

5. Tomographic investigations on mobility of c-nZVI **97**
5.0.1. Abstract . . . 97
5.1. Introduction . . . 98
5.1.1. Synchrotron observation . . . 98
5.1.2. Magnet resonance imaging (MRI] . . . 99
5.1.3. Objects of study . . . 100
5.2. Materials and Methods . . . 101
5.2.1. Synchrotron observation . . . 101
5.2.2. MRI . . . 102
5.3. Results and discussion . . . 104
5.3.1. Synchrotron radiation . . . 104
5.3.2. MRI . . . 106
5.4. Conclusion and outlook . . . 112
5.5. Acknowledgments . . . 112
5.6. Literature . . . 112

6. General discussion and final conclusions **117**
6.1. Summary of the achievements . . . 117
6.2. Outlook . . . 119

7. Literature **121**

A. Supporting Material to Chapter 2 **XXI**

B. Supporting Material to Chapter 3 **XXV**

C. Supporting Material to Chapter 4 **XXXI**

D. Miscellaneous **XXXVII**

1. Introduction

1.1. Water resources and contamination

The amount of freshwater in the global water cycle is about 2.5% of all water bodies. From this small amount the biggest part of 68.7% is bound in glaciers and only 30.1% is groundwater (Shiklomanov and Rodda, 2004; UNEP, 2006), but groundwater systems provide 25–40% of the world's drinking water (Morris et al., 2003). The European water supply of groundwater resources is higher than that, e.g. in Germany groundwater provides 72% of the required amount, 65% in France, and 84% in Switzerland, which makes groundwater an important resource, but more than 50% of groundwater resources is considered to be anthropogenically influenced (Kobus, 1996).
Contamination of groundwater with different classes of contaminants, such as chlorinated hydrocarbons, fuels or metallic ions, are potentially dangerous for human and environmental health. First surveys of groundwater pollution were performed in the 1960s and showed occurrence of tar derivates, synthetic detergents and pesticides in groundwater. Development of better analytical methods, such as gas chromatography, in the 1970s showed occurrence of many organic pollutants in groundwater in small concentrations (McCarthy, 2010). With increasing knowledge of the extent of contamination in soils and groundwater, the awareness of the need for restoration and maintenance of groundwater resources has increased.
Today the number of listed brown fields and contaminated sites is approx. 450,000 in the USA (USEPA, 2008). The Federal Environmental Agency of Germany (Umweltbundesamt) lists 14,409 sites in need of rehabilitation ("sanierungsbedürftige Altlasten") and 297,315 potentially contaminated sites ("altlastenverdächtige Flächen") (UBA, 2013). In Europe there are more than 400,000 potentially contaminated sites (Prokop and Schamann, 2000), as presented in Tab. 1. Another source (Swartjes, 2011) presents a number of 3 to 3.5 million

Type of site	No of sites
Potentially contaminated abandoned waste sites	90,517
Potentially contaminated abandoned industrial sites	112,368
Potentially contaminated abandoned former armament production sites	202,885
Potentially contaminated abandoned military sites	3,240
Potentially contaminated military sites owned by the Government	No official data
Total	409,010

Table 1.1.: List with numbers of potentially contaminated sites, listed by type in Europe (Prokop and Schamann, 2000).

sites with potential contaminations in the European Union and a market volume of €57 billion for remediation.

Maintaining and restoration of resources is one of the great challenges of our time, since quality of resources needs to be kept at a certain quality level in terms of sustainable management. Especially considering an expected growth of world population within the next decades, human and environmental demands need to be considered appropriate (UBA, 2010b). To meet the need for maintenance of water resources, legal frameworks were established in countries worldwide. Prokop and Schamann (2000) present an introduction to contaminated sites in Europe including references on the legal background and extent of problems in each country in Western Europe. In the USA contaminated sites are regulated under the Superfund Act (CERCLA) (US House of Representatives, 1980), the Superfund Amendments and Reauthorization Act (SARA) (US House of Representatives, 1986) and underlying regulations. In Germany the Federal Soil Conservation Act (BBodSchG, 1998) and the corresponding decree (BBodSchV, 1999) give the legal background. They define groundwater as the subject of protection ("Schutzgut") and the legal background on remediation of contaminated sites. The Federal Soil Conservation Act gives definitions, rules about registration of brownfield land, information of persons and authorities that might be concerned, investigations on the

degree of contamination, planning of remediation, and external and internal monitoring. The soil protection decree gives additional guidelines on investigations and assessment of contaminations, requirements on investigations and quality of the analytical process (Schwister, 2010).

1.2. Dealing with contaminated sites

Before remediation is directed, several steps from registration of potentially contaminated sites to risk assessments have to be carried out. Detailed descriptions are presented in literature (Entemann, 1998; Fleischauer and Falkenhain, 1996; Foerstner, 2008; Schwister, 2010). Decisions on remediation actions follow an integrated approach and consider not only contaminant concentrations, but additional aspects such as availability of contaminants and potential threat to human and environmental health. Additionally, these decisions also have to take economic and landscape planning issues under consideration (Domenico and Schwartz, 1990). However, the basic idea behind regulations is the protection of human and environmental health, which leads to four conceptual approaches for a possible long-term hazard control: (1) remediation and source removal, (2) plume control, (3) cut-off of transfer paths, and (4) restriction of use (UBA, 2010a). Depending on the authors, there are several other possibilities for processing: Domenico and Schwartz (1990) mention the additional possibility of monitoring approaches or alternative water supplies. These approaches might be applicable, when there is no acute threat for human and environmental health. Foerstner (2008) argues for remediation as treatment choice, since the other options shift the problem into the future, rather than solving it.

1.3. Classification of remediation technologies

Technological options for treatment of chlorinated compounds can be divided into on-site and off-site technologies and *in situ* and *ex situ* technologies (Fleischauer and Falkenhain, 1996). These classifications describe the location where the contamination is treated. With off-site technologies, excavated contaminated soil is brought to special treatment facilities, while on-site technologies operate on the field site. Ex situ technologies move the contamination out

of the ground for treatment and *in situ* technologies treat the contamination where it is. According to Fleischauer and Falkenhain (1996) the technological effort grows from *in situ* to off-site. Depending on the author and the intention of the authors, technologies can be sorted in different ways. Domenico and Schwartz (1990) consider remediation from a management perspective and present the groups with (1) management options, (2) containment, (3) containment removal and (4) *in situ* destruction, according to the management strategies presented in the chapter before. For *in situ* destruction (Schwister, 2010) suggests to the groups (1) physico-chemical treatment, (2) thermal methods and (3) biological treatments, which is similar to the classification made by Stroo and Ward (2010) for technological options.
An innovative remediation technology can be defined as a remediation technology which has reached a state of development that appears to be useful for environmental application, but has not reached a state-of-the-art technology and/or the generally accepted rules of technology (Koschitzky, 2010). Most authors consider pump-and-treat technologies and excavation as approved (non-innovative) technology and *in situ* technologies as innovative. However, the opinions on that vary between authors: for example, Koschitzky (2010) and Odensass and Schroers (2002) consider permeable reactive barriers innovative, but Gilham et al. (2010) consider iron-containing permeable reactive barriers (PRBs) as accepted standard practice. Several authors (Cook, 2009; Schaefer et al., 2003) already consider nZVI barriers as state-of-the-art technology. A reason for the difference in opinions might not only be the year of publication, but also the number of nZVI applications carried out so far in different geographical regions: while in North America application of nZVI has been carried out many times, the number of applications in Europe is very limited (Mueller et al., 2012), and therefore rather unknown.

1.4. *In situ* treatment of chlorinated compounds

1.4.1. Possible technologies for remediation of chlorinated compounds

Depending on the kind of contamination, e.g. organic compound, metallic ion or radioactive contamination, the proper treatment technology varies. But

already within the group of organic compounds there is a high variability in potential contamination, which might be fuel contamination or organic solvents, which might again be chlorinated or non-chlorinated. The chlorinated compounds may be dense non-aqueous-phase liquids (DNAPL) or light non-aqueous-phase liquids (LNAPL), which again are highly variable in physicochemical properties. According to McCarthy (2010), there are six possible technological options for treatment of chlorinated compounds:

- Conventional pump and treat
- Air injection
- Biodegradation
- Cosolvent and surfactant flushing
- *In situ* thermal destruction
- *In situ* chemical processes

Stroo (2010) takes a closer look at *in situ* technologies for remediation of chlorinated solvent plumes and lists advantages and limitations of each technology. Decision guidelines for method choice of *in situ* removal of chlorinated compounds can be found there as well.

1.4.2. Permeable reactive (iron) barriers

A reactive barrier is an artificial chemically active zone in the aquifer system, which aims for a transformation or mineralisation of chlorinated compounds. Groundwater passes the reactive barrier by natural groundwater flux and leaves the contaminant in the reactive barrier for transformation (Domenico and Schwartz, 1990). Several definitions of permeable reactive barriers (PRBs) are available (Birke et al., 2006; Odensass and Schroers, 2002; Stroo and Ward, 2010; USEPA, 2012), but all definitions refer to an engineered reaction zone in the subsurface, aiming for contaminant removal.
Reactive barriers can be constructed in several forms, for example as a full-scale reactive barrier or as a funnel-and-gate system. The full-scale system is filled with a reactive material for the whole transversal section, which has to be passed by contaminated water, and the funnel-and-gate system, which uses

pilling walls for creating a directed control of flow direction by construction of a funnel in front of the reactive system (Odensass and Schroers, 2002). For example McMahon et al. (1999) reports a funnel-and-gate system 366 m in length. Funnel-and-gate systems can be considered as a practical solution for big and diffuse sources (Domenico and Schwartz, 1990). However, based on the nature of a passive system, PRBs are only possible for remediation and control of the plume and not for source remediation. This makes reactive barriers to the technology of choice, when a pump-and-treat technology of source removal is technically not possible or too expensive, which is often the case for pollution from chlorinated compounds (Birke et al., 2006).

As a reactive agent not only redox active substances, but likewise a dense population of microorganisms, which might be able to biodegrade organic compounds (Domenico and Schwartz, 1990) or activated carbon for enrichment can be deployed in a PRB. Most applications in PRBs use an iron filling.Activated carbon as filling is only in Germany under discussion (Birke et al., 2006). Lists with tested fillings for permeable reactive barriers are available and contain different iron applications, oxygen-releasing compounds and sorptive material (Odensass and Schroers, 2002).

First experiments on chemical reduction of chlorinated compounds using ZVI have been published in the early 1990s (Gillham and O'Hannesin, 1994; Matheson and Tratnyek, 1994; Orth and Gillham, 1995). Field-scale chemical reduction with granular ZVI as reactive agent has been applied successfully since the mid-1990s, mostly in funnel-and-gate systems (McMahon et al., 1999; O'Hannesin and Gillham, 1998; Vogan et al., 1999; Wilkin et al., 2003), which are still state-of-the-art technology (Stroo and Ward, 2010).

Investigations on longevity lead to an expected reaction time of iron-containing PRBs of more than ten years up to several decades. For example Stroo and Ward (2010) calculate a durability of more than 100 years using a corrosion rate of 0.3 mol/kg Fe/d. Published data from field experiments show a high reaction of several years without decreasing trend and expect the PRB to work for many more years (O'Hannesin and Gillham, 1998; Vogan et al., 1999; Wilkin et al., 2003).

There are several limitations for PRBs and especially iron-containing PRBs. Birke et al. (2006) list potential limitations for application of this technology: the most important limitation is that there is no source removal and only

plume control. This creates a duration time of the remediation process up to several decades. The need for characterisation of the soil and groundwater on the location is very high in order to place the technology adequately, but this limitation accounts for all *in situ* technologies. Permeability and heterogeneity of the soil might be a more relevant factor than for classic pump-and-treat (Stroo and Ward, 2010). Additional limitations for technology choice are high costs in the beginning, a limitation of subsequent improvement and sometimes the *in situ* applied material has to be excavated after use (Birke et al., 2006). In addition to that, PRBs are limited for practical reasons to a construction depth of 15 m (Stroo and Ward, 2010) and construction might be impossible under sealed areas.
However, ideas on overcoming some limitations of iron-containing PRBs led to the idea of using nZVI as a reactive agent *in situ*. nZVI might be able to overcome delivery issues by injection of a slurry directly into the aquifer system (Grieger et al., 2010). A potentially high reaction rate due to high surface area could make nZVI an interesting approach not only for plume control in a PRB, but also interesting for source zone treatment, since the reactive agent could be directly injected into the source zone (Gilham et al., 2010).

1.5. Introduction to nanotechnology and colloid transport

1.5.1. Introduction

Nanotechnology is a rapidly growing sector in the world's economy, with thousands of products (Crane and Scott, 2012) for a high variety of applications. It is a broad field starting from pure nanosized particles to materials with nanostructured properties. The term "nano" means 10^{-9} and therefore the diameter of a nanoparticle reaches from 10^{-9} to 10^{-7} m (Frimmel and Delay, 2010). Nanoparticles can be defined according to this criteria as materials with size in the nanometre range of 1 to 100 nm in all three dimensions (ISO, 2008; Keane, 2010), two dimensions (ASTM, 2006; Frimmel and Delay, 2010) or at least one dimension (European Union, 2011).
Nanoparticles in the context of this thesis are a subgroup of colloids. Colloids are particles in a size range between 1 and 1,000 nm and therefore include a size

range of one order of magnitude more than nanoparticles. The term colloid can include bacteria, viruses, macromolecules, small droplets of non-aqueous phase liquids, inorganic rock or mineral fragments (Domenico and Schwartz, 1990), or the nZVI-containing nanocomposites, which are used in this study (See Fig. 1.1).

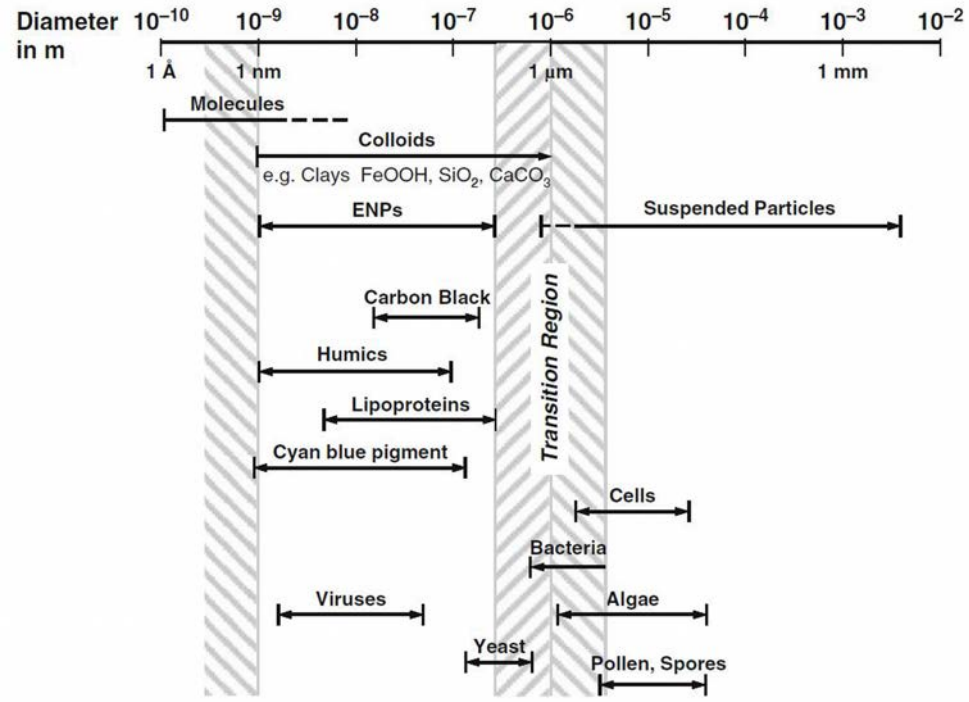

Figure 1.1.: Different natural and artificial particles and colloids which appear in aqueous systems. The figure was taken from Frimmel and Delay (2010).

Keane (2010) divides three kinds of nanoparticles (NP): natural NP, accidental NP and artificial NP. Typically, around 5% of the material in an aquifer is in the nm range (Baumann, 2010) and includes clays, weathered minerals, organic matter and metal oxides. Accidental nanoparticles are a by-product of combustion processes, production processes or erosion. Artificial nanoparticles are nanoparticles which were produced deliberately for a technical application (Keane, 2010; Nowack and Bucheli, 2007).
The most appealing property of nanoparticles in this context is the small size of a particle, and therefore a high specific surface (Frimmel and Delay, 2010).

The surface increases with smaller particle sizes (Nyer and Vance, 2001).
Nanoparticles, artificial and natural, and colloids have overlying definitions and therefore similar properties, but some specific differences as well. Natural nanoparticles and colloids usually show a wide range of particle size distribution, while artificial particles are usually defined to be monodisperse. Bigger colloids underlie the same forces (e.g. diffusion) to a different extent than nanoparticles. Anyhow, transport properties of both can be described with the same theoretical basis (Frimmel and Delay, 2010).

1.5.2. Theoretical background of colloid mobility

DLVO-theory

Even though natural nanoparticles and colloids occur in the environment, there are rather low concentrations of viruses and pathogens in groundwater, which leads to the conclusion that soil is an effective filter for nano- and colloidal-scale particles (Baumann, 2010). To understand transport properties of nanoparticles and colloids, the concept of single collector efficiency as a coefficient for description of particle deposition on a single collector, e.g. a sand grain or a glass bead, has been introduced.
Attachment of colloids was first described by Dejargin, Landau, Verwey and Overbeek (DLVO theory). They gave a theoretical description for stability of colloidal systems by describing steric, electrostatic and van der Waals forces. The classical DLVO theory describes the total interaction energy experienced by a colloid when it approaches another colloid or a surface. In aqueous environments the overlap of the diffuse electrostatic double layers, expressed as electrical charges near the surface of colloids, results in double-layer interactions. The energy of the interaction varies by the distance of the double layers. A further development of this theory, the extended DLVO theory (XDLVO) was developed to include steric interactions, magnetic forces (in case of iron colloids) and hydration forces (e. g. Petosa et al., 2010) for detailed information. The total interaction energy in the XDLVO theory can be expressed as

$$U^{XDLVO} = U^{LW} + U^{EL} + U^{AB} + U^{BO}$$

where

- U^{XDLVO} = the total interaction energy between two surfaces immersed in

water

- U^{LW} = the Liftshitz-van der Waals interaction term
- U^{EL} = the electrostatic interactions
- U^{AB} = the acid-base interaction term, and
- U^{BO} = the interaction energy due to Born repulsion.

Steric interaction should be considered additionally in case of presence of polymers or other long-chained molecules (Brant et al., 2007). If the energy is plotted as function of distance between two surfaces, the total interaction energy can be repulsive or attractive and varies as a function of distance between two surfaces. However, a low secondary minimum and a high repulsive barrier are favourable for low attachment and high transportability (Brant et al., 2007). Manipulation of the energy levels by addition of a polyanionic stabiliser is an approach used later for enhancing transportability of colloids.

Single collector efficiency

Yao et al. (1971) presented the first filtration model based on single collector efficiency: here, transport and deposition are described as the sum of three effects: transport by diffusion, interception and gravity (see Fig. 1.2).
The single collector contact efficiency, as presented by Yao et al. (1971), assumes that the three transport mechanisms are additive, following the formula $\eta_0 = \eta_D + \eta_I + \eta_G$, where

- η_0 = Single collector contact efficiency
- η_D = Transport by diffusion
- η_I = Transport by interception, and
- η_G = Transport by gravity.

Yao assumes that the three mechanisms are (amongst others mechanisms) dependent on particle size, so that a particle size with optimal transport properties and least possible attachment onto a granular collector exists, while smaller particles than the optimal size are strongly subject to diffusion, and

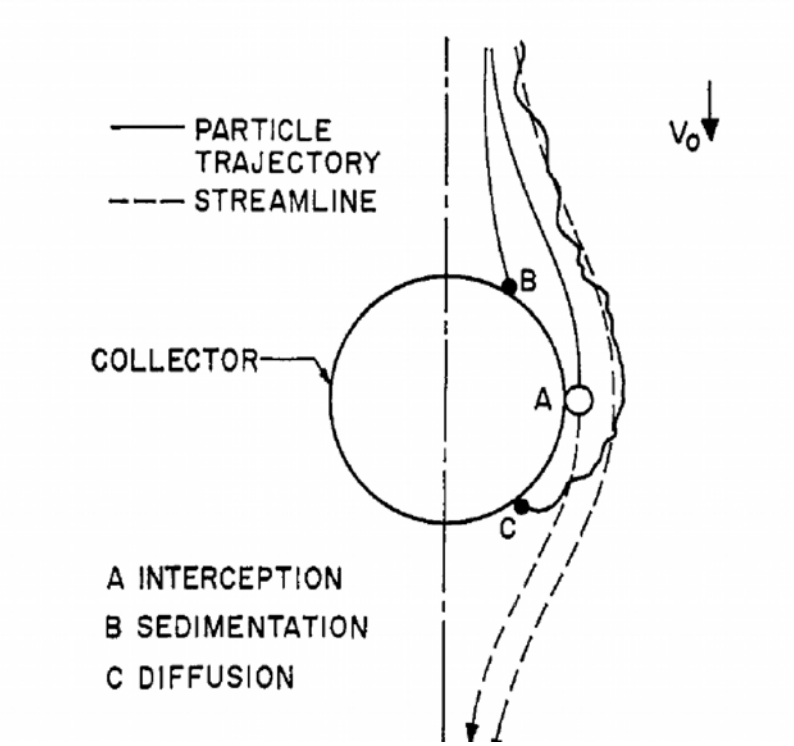

Figure 1.2.: Transport mechanisms of colloids according to Yao et al. (1971).

particles larger than that are attached by interception and sedimentation (Yao et al., 1971). See Fig. 1.3 for presentation of the three influencing factors on particles of different size and the resulting optimal colloid size in this example, which leads to least attachment.

Tufenkji and Elimelech (2004) argue that this model does not include hydrodynamic (viscous) forces and the universal van der Waals forces. Here, hydrodynamic forces play a major role in attachment of colloidal particles, which are larger than the two-digit nanometre range. Results from Tufenkji and Elimelech (2004) lead to a numerical solution for particle sizes, which show lowest single collector contact efficiency. The results in their examples show that particles between 0.5 and 2 µm size show lowest probability for contact between colloid and a surface or in-between colloids (see Fig. 1.4).

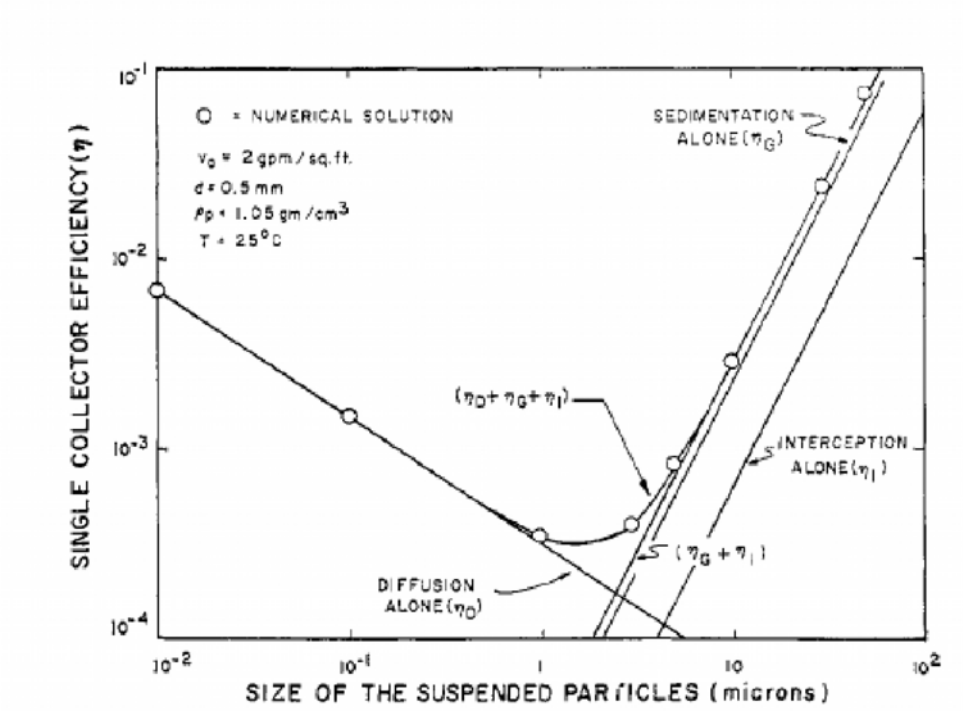

Figure 1.3.: Mechanisms of attachment of colloids and their influence on colloids of different size (Yao et al., 1971). Next to physicochemical drivers such as surface charges, the influence of the mechanisms diffusion, interception and sedimentation are relevant to different extents, depending on colloid size.

Single collector contact efficiency

Contact between a colloid and a surface does not necessarily lead to attachment of a colloid onto a surface. Tufenkji and Elimelech (2004) add an empirical factor η for calculating single collector contact efficiency:

$\eta = \eta_0 \, \alpha$

Here α is an empirical factor, which can be derived from porous media, suspended particles and solution chemistry following the formula:

$$\alpha = -\frac{2}{3}\frac{d_c}{(1-f)L\eta_0} ln(C/C_0)$$

where

- α = the empirical factor for single collector removal efficiency,

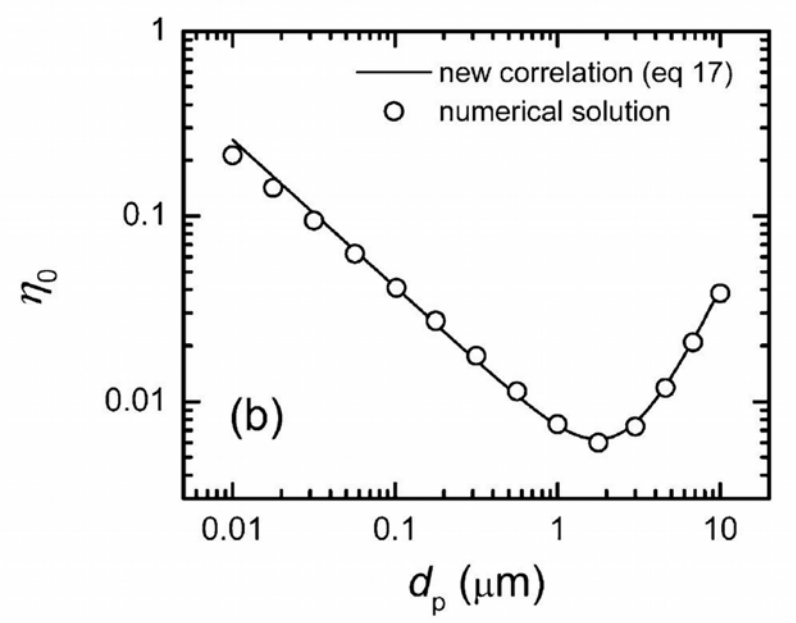

Figure 1.4.: Collector efficiency as function of particle size according to (Tufenkji and Elimelech, 2004). Here, an example for a numerical interpretation for collector efficiencies depending on colloid size is presented.

- d_c = diameter of the porous media, and
- f = porosity of a porous medium,
- L = filter medium packed length,
- η_0 = single collector contact efficiency
- C/C_0 = the normalised concentration of the influent concentration

Lutterodt et al. (2009) argue that transport in the theoretical models is assumed to occur at an invariant rate, but newer research hints on variation of the deposition rate coefficient for various reasons, such as heterogeneity in collectors and colloid or straining. These variations again lead to different extents of energy barriers.

Additional factors affecting transport

Several factors which influence attachment lie within the environment of the transport experiment; other factors can be influenced during transport or for a transport experiment. Roughness of the porous medium is a factor with a potentially high influence on the mobility of a colloid (Brant et al., 2007). For example, 30–50% higher deposition rates were found for bacterial transport on rough porous media than on smooth porous media (Shellenberger and Logan, 2002). Furthermore, chemical surface heterogeneities, such as surface charge inheterogeneities which might be derived from emplacements of metal in sand (Brant et al., 2007), can influence transport. Furthermore, the chemical characteristics of the transport medium, in most cases water, are important. Mono- and bivalent salts, natural organic matter, clays and microorganisms can have an influence, either alone or in combination (Brant et al., 2007). Larger macromolecules increase steric repulsion in the presence of monovalent salts. Bivalent cations can decrease steric repulsion of organic matter (Petosa et al., 2010). Generally, organic macromolecules are associated with higher steric repulsions (Aiken et al., 2011) and can be used to manipulate deposition and re-entrainment of colloids (Franchi and O'Melia, 2003). The effect of organic macromolecules can influence effective electrostatic forces or the hydrodynamic radius of colloids. This again can change the surface to be only dominated by the organic layer around the colloid (Brant et al., 2007).
Next to the factors which result from boundary conditions and which cannot be influenced, some factors can be influenced: within this work, increasing repulsive forces play a major role. General assumptions for potential stable colloid suspensions include a surface potential of more than –30 mV (International Organization for Standardization, 2010), which needs to be exceeded to obtain steric stabilisation. Addition of organic matter can increase steric forces and stabilise colloids by increasing zeta potential. Surface modifications can effect interactions between a colloid and a surface or another colloid by a factor of 100 (Baumann, 2010; Pelley and Tufenkji, 2008; Saleh et al., 2008). This is used very often for increasing colloid transport as presented and used later. If colloids are stable in terms of low collision and low attachment, they are potentially very mobile in porous media. Generally negatively charged molecules are considered to be the most mobile, since most aquifer materials

have a negative surface charge (Domenico and Schwartz, 1990).

1.6. Current state on research on nanoscale zero-valent iron (nZVI)

1.6.1. Introduction

The current state of nZVI technology begins with the first publication of this idea in 1994. Gillham and O'Hannesin (1994) suggested application of smaller particles than granular ZVI in order to increase reaction rates of ZVI. In 1997, the first study was published on mobility of granular ZVI of 2 µm size in column experiments (Cantrell and Kaplan, 1997), which concludes very high gravitational influence on transport, but the idea of injection of ZVI colloids into the subsurface was born. Depending on the author, as discussed in the chapters above, reactive barriers filled with nZVI is considered state-of-the-art technology (Baumann, 2010; Schaefer et al., 2003). In this study it is considered as innovative technology for the simple reason that this technology never reached the state of full-scale application in Germany. However, classical reactive barriers can only be applied downstream a source of contamination. The solution for this issue might be the direct deployment of nZVI in the source zone of a contamination (Baumann, 2010). This technology might be more cost-effective than installation of a PRB of ZVI (Cai et al., 2006; Marcus and Bonds, 1999). Generally, nZVI is considered to be a promising approach for groundwater remediation (Crane and Scott, 2012).

1.6.2. Reactivity

ZVI is known to be a reactive agent in a PRB for two decades (Gillham and O'Hannesin, 1994). The same reactive process is given for nZVI, but as a consequence of small size a high specific surface is given (Frimmel and Delay, 2010), which leads to high reaction rates and a rapid decrease of contaminant concentration levels (Baumann, 2010). The dechlorination of perchloroethene (PCE, C_2Cl_4) follows in a simple form the reaction equation

$$Fe^0 + H_2O + X - Cl \rightarrow Fe^{2+} + OH^- + X - H + Cl^-$$

(Nyer and Vance, 2001), or in complete stochiometry for TCE

$$C_2Cl_4 + 4Fe^0 + 4H^+ \rightarrow C_2H_4 + 4Fe^{2+} + 4Cl^-$$

(Zhang, 2003). Following that logic PCE can be reduced to acetylene (Lowry, 2007). TCE dechlorination requires three moles of nZVI per mole of TCE, which is 1.0 g nZVI per 1.3 g TCE (Baumann, 2010). The dechlorination process follows mostly a pathway of beta elimination or reductive dechlorination. In this reaction, nZVI provides electrons and corrodes (Arnold and Roberts, 2000; Nyer and Vance, 2001). In this elimination process, the C-Cl bond is broken and Cl^- is released into the surrounding medium (Elschenbroich, 2006). Another published reaction process leads from PCE to TCE, to DCE and at last to VC (Elschenbroich, 2006). However, not every contaminant can be remediated using nZVI: for example, aromatic ring systems cannot be broken by the reductive energy of nZVI (UBA, 2012).
In field applications nZVI has been evaluated and was shown to be highly reactive. Comba et al. (2011) wrote a review on 112 field applications of ZVI of millimetric, micrometric and nZVI. Millimetric ZVI showed cleaning efficiencies of 97%, followed by micrometric ZVI with 93% and nanoscale ZVI with 63%. Macé et al. (2006) reviewed several applications of nZVI made by the company Golder and concludes generally a decrease of concentrations of chlorinated solvents over a short period of time, which supports the results by Comba et al. (2011). However, results vary in different applications. Comba et al. (2011) explain smaller cleaning efficiencies for nZVI by application issues, which need to be improved in order to achieve higher cleaning efficiencies. This will be discussed in the chapters on stability and mobility of nZVI.

1.6.3. Production

Several production pathways for nZVI have been published. All methods have their specific advantages and disadvantages. Methods for production are listed in a publication by the German Federal Environmental Agency (UBA, 2012) and are:

- mechanical crushing of bigger particles
- chemical reduction of iron salts, e.g. iron chloride, by sodium borohy-

dride in water. The resulting particles reach a size of 10 to 100 nm with a medium size of 50 nm and a specific surface of 15 – 50m^2/g.

- reduction of iron oxide at high temperatures of 300–600 °C together with hydrogen. Mean particle size is 70 nm and specific surface is 30 m^2/g
- heating of ironpentacarbonyle up to 250°C. Mean particle size is 5 nm.

For enhancement of reactivity small amounts of a noble metal, such as palladium, might be added during the production process. In laboratory studies 0.1% in mass as addition of noble metals to the nZVI can enhance reactivity by two orders of magnitude (Cook, 2009), but field-scale applications show no increased decomposition of chlorinated contaminants (Comba et al., 2011). After production, particles have to be stabilised due to pyrophoric properties. For example, Sohn et al. (2006) stabilised nZVI by producing an iron oxide shell around the particles. Addition of a polyanionic stabiliser was observed to have an influence on reactivity of nZVI in both ways, positive and negative. This influence is detectable, but not to a relevant extent (Tratnyek et al., 2001).

1.6.4. Mobility

Mobility of different nZVI applications has been tested, from small laboratory experiments to field experiments. Bare nZVI is almost non-mobile in column experiments (Schrick et al., 2004). Stabilised nZVI, as presented in the chapter on stability, is more mobile, but highly variable in expected transport ranges. This depends on the design of the study: results are in a range between 0.3 and 2 m at 99.99% filtration level (Laumann et al., 2013; Tiraferri and Sethi, 2009), but higher possible transportation distances can be achieved under artificial conditions (Saleh et al., 2008). Comparison in column experiments show higher breakthrough rates for stabilised particles than for unstabilised particles (Jiemvarangkul et al., 2011; Johnson et al., 2009; Tiraferri and Sethi, 2009). He et al. (2009) showed higher transport rates in glass beads, used as porous media, than in sand as porous media. Raychoudhury et al. (2012) found concentration-dependent changes in breakthrough: if the concentration of nZVI in a suspension is higher, the relative breakthrough rate is lower. In difference to breakthrough behaviour of conservative tracers such as salts, full breakthrough cannot be reached. Often, no steady state breakthrough

level is reached but a fast rise in breakthrough level in the beginning and then a change in speed to a very slowly growing breakthrough level can be observed (Raychoudhury et al., 2012). Generally, the transport behaviour of nZVI follows the general rules of colloid transport as reviewed by Kanti Sen and Khilar (2006) and Ryan and Elimelech (1996).
Bigger-scaled laboratory experiments have been performed in two- and three-dimensional laboratory aquifer tanks. Phenrat et al. (2010) observed transport of stabilised nZVI in a 2D flow cell of 30 x 18 x 2.5 cm. In that study, the breakthrough time is comparable to breakthrough of a conservative tracer and the breakthrough level is about 50% of the injected concentration. In another study using the same flow cell, flow bypass of nZVI around lenses with lower hydraulic conductivity was observed (Phenrat et al., 2011). Kanel et al. (2008) used a 2D aquifer tank with a length of 50 cm and a height of 28.5 cm, see Fig. 1.5. In that study transport properties of tracer, unstabilised and stabilised nZVI were observed in silica beads of 1.1 mm diameter in a vertical flow field. Unstabilised nZVI was hardly mobile at all, while stabilised nZVI showed a similar transport speed in terms of vertical flow compared to tracer, but a strong gravitational influence was observed. Johnson et al. (2013) performed a laboratory study in field scale size by using a 3D container of 10 x 10 x 2.4 m size. In that study, CMC-stabilised iron was injected under aggressive flow conditions and reached a transport distance of 2.5 m. The distribution of nZVI was rather uneven in that study: approx. 70% of the injected nZVI reached 25 cm distance, 45% reached 50 cm and after 1 m only 2% of the injected nZVI was found.
In field experiments, transport ranges have been observed to be maximal 4.5 m, from the point of injection. Most studies follow the approach of an artificial stimulated flow field. Usually, an nZVI containing suspension is injected into a well and is extracted at another well. In most studies, observation wells are installed to collect groundwater samples. Exemplarily, a set-up of a field experiment is presented in a study by Elliott and Zhang (2001). Limited mobility in aquifer systems result in reduced contaminant concentration only close to the injection wells (Zhang, 2003). See Tab. 1.2 for a compilation of the current knowledge on transport distances, which were reached in field experiments on mobility of nZVI.

Transport range	Application	Soil characterisation	Source
4.5 m	Recirculation of bimetallic-doted nZVI. Recirculation for two days. Injection of 1.7 kg. Concentrations of 20–30 mg/L were found at the observation wells.	Hydraulic conductivity (K) = 0.2 cm/s Porosity = 0.25	Elliot & Zhang, 2001
0.54 – 1.3 m	Injection and observation, push-pull-test	Holocene and Pleistocene alluvial sediments, predominantly silts and clays, and coarse grained sediment deposits along ancient stream beds	Bennett et al., 2010
Close to injection wells	Visual evidence of nZVI transport in soil cores close to injection wells	Medium to coarse grained sand	Quinn et al. 2005
1.5 - 3 m	Pd-doted nZVI, 70% normalised to tracer after 1.5 m. After 3 m almost no recovery.	Silty clay with sand and gravel	He et al., 2010
1.06 m	Observation of coloured water, recirculation of Pd-doted nZVI slurry.	Clayey sand or silty very fine-to-fine sand	Henn and Wadilll, 2006
3 m	Gravity injection of approx. 40 kg nZVI with small traces of palladium	Medium to coarse sand and few silt	Wei at al., 2010

Table 1.2.: Compilation of published studies dealing with mobility of nZVI in field experiments.

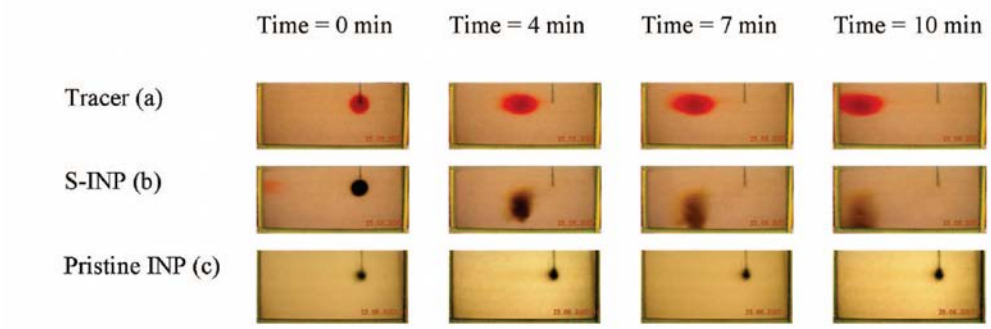

Figure 1.5.: Transport of tracer, stabilised iron nanoparticles and pristine iron nanoparticles in a 2D aquifer container filled with glass beads (Kanel et al., 2008). In this example a vertical flow field from the right to the left side is applied. While transport of tracer (a) follows the flow of water, stabilised nZVI (b) is mobile, but underlies a strong influence of gravity. Unstabilised nZVI (c) is hardly mobile at all under these experimental conditions.

1.6.5. Limitations

The current state of nZVI application shows many advantages compared to established technologies for remediation of chlorinated contaminations, such as pump-and-treat, or other innovative technologies, such as permeable reactive barriers, but there are flaws. One is the lack of reaching the water-NAPL interface (Baumann, 2010), therefore direct contact between organic compounds and reactive iron seems hardly possible. The second is limited mobility of pure and stabilised nZVI, caused by aggregation and sedimentation (Phenrat et al., 2007). This limited mobility might additionally lead to pore clogging and water fluxes around the nZVI (Crane and Scott, 2012). High iron concentrations of more than 500 g per kg sediment might lead to potentially harmful conditions for organisms (Adeleye et al., 2013). There are only few studies on toxicology of nZVI, but generally the assumption is nZVI shows no additional threat to humans and the environment when applied in contaminated areas (Grieger et al., 2010). Nevertheless, nZVI is bactericidal in low mg/L ranges (Li et al., 2010). In case of bimetallic nZVI nanoparticles, concerns about the release of a noble metal into the environment were mentioned in literature (Crane and Scott, 2012).

1.6.6. Colloid enhanced mobility

To overcome the main limitations of nZVI applications, the idea of using bigger particles as carrier for nZVI, according to filtration theory (Tufenkji and Elimelech, 2004), has been mentioned several times in literature. Bigger particles might decrease aggregation (Phenrat et al., 2009) and lead to lower attachment coefficiencies (Schrick et al., 2004). This idea has been followed by several authors and led to the development of nanostructured composites made from silica (Zheng et al., 2008), carbon black (Hoch et al., 2008), kaolinite (Chen et al., 2013), graphite (Zhang et al., 2006), carbon microspheres (Sunkara et al., 2010; Sunkara et al., 2011; Zhan et al., 2011), bentonite (Shi et al., 2011) or activated carbon (Bleyl et al., 2012; Mackenzie et al., 2012; Zhuang et al., 2011). Hydrophilic substances, e.g. activated carbon (Schrick et al., 2004), could create a composite which could overcome the interface between water and the NAPL phase.
Mobility of composites is not studied well. Carbon microspheres were observed to have high breakthrough rates in 3-cm-sized column experiments (Sunkara et al., 2011; Zhan et al., 2011). The same set-up was used for silica-based material and 70% breakthrough of colloids was observed (Zhan et al., 2008). One experiment using activated carbon-based material has been published and shows 80% breakthrough in a 22 cm column (Mackenzie et al., 2012). The material from the last experiment is presented later in detail in the material description of carbon-supported nZVI.

1.7. Carbon-colloid supported nZVI (c-nZVI)

1.7.1. Introduction

The material used in this study is called Carbo-Iron colloid (CIC). Here, crushed activated carbon is used as a carrier colloid for nZVI. The material properties are favorable for transport in aquifer material.

1.7.2. Material production

A complete description of the production process can be found in a study by Bleyl et al. (2012). Colloids of activated carbon are wet-impregnated with a precursor solution of an iron salt. Iron is immobilised in the colloid by alkali

washing or evaporation of the water. In this state iron exists as iron oxide and hydroxide in the pore space. The next step is thermal reduction of the iron to ZVI. This can be done at 500 °C in a reducing atmosphere with H_2 and N_2 or at 700 °C in inert gas (Bleyl et al., 2013; Bleyl et al., 2012). The last step is inactivation by small amounts of hydrochloric acid (Mackenzie et al., 2012).

1.7.3. Reactivity

Mackenzie et al. (2012) performed an exemplary experiment and found higher reactivity for CIC than for pure nZVI. A batch experiment showed 15 times more effective reactivity than pure nZVI without activated carbon as carrier. An attempt to explain this effect is presented by Bleyl et al. (2013). There it is assumed that sorptive enrichment of PCE in the pore space of the activated carbon causes the observed effect. Therefore, the already-mentioned interface problem between water and NAPL (Baumann, 2010) can be solved by this carrier. An experiment in columns, where CIC was immobilised by mixing with sediments, showed very similar reaction rates in the batch experiments (Bleyl et al., 2013).

1.7.4. Stability and mobility

Since the iron is in the pore space of the activated carbon, the transport characteristics of this material are dominated by the properties of activated carbon (Mackenzie et al., 2012). At a pH value of 7, the zeta potential of CIC is between –7 and –29 mV (Mackenzie et al., 2012). Pure iron shows a zeta potential of +20 mV (Mackenzie et al., 2012) to –1.45 mV (Cirtiu et al., 2011). Based on zeta potential, CIC alone is not mobile enough for transport and needs the addition of a polyanionic stabiliser. To achieve high-enough negative zeta potential, 3% in mass should be enough, and an addition of 7% leads to full charging of the surface. More than 15% addition of CMC in deionised water does not lead to a higher stabilising effect (Bleyl et al., 2013; Mackenzie et al., 2012). Particle properties are shown in Tab. 1.3.
A column experiment to test whether nZVI and iron stick together and do not become separated during the transport process was performed in a 22-cm-long column. The experiment showed a breakthrough of 80% of the injected concentration. In this experiment carbon and ZVI were measured and showed

Surface BET	550 - 800 m^2/g
Particle size D_{50}	0.8 µm
Fe^0 content	10-25%
carbon content	50 - 50%
Density	1.6 - 1.7 g/cm^3
Iron cluster size	20 - 50 nm
Electrostatic potential	-30 mV

Table 1.3.: Particle characteristics of Carbo-Iron colloids (CIC) (Bleyl et al., 2013; Bleyl et al., 2012; Mackenzie et al., 2012).

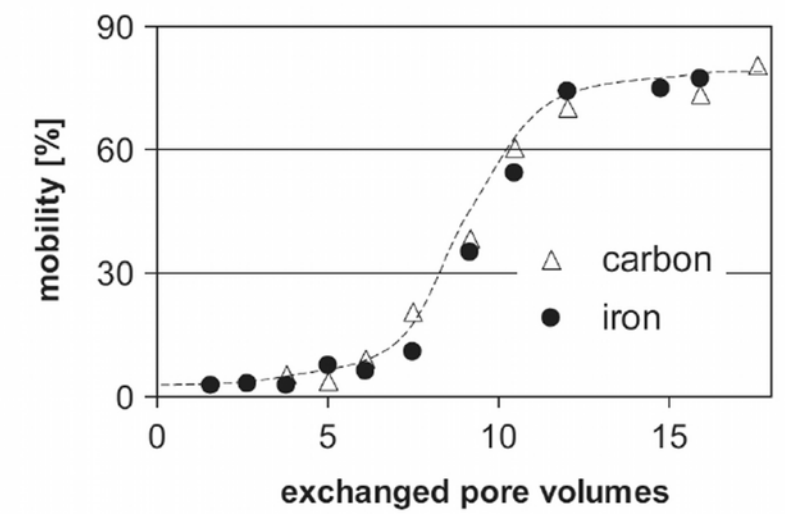

Figure 1.6.: Comparison of iron and carbon concentration in a CIC transport experiment according to Mackenzie et al. (2012). Iron and Carbon breakthrough curves show the same shape, therefore it can be assumed that CIC is a stable material.

identical breakthrough behaviour, which means direct attachment of carbon and nZVI in a composite and therefore in the transport experiment (Fig. 1.6). Stabilised nZVI from Toda Corporation (Japan) had 10% breakthrough in the same experiment. Therefore CIC seem to be more mobile in column experiments than pure nZVI.

1.8. Aim of this study

This research was conducted as part of the research project Fe-Nanosit (Eisenbasierte Nanopartikel und Nanokompositstrukturen zur Schadstoffentfernung aus Grund- und Abwässern – Iron-based nanoparticles and nano-composites for removal of contaminants in groundwater and sewage), which aimed at exploration of the potential of nanomaterial applications in the context of wastewater treatment and groundwater remediation. Within this project the task of this subproject was to investigate the mobility of a newly developed nano-composite material for groundwater remediation.
In the forefront of this study, application of nZVI was described as a possible innovative technology for remediation of chlorinated compounds in aquifer systems. To overcome the limitation of very limited mobility of nZVI in laboratory and field-scale investigations, CIC were developed. They were expected to have possible superior characteristics compared to nZVI.
The aim of this research was to investigate and evaluate transport properties of carbon-supported nZVI. The research consisted of identification of methods and experimental set-ups for transport experiments. Transport experiments were conducted on different scales from small sized laboratory experiments in column experiments (chapter 2) over 2-D laboratory experiments (chapter 3) to a field experiment (chapter 4). method development of non-invasive methods is presented (chapter 5). The last step was to integrate the results aiming for an overall assessment of transport properties.
Results of this cumulative thesis have already been published (Busch et al., 2014a; Busch et al., 2014b) or are submitted (Busch et al., 2014c). An additional study on imaging approaches is presented (chapter 5).

For literature references see chapter 7.

2. Transport of carbon colloid supported nanoscale zero-valent iron in saturated porous media

Article published as J. Busch, T. Meißner, A. Potthoff & S.E. Oswald (2014): Transport of carbon colloid supported nanoscale zero-valent iron in saturated porous media. Journal of Contaminant Hydrology 164 p.25-34

2.0.1. Abstract

Injection of nanoscale zero-valent iron (nZVI) has recently gained great interest as emerging technology for In situ remediation of chlorinated organic compounds from groundwater systems. Zero-valent iron (ZVI) is able to reduce organic compounds and to render it to less harmful substances. The use of nanoscale particles instead of granular or microscale particles can increase dechlorination rates by orders of magnitude due to its high surface area. However, classical nZVI appears to be hampered in its environmental application by its limited mobility. One approach is colloid supported transport of nZVI, where the nZVI gets transported by a mobile colloid. In this study transport properties of activated carbon colloid supported nZVI (c-nZVI; d_{50} = 2.4 µm) are investigated in column tests using columns of 40 cm length, which were filled with porous media. A suspension was pumped through the column under different physicochemical conditions (addition of a polyanionic stabilizer and changes in pH and ionic strength). Highest observed breakthrough was 62% of the injected concentration in glass beads with addition of stabilizer. Addition of mono- and bivalent salt, e.g. more than 0.5 mM/L $CaCl_2$, can decrease mobility and changes in pH to values below six can inhibit mobility at all. Measurements of colloid sizes and zeta potentials show changes in the mean particle size by a factor of ten and an increase of zeta potential from -62 mV to -80 mV during the transport experiment. However, results suggest potential applicability of c-nZVI under field conditions.

2.1. Introduction

Contamination of groundwater with organic and inorganic pollutants, such as chlorinated hydrocarbons, fuels and metallic ions, is a threat for environmental and human health. Remediation of groundwater resources has been a subject to science for several decades, but conventional remediation and treatment technologies, such as pump-and-treat, have shown limited effectiveness in reducing contamination and are expensive (Mueller and Nowack, 2010; Savage and Diallo, 2005). One new strategy to address this issue is the application of nanotechnology, which can be considered as a beneficial technology for sustainable groundwater management (Grieger et al., 2010). Several classes of functional nanomaterials have been developed within the last years such as (1) metal containing nanoparticles, (2) carbonaceous nanomaterials, (3) zeolites, and (4) dendrimers. Different kinds of particles show a variety of physicochemical properties and are therefore interesting for different applications (Savage and Diallo, 2005). The first class of metal containing nanoparticles shows high potential for groundwater and soil remediation and could probably be applied alongside to classical methods or could be installed as *in situ* permeable reactive barrier. Especially using nanoscale zero-valent iron (nZVI) as a reactive agent seems to be a promising approach for groundwater remediation (Crane and Scott, 2012).
Permeable reactive barriers (PRBs) build with granular zero-valent iron (ZVI) are established technology for almost two decades (Gillham and O'Hannesin, 1994; Matheson and Tratnyek, 1994). By changing the particle size from millimetric to nanoscale, the reactivity of iron increases several orders of magnitude due to a higher surface of nZVI (Mueller and Nowack, 2010). The Surface of a particle increases by a factor of 1000 by reducing particle size with the same factor, e.g. from 0.1 mm to 100 nm (Sellers et al., 2008). NVZI is highly reactive with chlorinated organic compounds (Joo and Cheng, 2006; Li et al., 2006; Wiesner and Bottero, 2007; Zhang, 2003). An advantage of direct injection of mobile colloids could be an easier installation of a PRB, since a direct injection of nZVI into a contaminated aquifer could be more cost effective and feasible than the installation of a PRB by excavation of large volumes and direct installation into the aquifer, e.g. for deep aquifers and fractured rock aquifers (Cai et al., 2006; Marcus and Bonds, 1999).

Several field applications for ZVI and nZVI have been reported to show high cleaning efficiency for different ZVI-applications, but a review concludes a need to research on nZVI technologies, since other ZVI-technologies show a higher efficiency. In that study, millimetric and micrometric iron was described to remove 97% and 91% of contamination, while nZVI applications only remove 67% of contaminants (Comba et al., 2011). Fast aggregation of nZVI to bigger aggregates and subsequent sedimentation was identified to be the main limitation for application of nZVI (Phenrat et al., 2007). Laboratory (Schrick et al., 2004), field scale experiments (Johnson et al., 2013) and field experiments (He et al., 2010; Quinn et al., 2005) show limited transport for nZVI, which might not be enough to install PRBs *in situ*, since a reduction of contaminant concentrations can only be observed close to the injection well (Zhang, 2003). Different approaches have been made to enhance mobility of nZVI. One approach is to use surface modifiers, which increases electrostatic repulsion by increasing negative surface charges. Several polyanionic stabilizers are under discussion, such as carboxymethylcellulouse (CMC) (He et al., 2009), guar gum (Tiraferri and Sethi, 2009), or others (Jiemvarangkul et al., 2011; Kim et al., 2009; Phenrat et al., 2008). Another approach aims for a suited carrier particle that contains nZVI, since filtration theory proposes that colloids of a size around 1 µm show the highest mobility in soils (Tufenkji and Elimelech, 2004). Detailed insight into filtration theory and nanomaterial transport is presented in reviews (Brant et al., 2007; Petosa et al., 2010). Several approaches to create a mobile composite material have been published recently: Carrier materials could consist of silica (Zheng et al., 2008), carbon black (Hoch et al., 2008), graphite (Zhang et al., 2006), carbon microspheres (Sunkara et al., 2010; Sunkara et al., 2011; Zhan et al., 2011), or activated carbon (Bleyl et al., 2012; Mackenzie et al., 2012). The last approach creates a composite material called "Carbo-Iron® colloids" (CIC), which shows material properties that are favorable for mobility. The mean particle diameter (d_{50}) of 0.8 µm (Bleyl et al., 2012) to 2.4 µm (this study) is in the relevant range for possible transport, the density is 1.7 g/cm³, and the composite contains 10-25 wt.-% of nZVI. Additionally to that, the activated carbon is able to absorb organic compounds and to accumulate at interfaces of groundwater and non-aqueous phase liquids (NAPL). Degradation of TCE by CIC has already been shown (Mackenzie et al., 2012).

Transport of colloids in porous media is usually described by the DLVO theory. The DLVO theory expresses the interaction energy between surfaces, e.g. particle-particle interactions or particle-surface interactions, as sum of van der Waals forces and electrostatic interactions. The DLVO theory has been extended for additional driving forces such as acid base interactions and Born repulsion forces. Additional forces, e.g. steric interactions, show additional influence on colloid transport and might be directly manipulated by macromolecules. Qualitative predictions from DLVO models suggest increased agglomeration and deposition of colloids at high ionic strength and pH values close to the point of zero charge due to reduction of repulsive forces. (Brant et al., 2007). The transport and attachment of colloids in porous media is described in filtration theory by the mechanisms of Interception, gravitational sedimentation and Brownian diffusion which are additive. Depending on the colloid size, the mechanisms are developed to another extent, which leads to a possible colloid size with the smallest contact and attachment probability (Tufenkji and Elimelech, 2004; Yao et al., 1971). In our study we investigate the mobility of activated carbon colloid supported nZVI (c-nZVI) in column tests using particles, produced as a variant of CIC with a bigger mean diameter of 2.4 µm than the optimal size range of 0.5-2 µm for transport in aquifer systems according to Tufenkji and Elimelech (2004). We want to examine whether an anionic stabilizer can affect the mobility of c-nZVI, if the porous media have an influence on the transport, and which environmental conditions are suited for injecting c-nZVI for groundwater remediation. Here the influence of ionic strength (NaCl and $CaCl_2$) and pH is examined. Additionally changes in zeta potential and particle size distribution are observed during a transport experiment.

2.2. Materials and Methods

A sample of c-nZVI was provided by the Helmholtz Centre for Environmental Research UFZ (Leipzig, Germany). CMC, HCl, NaCl and $CaCl_2$ were of analytical grade (p.a.) and purchased from Carl Roth (Karlsruhe, Germany). Deionized water was produced using an ion exchange resin containing cartridge. Potassium hydrogen phthalate (KHP) was of analytical grade and provided by Elementar (Hanau, Germany).

The particle size distribution was measured by static light scattering using a Mastersizer 2000 (Malvern GmbH, Herrenberg, Germany). Suspensions were obtained by probe sonication using a Branson Sonifier 450 (Branson Ultrasonics Corporation, Danbury, CT, USA) for particle characterization. Specific surface area (BET method) was obtained by taking an ASAP 2010 accelerated surface area and porosimetry analyzer (Micromeritics GmbH, Mönchengladbach, Germany). Zeta potential was measured by using a Zetasizer Nano (Malvern GmbH, Herrenberg, Germany).

Samples for sedimentation experiments were prepared by purging 1 L of deionized water with nitrogen for 1 h to remove oxygen. For one experiment, an amount of 200 mg CMC was added and dissolved by sonication and a sample was taken for detecting background carbon concentration. A second experiment was performed without addition of CMC. Both experiments were performed twice. 1000 mg/l of c-nZVI was added to the CMC containing solution and dispersed for 30 min at 24,000 rpm using an Ultra-Turrax T25 Digital by IKA (Staufen, Germany) with an S25N-18G dispersing element. Three samples were taken to determine initial carbon concentration. After taking the samples, the sonication device was removed and the suspension was left without further movement. Samples were taken automatically in defined time steps by the analyzer in 7.5 cm height in a 15 cm high bottle. Results were calculated by subtraction of carbon content provided by the background concentration of CMC and normalized to the initial concentration of c-nZVI.

For sample preparation of column tests, 1 L of deionized water was purged by nitrogen for at least 1 h. A defined amount of CMC (0-200 mg/L) was added and dissolved by sonication and background carbon concentration was measured. Subsequent, a defined amount of 500 or 1000 mg of c-nZVI was added and dispersed for at least 30 min at 24,000 rpm. Additional amounts of salts were added after dispersing the colloids, but dispersion was continued for another 30 min until the concentration in the storage tank was measured. Adjustments of pH were made by addition of diluted HCl or NaOH into the suspension after dispersing, but before measurement of the concentration in the storage tank. During the transport experiment the Ultra Turrax device was kept in the storage tank at 10,000 rpm to keep colloids in suspension and prevent them from sinking, and aiming for a constant injection concentration of c-nZVI. Samples for zeta potential measurements and particle size distribution

before and after a column tests were taken from the storage tank and from the end of the column and stored in glass bottles. Samples were transported into another laboratory and were approximately one week old before measurement. They were not deagglomerated again by a Branson Sonifier or an Ultra Turrax before size measurements, but only with the sonication bath offered by the static light scattering device. Before size or zeta potential measurement, samples were diluted with deionized water to the optimal measuring concentration of the respective device. All experiments, unless stated otherwise, were performed at pH 10.4. Several porous media were included in the experiments, including two sizes of glass beads, sand from two commercial suppliers and aquifer material from two field sites (Tab. 2-1). Porous media A, B1, B2, D1, and D2 show a crushed uneven shape with sharp edges, while porous media C, E1, and E2 show a very even round shape. Glass beads (E1 and E2), and sands A and B were cleaned by soaking overnight in HCl (2M), washing with deionized water until reaching neutral pH, subsequent soaking overnight in NaOH (2M) and washing with deionized water. The porous media were dried in a drying-oven at 104° C and stored until usage. Samples from field sites were dried and fractioned by sieve fractioning. Prior to transport experiments the fractions (C, D1, and D2) were soaked overnight in HCl (2M) and washed with deionized water until neutral pH was reached prior to column experiments. Cleaning of porous media using acid washing in different variation and combination with other treatments is an established procedure in colloid transport experiments (Solovitch et al., 2010; Tiraferri and Sethi, 2009).
Column experiments were performed in columns with a height of 40 cm and an inner diameter of 2 cm (Lenz Laborglas GmbH & Co. KG, Westheim, Germany). 125 mL of porous media were filled wet into the column. Porosity was 0.38-0.39. The experiments were performed using a piston pump (Ismatec MCP equipped with a FMI 2.05 piston head) equipped with two air filled blind tubes after the piston to decrease pulsation. Before performing breakthrough tests the filled columns were equilibrated with ten pore volumes of a background solution containing the same amount of CMC and salt as the colloid suspension. The suspension was pumped with a constant speed of 3.4 mL/min or 2.45 cm/min vertically against gravity. Column experiments are often performed faster than natural groundwater velocities, for practical reasons; here this is rectified further by representing an injection scenario via a

Name	Type	Grain size (sand type)	Supplier
A	QS	1-2 mm	Euroquarz, Laußnitz
B1	QS	0.1-0.5 mm (fine to medium)	Sand Schulz, Berlin
B2	QS	0.2-1 mm (coarse to medium)	Sand Schulz, Berlin
C	AS	0.2-0.63 mm (medium)	Field site A (Lower Saxony)
D1	AS	0.2-0.63 mm (medium)	Field site B (Saxony)
D2	AS	0.63 - 0.2 mm (fine)	Field site B (Saxony)
E1	GB	0.25-0.51 mm	Roth, Karlsruhe
E2	GB	0.75-0.1 mm	Roth, Karlsruhe

Table 2.1.: List of porous media used in column experiments. The list contains abbreviation, type of porous medium, grain size and supplier. Abbreviations: QS = Quartz sand, AS = Aquifer sample, GB = Glass beads

well into an aquifer with velocities larger than the background groundwater flow. Sketches of comparable experimental setups can be found in the literature (Bradford et al., 2002; Jiemvarangkul et al., 2011).
Samples at the column effluent were taken periodically every 10 – 15 min. Analysis of samples was performed using a Vario TOC select carbon analyzer by Elementar (Hanau, Germany) using a total carbon detection method with high temperature liquid combustion at 850° C and NDIR-photometer detection. Injection volume was set to 0.1 mL. Samples containing amounts of carbon above the detection range, as given in terms of maximum peak size by the manufacturer, were diluted with deionized water prior to analysis up to a factor of four.

2.3. Results and Discussion

2.3.1. Particle Characterization

The mean particle size using probe sonication was 2.4 µm and the surface area was measured to be 588 m^2/g. This particle size is at the upper end of the range that enables highest mobility in aquifers (Tufenkji and Elimelech, 2004). The difference in the size of the particle in comparison to studies by Bleyl et al. (2012) and Mackenzie et al. (2012), who reported a mean diameter of 0.8 µm, reflects variance in the current production process. Thus, the results following from this particle size will rather show the lower limit of the possible mobility,

and higher mobility and travel lengths might be feasible by fine tuning of this product to an optimized mean size. Since the production is based on crushed activated carbon, there will clearly be a considerable size range of colloid size. According to the work of Tufenkji and Elimelech (2004) the single collector contact efficiencies, and therefore the range of mobility, might be changing drastically by variations in size of particles, but the optimal size is depending on aquifer properties and other specific properties of the colloid such as specific weight. An experiment by Kim et al. (2008), could show a significant influence of particle size on transport of silica particles. In that study columns of 10 cm length and 3.5 cm diameter were filled with glass beads and colloids were pumped with a velocity of 5 m/h through the porous medium. The large surface area of c-nZVI can be attributed to the porosity of activated carbon. Activated carbon additionally provides a surface, which is favorable for contact with organic phases and might be able to absorb contaminants close to the reduction agent nZVI (Mackenzie et al., 2012).

2.3.2. Quality control and assurance of carbon analysis and column transport experiments

A method for detection of c-nZVI concentrations using carbon analysis was tested, and in the following passage standard quality control and assurance parameters are presented. A calibration series (n=8) using KHP as calibration standard yielded an R^2 = 0.99. The limit of detection (LOD) and quantification (LOQ) for the detection of carbon by means of blank plus three and ten times standard deviation was calculated to be 0.02 and 0.05 mg/L, respectively. A corresponding calibration series of c-nZVI was made using a background concentration of 200 mg/L of CMC, as used in the experiments for variation of physicochemical parameters. This calibration yielded R^2 = 0.98. The limit of detection and quantification of c-nZVI was calculated to be 2.01 (LOD) and 3.21 (LOQ) mg c-nZVI /L in the presence of 200 mg/L CMC. The upper detection limit was 630 mg c-nZVI in the presence of 200 mg/L CMC. A concentration of 60% carbon in the colloid was found (by comparison of the calibration of carbon in KHP and c-nZVI) and represents the expected amount of carbon in c-nZVI, which results from a nZVI content of 20% in the colloid, the mass of the oxide shell around the nZVI and production residuals, such as ash (Bleyl et

al., 2012). Reproducibility of measurements was examined by measuring one sample containing 100 mg c-nZVI/L eight times and standard deviation was 4.48%. Reproducibility of column experiments was examined by performing one experiment six times under identical experimental conditions (1000 mg/L c-nZVI, 200 mg/L CMC, sand B1). Standard deviation was calculated to be 14% by means of deviation of average breakthrough concentration of c-nZVI after ten exchanged pore volumes of a c-nZVI containing suspension (1000 mg/L c-nZVI, 200 mg/L CMC, sand B1, see Supporting Material).

2.3.3. Electrostatic potential of c-nZVI suspensions

Zeta potential was measured in the presence of different amounts of CMC (see Fig. 2.1). Standard deviations of measurements were 0.50 – 5.53 mV, with an average deviation of 1.4 mV and a median value of 0.89 mV standard deviation (See Supporting Material). Without addition of CMC zeta potential of the suspension is in a very low negative range of around -6 mV and decreases with addition of CMC. Zeta potential exceeds 30 mV using 5% CMC in relation to c-nZVI and grows with additional CMC to more than -50 mV with a content of 40% CMC. According to ISO 14887:2000, zeta potentials above 30 mV and below 30 mV are defined as threshold for a sufficient electrostatic stabilization (International Organization for Standardization, 2010). For transport in porous media a high absolute value of the zeta potential is favorable, since electrostatic repulsion decreases the chance for attachment between particle and porous medium. The results will be discussed later (see sections 3.5 and 3.6) together with results from transport experiments using different amounts of CMC. Zeta potential of c-nZVI has been observed without addition of CMC as a function of pH with a point of zero charge at pH 6.2 and increasing trend with higher pH values. This results in a zeta potential of less than -30 mV at measurements above pH 10 (Mackenzie et al., 2012).

2.3.4. Stability of a c-nZVI suspension

Stability of a suspension was examined by observing carbon content in an unmoved suspension for 11 h. After subtraction of the background carbon concentration, caused by 200 mg/L CMC, a decreasing carbon concentration

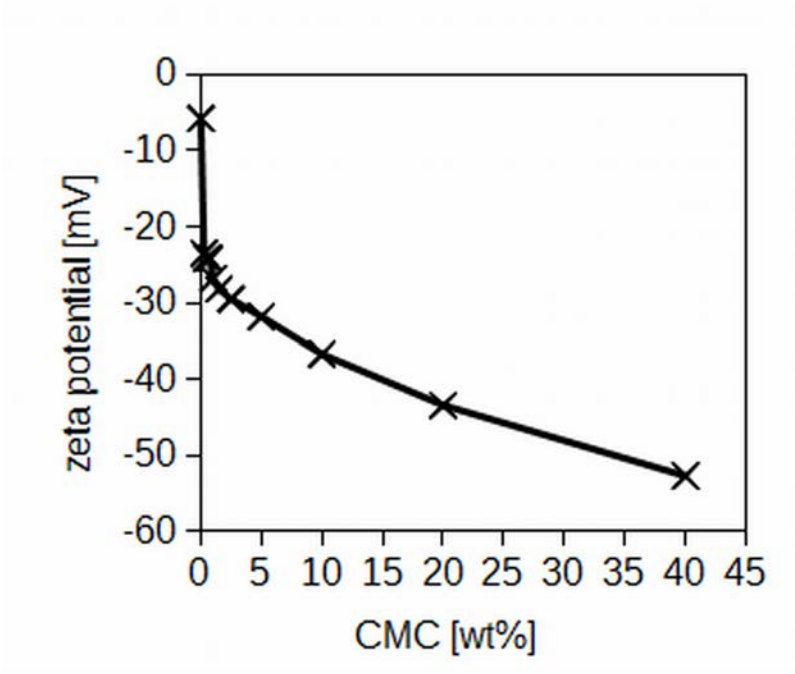

Figure 2.1.: Zeta potential of c-nZVI suspension in the presence of different amounts of CMC. The amount of CMC is described as percentual content related to the c-nZVI Content of 100 mg/L. Average standard deviation is 1.43 mV (See Supporting Material). The experiment was performed at pH 10.

over time was observed for unstabilized and stabilized c-nZVI (see Fig. 2.2). In the experiment without addition of CMC, the carbon concentration fell to 27% of the initial concentration within 12 min, to 10% within 1 h and to 5% within 2 h. In the experiment with addition of 200 mg/L CMC, a decrease of carbon concentration to 76% was observed within 25 min from the initial concentration. Within 1 h the carbon concentration decreases to 65% and within 2 h to 60% of the initial concentration. During the remaining time of the experiment the carbon concentration approaches a carbon concentration of 40% after 11 h in comparison to the initial concentration.
Data from this experiment suggest three things: At first, addition of a polyanionic stabilizer decreases sedimentation rates of c-nZVI, compared to a colloid without stabilizer. Sedimentation rates of 2.5 cm/min for unstabilized c-nZVI and 0.046 cm/min for stabilized c-nZVI were calculated according to the Stokes law. This is a factor of 50 between the sedimentation rates of unstabilized and

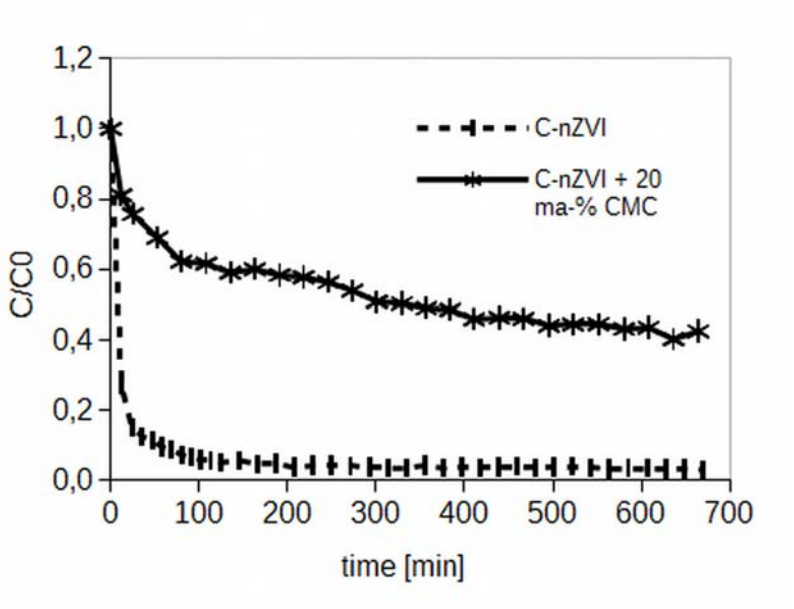

Figure 2.2.: Relative c-nZVI concentration in a sedimentation experiment in dependence to time after the beginning of the experiment. The experiment was performed once without a polyanionic stabilizer and once using a background concentration of 200 mg/L of CMC and contained 1000 mg/L c-nZVI. Duplicates are not presented.

stabilized colloids. Bleyl (2013) calculated a theoretical sedimentation rate of 0.17 cm/h for c-nZVI with a mean diameter of 0.8 µm, but already mentioned the effect of agglomeration on sedimentation speed. The second result is, without stabilization the colloids are not stable in suspension and with addition of a stabilizer, there is still a fraction of particles that are not stable in the suspension and sediments within less than 1 h. This fraction can be found after the experiment as film on the ground of the storage bottle of the stock suspension. Therefore, this fraction will most likely be not mobile in the subsequent following column transport experiment, since agglomeration and gravity will immobilize this fraction within endurance of the transport experiment. The third suggestion following from that is the existence of a rather stable fraction of particles which remain stable in an unmoved suspension for at least 11 h. This stable fraction, which remains in suspension for longer than the duration of the transport experiment, should be mobile in column experiments using inert porous media, as long as no other effects on mobility prevent them from

being mobile. Stability of colloids in suspension is one of the major factors that limit mobility of colloids in porous media and fast aggregation of pure nZVI has been identified as one of the major challenges in *in situ* iron delivery (Phenrat et al., 2007). Nevertheless stability of c-nZVI as shown here is at the upper end of published data of stability, compared to other nZVI formulations (Phenrat et al., 2008; Phenrat et al., 2007). In these studies sedimentation was strongly depending on colloid concentration. Comparable concentrations of classical nZVI show a comparable sedimentation rate to unstabilized c-nZVI. Stabilized c-nZVI shows a slower sedimentation rate than surface modified nZVI.

2.3.5. Effect of a polyanionic stabilizer

A set of experiments was performed to investigate on the effect of a polyanionic stabilizer, here CMC, which aims to increase electrical charges at the surface of the particle. Defined amounts of CMC (0-100 mg/L; 0-20% related to the weight of c-nZVI) were added to a suspension of 500 mg c-nZVI/L and pumped through porous medium B1. Experiments show that concentrations at the column effluent are 36% in both experiments after ten exchanged pore volumes, relative to the injection concentration using 10% or 20% CMC. The addition of 2.5% and 5% CMC shows a breakthrough of 30% and 2% after ten exchanged pore volumes. Compared to the reproducibility experiment done with 20% CMC (n=6), at CMC concentrations of 2.5% or lower the concentration was more than two standard deviations lower than the mean breakthrough level of the breakthrough reproducibility experiment with 20% CMC. Without addition of CMC no breakthrough was observed. The slope of the breakthrough curves for suspensions containing any concentration of CMC are similar for all samples for the first three pore volumes: After the first exchanged pore volume breakthrough of particles begins and rises for two more exchanged pore volumes. After the third exchanged pore volume the characteristic of the shape of breakthrough curves vary: The breakthrough concentration of the suspension containing 0.5% CMC decreases after the third exchanged pore volume, and the breakthrough concentration of the suspension containing 1% CMC decreases after the fifth pore volume, while the breakthrough curves of higher concentrated suspensions stabilize on a slowly increasing trend. A

breakthrough experiment using 20% of CMC was extended to 25 exchanged pore volumes and a slightly increasing trend was observed during the whole time.

Transport and stability in porous media strongly depends on electrostatic properties of the porous media, colloids and additives. Adding a polyanionic stabilizer increases the negative zeta potential of the colloidal suspension, as shown before. The addition of CMC is often used in laboratory (He et al., 2009; He et al., 2007) and field experiments (Bennett et al., 2010; He et al., 2010) for enhancing transport of nZVI by increasing the negative zeta potential and therefore increasing electrostatic repulsion between particles among each other and among the porous medium (Phenrat et al., 2008). In Fig. 2.1, a dataset showing zeta potential in relation to CMC content is presented: With addition of CMC zeta potential decreases and therefore increases the potential mobility of c-nZVI, which supports the observation of increased transport with increased CMC content (Fig. 2.3). There are several polyanionic stabilizers available and generally dissolved organic material has a positive impact on colloid stability and mobility (Aiken et al., 2011). Transport can be reduced by high ionic strength and low pH (see sections 3.8 and 3.9); therefore it seems to be adequate to provide CMC exceeding the necessary amount of 10% in relation to c-nZVI concentration to achieve the highest mobility in practical applications. Therefore in following experiments 20% of CMC compared to the amount of c-nZVI was used. The Advantages of CMC as a polyanionic stabilizer are easy availability, cost efficiency and environmental compatibility.

2.3.6. Change of particle properties during transport in a column experiment

An additional experiment was performed under equal conditions as in the set of experiments before (see section 3.5) to observe changes in particle size distribution and zeta potential within a column experiment. Zeta potential was detected from a sample containing 20% CMC in relation to c-nZVI content before injection at a level of -60 mV and after breakthrough at a level of -75 to -80 mV. Therefore, measured zeta potential decreases during the experiment. Additional to that, sizes of particles were detected before and after the column experiment (see Fig. 2.4).

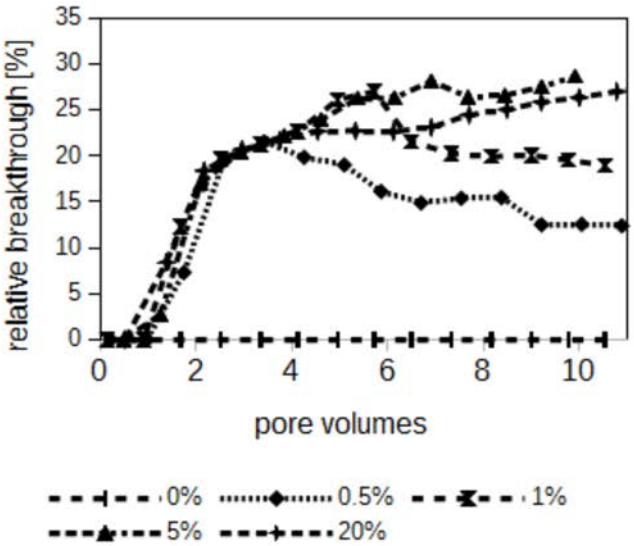

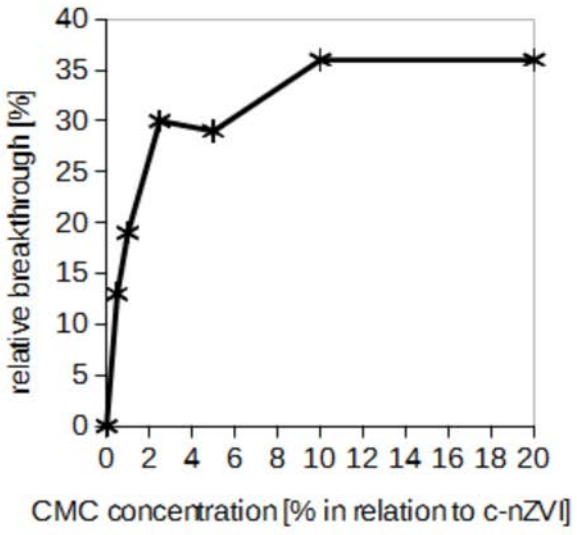

Figure 2.3.: Panel a shows four selected breakthrough curves for a c-nZVI (500 mg/L) suspension containing different amounts of CMC (0, 0.5, 1, 5, and 20% related to 500 mg/l c-nZVI). Panel b shows breakthrough level of c-nZVI after ten exchanged pore volumes of c-nZVI (500 mg/L) in porous medium B1 in relation to the addition of the polyanionic stabilizer CMC.

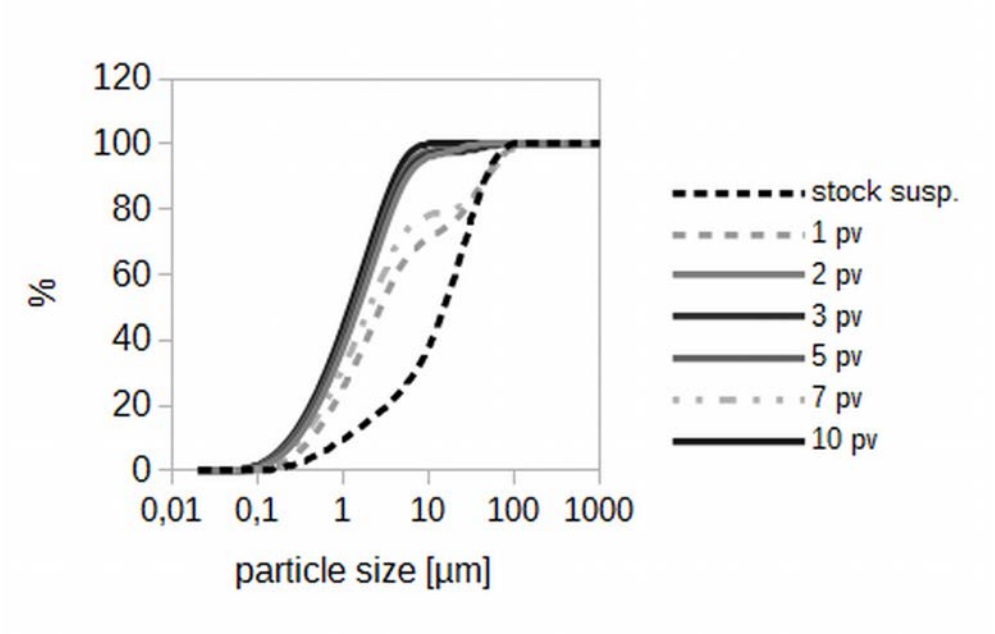

Figure 2.4.: Particle size distribution of a c-nZVI suspension of a sample from the storage tank, before injection, and samples taken from the column outlet. The sample from the storage tank represents 100% of the concentration, while the samples taken after one and two pore volumes represent a concentration of 8% and 18% at this time in the outflow, and the other samples represent 25 – 36% of the injected concentration.

Samples were taken from the storage tank and after the column after 1 – 10 exchanged pore volumes, sampled to glass bottles and were sent via post to another laboratory for analysis. Samples were approximately one week old before measurements and injection into the static light scattering device. Therefore measured particle size reflects not only on the properties at the column outflow, but also on aggregation effects occurring after the column transport experiment, and moreover, suspensions used for the column experiment were prepared by a stirring dispersing machine (Ultra Turrax) and not by probe sonication (Branson sonifier). See recent studies by Meissner et al. (2014) or Misra et al. (2012) for more information. So, particle size distribution of c-nZVI from the storage tank and subsequently after exchanged pore volumes might be larger from the beginning. For this reason we assume the result only to be correct relatively to each other, nevertheless it might give a hint on filtration

processes in the column. The sample taken from the storage tank showed a mean particle size of 15 µm in terms of mass distribution, a sample from the outflow of the column taken from the first to second exchanged pore volume was 3 µm in size and later taken samples (from two to ten exchanged pore volumes) were between 1 µm in size, except one sample taken after 7 pore volumes with 2 µm size, which might be an outlier. These results suggest a fractionation of particles during the experiment: The decreasing zeta potential might result from higher relative CMC amounts in the suspension per c-NZVI particle, since only one third of the injected c-nZVI reaches the end of the column. The increased amount of CMC adsorbs on c-nZVI, resulting in a decrease of the zeta potential. Smaller mean particle sizes after the column experiment might be explainable by a physical filtration of bigger particles, according to filtration theory (Brant et al., 2007; Tufenkji and Elimelech, 2004; Tufenkji and Elimelech, 2005). Therefore the smaller fraction of particles might travel better than the bigger sized fraction and reaches the end of the column. This can be supported by a visual observation of sedimentation in the first 5 cm of a column, by a changing color from sand colored to black. Therefore estimations of distribution ranges should take a strong straining in the beginning into account. A strong straining in the beginning of a column experiment has been observed before for other particles (Bradford et al., 2002).

2.3.7. Effect of porous media

All experiments with different porous media (Tab. 1) were performed with C_0 = 500 mg/L nZVI and 100 mg/L CMC. Breakthrough curves are shown in Fig. 2.5. Relative concentrations at the column effluent after 10 pore volumes are between 23% (porous medium D1) and 62% (C1) compared to the injected concentration.

Soil characteristics have a clear influence on the mobility of particles. Size, shape, surface, organic content, pore geometry, and electrostatic properties of the porous media can influence colloid behavior. Due to increased surface area and depositional sites (Mattison et al., 2011), it is reasonable to see an effect of porous medium grain size on the breakthrough of c-nZVI. Comparison of two sizes of glass beads (porous media E) and two size fractions of porous media (B and D) shows this effect under the assumption that other characteristics within

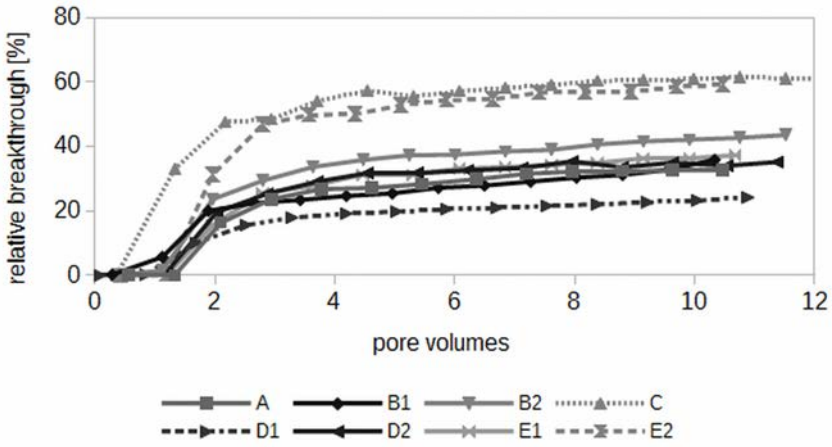

Figure 2.5.: Breakthrough curves for c-nZVI in different porous media under identical experimental conditions (500 mg/L c-nZVI, 100 mg/L CMC. Used sand types are quartz sand (A: 1-2mm grain size, B1: 0.1-0.5, B2:0.2-1) Aquifer samples (C: 0.2-0.63, D1: 0.2-0.63, D2: 0.63-2) and glass beads (E1: 0.25-0.51, E2 0.75-1mm, see table 1 for detailed information). Sand "B1" is the same sample as sample "20%" in Fig. 2.3.

the porous media are equal. The difference in breakthrough maxima after ten exchanged pore volumes between smaller and coarser grained fractions of the sand is 10% absolute and the difference between the glass beads is 20% absolute.

Another effect which might be observable in the experiments here might be the influence of porous medium shapes. While glass beads (E) and sand C have a smooth surface and round shape, the other porous media (A, B and D) exhibit a rough surface and are rather edgy than roundly shaped. Increased retention due to an edgy shape of grain might explain most of the differences observed here for similar grain sizes. Surface roughness and heterogeneity have already been investigated and found to be relevant for deposition and transport of colloids (Shellenberger and Logan, 2002). Noticeable differences of breakthrough maxima in different porous media have already been observed for other particles (He et al., 2009). Results from all sands show a slight increase in the slope of the breakthrough curve after the third exchanged pore volume until the end of the experiments, without reaching a steady state plateau level.

This has been observed before in column experiments using microspheres (Bradford and Bettahar, 2006) and CMC-stabilized nZVI (Raychoudhury et al., 2012). In the first study asymmetric breakthrough curves are explained to origin from aggregation and filtration and in the second study the continuous increasing breakthrough curve was explained to origin from detachment of colloids from the porous medium, rather than from changes in the flow regime by aggregation and blocking of pores.

2.3.8. Effect of ionic strength

A next set of experiments was performed to investigate the effects of ionic strength. Defined concentrations of NaCl (0 – 400 mM/L) and $CaCl_2$ (0-200 mM/L) were added to a suspension of 1000 mg/L c-nZVI and 200 mg/L CMC. The injection was pumped through porous medium B1. Figures 2.6 and 2.7 show the corresponding breakthrough curves. In the presence of NaCl the relative breakthrough maximum concentration of c-nZVI after ten exchanged pore volumes is between 25% and 38% in comparison to the input concentration. At 200 and 400 mM/L ionic strength of NaCl the breakthrough decreases at higher ionic strength in comparison to lower concentrations. In the presence of CaCl2 the relative breakthrough of c-nZVI after ten exchanged pore volumes is between 2.3% and 33%, respectively, in comparison to the input concentration. The breakthrough decreases at concentrations higher than 0.5 mM/L $CaCl_2$ and decreases more with growing ionic strength. At 200 mM/L ionic strength the breakthrough increases for the first three pore volumes up to 5% and then decreases again, as already observed in section 3.7 for low pH conditions.
Ionic strength shows an influence on the transport of c-nZVI. In suspensions containing high ionic strengths mobility of c-nZVI decreases. This decrease happens in suspensions containing divalent ions (Ca^{2+}) stronger than in suspensions containing monovalent ions (Na^{+}). Higher effects of divalent ions in the order of one to two magnitudes have been reported, e.g. the effect of KCl and $CaCl_2$ on breakthrough behavior of hydroxyapatite (Wang et al., 2011). Decreasing surface charges of colloids have been observed with increasing ionic strengths of NaCl (Tiraferri et al., 2011) and have been attributed to bivalent cations (Ryan et al., 1999) before. This mechanism might explain the decrease in mobility here. A general review on that topic is available (Petosa et al., 2010).

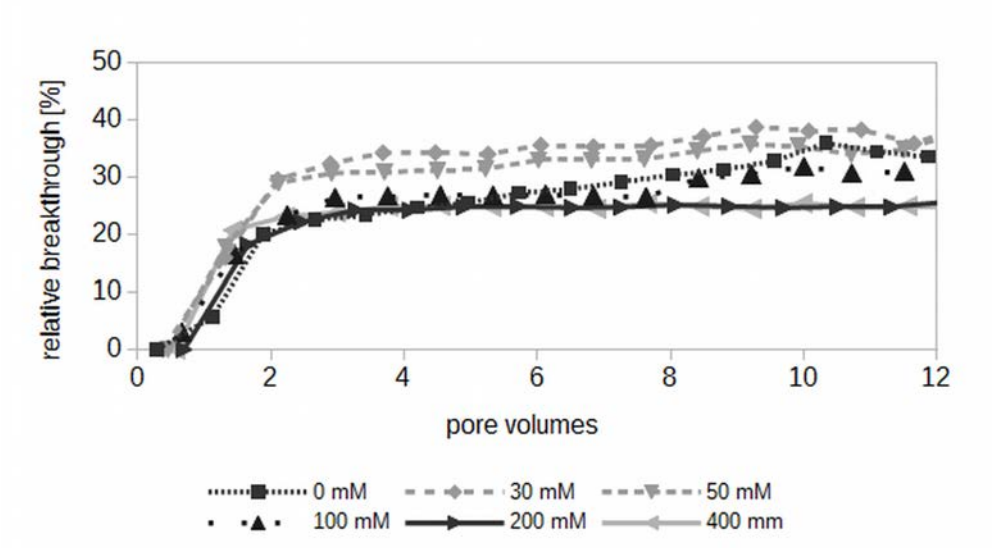

Figure 2.6.: Breakthrough curves of c-nZVI (1000 mg/L) with a background concentration of CMC (200 mg/L) in the presence of different amounts of NaCl. Sample "0 mM" equals sample "20%" in Fig. 2.3, and "B1" in Fig. 2.5.

In the literature 2 mM of Ca^{2+} and 10 mM of Na^{+} are assumed to be a natural background concentrations for groundwater in literature (Tiraferri and Sethi, 2009) and do not have a negative effects on transport. These concentrations might vary regionally, and in contaminated aquifers the salinity might be higher.

2.3.9. Effect of pH

A set of experiments was performed to investigate on the effects of pH on the breakthrough by adjusting pH in a suspension containing 1000 mg c-nZVI/L and 200 mg/L CMC to values between 4 and 12. The pH of a suspension prepared without an additional acid or a base is 10.4. Results show breakthrough maximum between 8% and 34% in porous medium B1. At a pH of 4 the smallest breakthrough maximum compared to higher pH values was observed. At pH values of six or higher, no statistical significant trend in respect to pH could be observed. The pH was monitored in the storage tank and in the column effluent. It was observed that pH increases within 2 h from pH 4 to 6 and from pH 6 to 7 in the storage tank. The same increased pH value was found at the

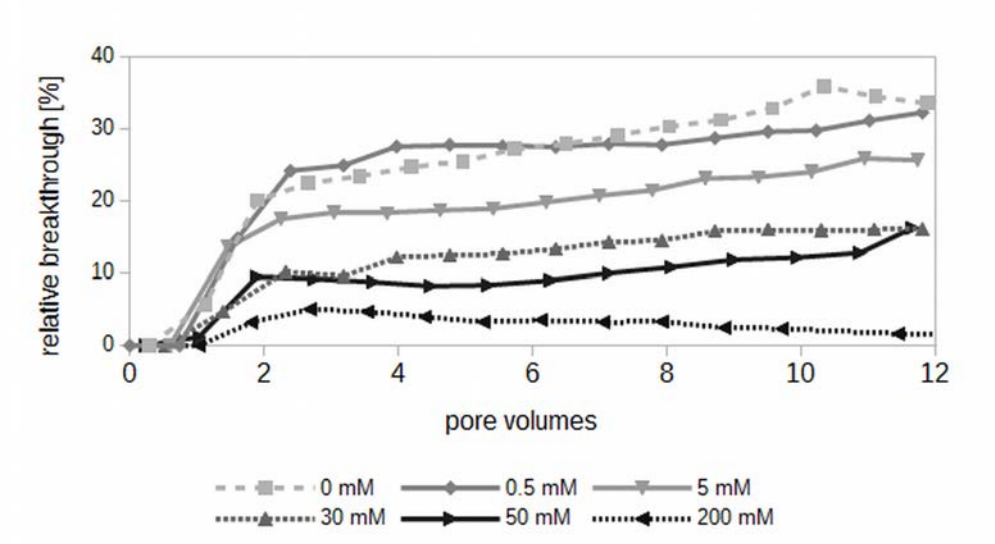

Figure 2.7.: Breakthrough curves of c-nZVI (1000 mg/L) with a background concentration of CMC (200 mg/L) in the presence of different amounts of $CaCl_2$. Sample "0 mM" equals sample "0 mM" in Fig. 2.6, "20%" in Fig. 2.3, and "B1" in Fig. 2.5.

end of the column.

The influence of pH on transport of c-nZVI is only substantial at low pH values of the suspension. The point of zero-charge for pure nZVI is at pH 5-6 (Nyer and Vance, 2001) and for activated carbon around 8 (Noh and Schwarz, 1990). Above these pH levels the expected surface charge is negative, and therefore electrostatic repulsion forces can stabilize particles. The addition of CMC increases zeta potential for c-nZVI, which leads to additional stability. A similar result has been observed for CMC-stabilized ZnO-nanoparticles before (Kanel and Al-Abed, 2011). Generally, a pH of 5 can be assumed to be the lower limitation for effective particle transport in porous media (Ryan and Elimelech, 1996; Zhou et al., 2011), because colloids and aquifer material reach an uncharged state, by means of a negligible or positive zeta potential at this pH value. An additional explanation for a decreasing breakthrough after an initial breakthrough maximum after two exchanged pore volumes under unfavorable transport conditions might be colloid agglomerations which block the pore space for colloid transport at all. Nevertheless, the pH in a c-nZVI-suspension tends to be around 10.4 and suspensions which were adjusted to lower pH

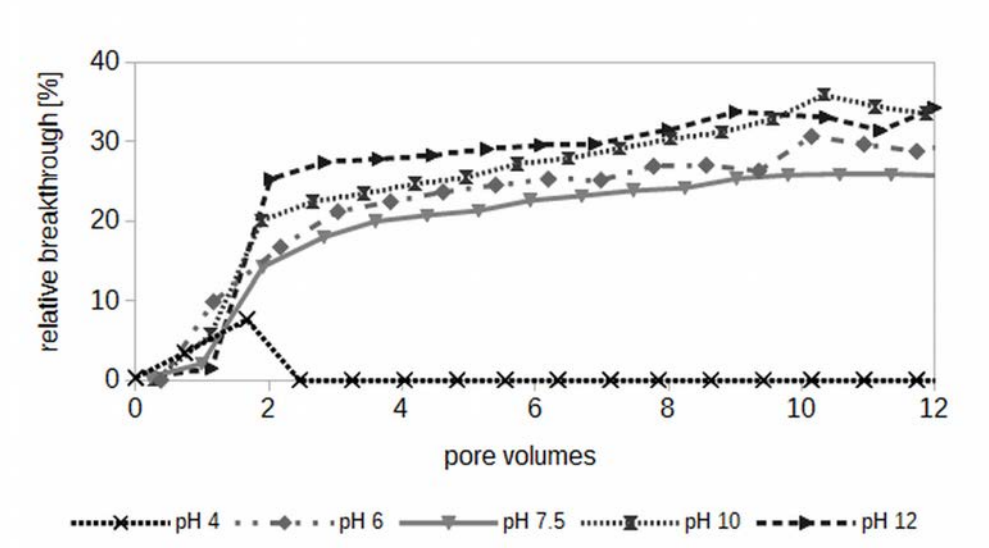

Figure 2.8.: Breakthrough curves of c-nZVI (1000mg/L) with a background concentration of CMC (200 mg/L) in porous medium B1 at different pH values. Sample "pH 10" equals sample "0 mM" in Fig. 2.5 and 2.6, "20%" in Fig. 2.3, and "B1" in Fig. 2.5.

increase their pH with time. For lower pH values the increasing pH can be interpreted as reaction of nZVI with acid, since iron generated hydroxyls (OH^-) react with hydronium (H_3O^+) (Nyer and Vance, 2001). A reaction with oxygen is rather unlikely, since oxygen was purged in the beginning.

2.3.10. General discussion and conclusion

It is difficult to transfer results from column tests to aquifer systems, for results from column tests can vary drastically by settings of boundary conditions and experimental setup, such as the selection of column size, porous media or injection speed. Several more parameters than the ones tested have an influence on colloid transport, such as injection speed (Chowdhury et al., 2011; Espinasse et al., 2007; He et al., 2009) and particle concentration (Bradford and Bettahar, 2006; Chowdhury et al., 2011; Liu et al., 1995). Furthermore we expect c-nZVI not to follow a linear function of particle attachment with transport distance in porous media, but a strong straining in the beginning and after that a rater equal particle attachment distribution to the porous media. In our experiments a relative breakthrough maximum of 23 - 62% after ten

exchanged pore volumes was observed in 40 cm long columns, which suggests possible transport ranges of several meters. Filtration coefficients suggest a transport range of 3.1 - 4.1 m at a filtration rate of 99%, or 7.7 - 8.7 m at 99.99% filtration level. Transport ranges calculated for polyanionic stabilized nZVI have been published in ranges from few centimeters (Schrick et al., 2004) to 1 or 2 m at 99.99% filtration level (Laumann et al., 2013; Tiraferri and Sethi, 2009), or up to more than 100 m for preselected particles (Saleh et al., 2008). Though a field injection set-up still needs to be designed in detail, the concept of c-nZVI already shows promising characteristics to be applied in the field and to achieve a substantial distribution of nZVI of several meters of distance around the injection well *in situ*. However in evaluating optimal particle size for individual applications economic considerations of production might have an influence as well. Given that, the general concept of c-nZVI, seems to be an approach suited for efficient iron delivery. Future research will focus on a larger scale of transport experiments with observations in a 2D-laboratory-aquifer experiment, comparable to other nZVI studies (Kanel et al., 2008; Loveland et al., 2003). Additional future research should take a closer look on optimal particle size of this material and experiments in the field should be performed to aim for *in situ* generated data on the feasibility and design of this technology.

2.4. Acknowledgments

This study was supported by the German Ministry for Education and Research (Bundesministerium für Bildung und Forschung, BMBF) in the project Fe-NANOSIT (Iron based nanoparticles and nano-composite structures for remediation of ground- and wastewater). We want to thank Stefan Scholz of the department of Bioanalytical Ecotoxicology and the staff of the department Environmental Engineering from the Helmholtz Centre for Environmental Research UFZ (Leipzig, Germany) for provision of particles and technical support.

2.5. Literature

Aiken, G.R., Hsu-Kim, H. and Ryan, J.N., 2011. Influence of Dissolved Organic Matter on the Environmental Fate of Metals, Nanoparticles, and Colloids. Environmental Science & Technology, 45(8): 3196-3201.

Bennett, P., He, F., Zhao, D.Y., Aiken, B. and Feldman, L., 2010. *In situ* testing of metallic iron nanoparticle mobility and reactivity in a shallow granular aquifer. Journal of Contaminant Hydrology, 116(1-4): 35-46.
Bleyl, S., Kopinke, F.-D., Georgi, A. and Mackenzie, K., 2013. Carbo-Iron – ein maßgeschneidertes Reagenz zur *in situ*-Grundwassersanierung. Carbo-Iron – A Tailored Reagent for *in situ* Groundwater Remediation. Chemie Ingenieur Technik, 85(8): 1302-1311.
Bleyl, S., Kopinke, F.-D. and Mackenzie, K., 2012. Carbo-Iron® Synthesis and stabilization of Fe(0)-doped colloidal activated carbon for *in situ* groundwater treatment. Chemical Engineering Journal, 191: 588-595.
Bradford, S.A. and Bettahar, M., 2006. Concentration dependent transport of colloids in saturated porous media. Journal of Contaminant Hydrology, 82(1-2): 99-117.
Bradford, S.A., Yates, S.R., Bettahar, M. and Simunek, J., 2002. Physical factors affecting the transport and fate of colloids in saturated porous media. Water Resources Research, 38(12).
Brant, J., Labille, J., Bottero, J.Y. and Wiesner, M.R., 2007. Nanoparticle Transport, Aggregation, and Deposition. In: M.R. Wiesner and J.Y. Bottero (Editors), Environmental Nanotechnology: Applications and Impacts of Nanomaterials. The McGraw-Hill Companies, Wiesner, M.R., Bottero, J.-Y., 2007. Environmental Nanotechnology: Applications and Impacts of Nanomaterials. The McGraw-Hill Companies, New York, Chicago, San Francisco, Lisbon, London, Madrid, Mexico City, Milan, New Delhi, San Juan, Seoul, Singapore, Sydney, Toronto.
Cai, Z.S., Thomson, N.R., Wilson, R.D. and Oswald, S.E., 2006. A lumped parameter approach to model the treatment of organic contaminants by a granular iron filled fracture. Advances in Water Resources, 29(4): 624-638. Chowdhury, I., Hong, Y., Honda, R.J. and Walker, S.L., 2011. Mechanisms of TiO(2) nanoparticle transport in porous media: Role of solution chemistry, nanoparticle concentration, and flowrate. Journal of Colloid and Interface Science, 360(2): 548-555.
Comba, S., Di Molfetta, A. and Sethi, R., 2011. A Comparison Between Field Applications of Nano-, Micro-, and Millimetric Zero-Valent Iron for the Remediation of Contaminated Aquifers. Water Air and Soil Pollution, 215(1-4): 595-607.
Crane, R.A. and Scott, T.B., 2012. Nanoscale zero-valent iron: Future prospects for an emerging water treatment technology. Journal of Hazardous Materials, 211–212(0): 112-125.
Espinasse, B., Hotze, E.M. and Wiesner, M.R., 2007. Transport and Retention of Colloidal Aggregates of C60 in Porous Media: Effects of Organic Macromolecules, Ionic Composition, and Preparation Method. Environmental Science & Technology, 41(21): 7396-7402.
Gillham, R.W. and O'Hannesin, S.F., 1994. Enhanced Degradation of Halogenated Aliphatics by Zero-Valent Iron. Ground Water, 32(6): 958-967.
Grieger, K.D. et al., 2010. Environmental benefits and risks of zero-valent iron nanoparticles (nZVI) for *in situ* remediation: Risk mitigation or trade-off? Journal of Contaminant Hydrology, 118(3-4): 165-183.
He, F., Zhang, M., Qian, T. and Zhao, D., 2009. Transport of carboxymethyl cellulose stabilized iron nanoparticles in porous media: Column experiments and modeling. Journal of Colloid and Interface Science, 334(1): 96-102.
He, F., Zhao, D., Liu, J. and Roberts, C.B., 2007. Stabilization of Fe-Pd nanoparticles with sodium carboxymethyl cellulose for enhanced transport and dechlorination of trichloroethylene in soil and groundwater. Industrial & Engineering Chemistry Re-

search, 46(1): 29-34.
He, F., Zhao, D. and Paul, C., 2010. Field assessment of carboxymethyl cellulose stabilized iron nanoparticles for *in situ* destruction of chlorinated solvents in source zones. Water Research, 44(7): 2360-2370.
Hoch, L.B. et al., 2008. Carbothermal synthesis of carbon-supported nanoscale zero-valent iron particles for the remediation of hexavalent chromium. Environmental Science & Technology, 42(7): 2600-2605.
International Organization for Standardization, 2010. ISO 14887:2000. Sample preparation - dispersing procedures for powders in liquids.
Jiemvarangkul, P., Zhang, W.X. and Lien, H.L., 2011. Enhanced transport of polyelectrolyte stabilized nanoscale zero-valent iron (nZVI) in porous media. Chemical Engineering Journal, 170(2-3): 482-491.
Johnson, R.L. et al., 2013. Field-Scale Transport and Transformation of Carboxymethylcellulose Stabilized Nano Zero-Valent Iron. Environmental Science & Technology, 47(3): 1573-1580.
Joo, S.H. and Cheng, I.F., 2006. Literature Review, Nanotechnology for Environmental Remediation. Modern Inorganic Chemistry. Springer New York, pp. 5-23.
Kanel, S.R. and Al-Abed, S.R., 2011. Influence of pH on the transport of nanoscale zinc oxide in saturated porous media. Journal of Nanoparticle Research, 13(9): 4035-4047.
Kanel, S.R., Goswami, R.R., Clement, T.P., Barnett, M.O. and Zhao, D., 2008. Two dimensional transport characteristics of surface stabilized zero-valent iron nanoparticles in porous media. Environmental Science & Technology, 42(3): 896-900.
Kim, H.-J., Phenrat, T., Tilton, R.D. and Lowry, G.V., 2009. Fe0 Nanoparticles Remain Mobile in Porous Media after Aging Due to Slow Desorption of Polymeric Surface Modifiers. Environmental Science & Technology, 43(10): 3824-3830.
Kim, J., Nason, J.A. and Lawler, D.F., 2008. Influence of surface charge distributions and particle size distributions on particle attachment in granular media filtration. Environmental Science & Technology, 42(7): 2557-2562.
Laumann, S., Micić, V., Lowry, G.V. and Hofmann, T., 2013. Carbonate minerals in porous media decrease mobility of polyacrylic acid modified zero-valent iron nanoparticles used for groundwater remediation. Environmental Pollution, 179: 53-60.
Li, X.-q., Elliott, D.W. and Zhang, W.-x., 2006. Zero-valent iron nanoparticles for abatement of environmental pollutants: Materials and engineering aspects. Critical Reviews in Solid State and Materials Sciences, 31(4): 111-122.
Liu, D., Johnson, P.R. and Elimelech, M., 1995. Colloid deposition dynamics in flow-through porous media: role of electrolyte concentration. Environmental Science & Technology, 29(12): 2963-2973.
Loveland, J.P., Bhattacharjee, S., Ryan, J.N. and Elimelech, M., 2003. Colloid transport in a geochemically heterogeneous porous medium: aquifer tank experiment and modeling. Journal of Contaminant Hydrology, 65(3-4): 161-182.
Mackenzie, K., Bleyl, S., Georgi, A. and Kopinke, F.-D., 2012. Carbo-Iron An Fe/AC composite As alternative to nano-iron for groundwater treatment. Water Research, 46(12): 3817-3826.
Marcus, D.L. and Bonds, C., 1999. Results of the reactant sand-fracking pilot test and implications for the *in situ* remediation of chlorinated VOCs and metals in deep and fractured bedrock aquifers. Journal of Hazardous Materials, 68(1-2): 125-153.
Matheson, L.J. and Tratnyek, P.G., 1994. Reductive dehalogenation of chlorinated methanes by iron metal. Environmental Science & Technology, 28(12): 2045-2053.
Mattison, N.T., O'Carroll, D.M., Kerry Rowe, R. and Petersen, E.J., 2011. Impact of

Porous Media Grain Size on the Transport of Multi-walled Carbon Nanotubes. Environmental Science & Technology, 45(22): 9765-75.
Meissner, T., Oelschlägel, K. and Potthoff, A., 2014. Dispersion of nanomaterials used in toxicological studies: a comparison of sonication approaches demonstrated on TiO2 P25. Journal of Nanoparticle Research, 16(2): 1-13.
Misra, S.K., Dybowska, A., Berhanu, D., Luoma, S.N. and Valsami-Jones, E., 2012. The complexity of nanoparticle dissolution and its importance in nanotoxicological studies. Science of The Total Environment, 438(0): 225-232. Mueller, N.C. and Nowack, B., 2010. Nanoparticles for Remediation: Solving Big Problems with Little Particles. Elements, 6(6): 395-400.
Noh, J.S. and Schwarz, J.A., 1990. Effect of HNO3 treatment on the surface acidity of activated carbons. Carbon, 28(5): 675-682.
Nyer, E.K. and Vance, D.B., 2001. Nano-Scale Iron for Dehalogenation. Ground Water Monitoring & Remediation, 21(2): 41-46.
Petosa, A.R., Jaisi, D.P., Quevedo, I.R., Elimelech, M. and Tufenkji, N., 2010. Aggregation and Deposition of Engineered Nanomaterials in Aquatic Environments: Role of Physicochemical Interactions. Environmental Science & Technology, 44(17): 6532-6549.
Phenrat, T. et al., 2008. Stabilization of aqueous nanoscale zerovalent iron dispersions by anionic polyelectrolytes: adsorbed anionic polyelectrolyte layer properties and their effect on aggregation and sedimentation. Journal of Nanoparticle Research, 10(5): 795-814.
Phenrat, T., Saleh, N., Sirk, K., Tilton, R.D. and Lowry, G.V., 2007. Aggregation and sedimentation of aqueous nanoscale zerovalent iron dispersions. Environmental Science & Technology, 41(1): 284-290.
Quinn, J. et al., 2005. Field Demonstration of DNAPL Dehalogenation Using Emulsified Zero-Valent Iron. Environmental Science & Technology, 39(5): 1309-1318.
Raychoudhury, T., Tufenkji, N. and Ghoshal, S., 2012. Aggregation and deposition kinetics of carboxymethyl cellulose-modified zero-valent iron nanoparticles in porous media. Water Research, 46(6): 1735-1744.
Ryan, J.N. and Elimelech, M., 1996. Colloid mobilization and transport in groundwater. Colloids and Surfaces a-Physicochemical and Engineering Aspects, 107: 1-56.
Ryan, J.N., Elimelech, M., Ard, R.A., Harvey, R.W. and Johnson, P.R., 1999. Bacteriophage PRD1 and silica colloid transport and recovery in an iron oxide-coated sand aquifer. Environmental Science & Technology, 33(1).
Saleh, N. et al., 2008. Ionic strength and composition affect the mobility of surface-modified Fe-0 nanoparticles in water-saturated sand columns. Environmental Science & Technology, 42(9): 3349-3355.
Savage, N. and Diallo, M.S., 2005. Nanomaterials and water purification: Opportunities and challenges. Journal of Nanoparticle Research, 7(4-5): 331-342.
Schrick, B., Hydutsky, B.W., Blough, J.L. and Mallouk, T.E., 2004. Delivery vehicles for zerovalent metal nanoparticles in soil and groundwater. Chemistry of Materials, 16(11): 2187-2193.
Sellers, K. et al., 2008. Nanotechnology and the Environment. Taylor & Francis, Boca Raton. Shellenberger, K. and Logan, B.E., 2002. Effect of molecular scale roughness of glass beads on colloidal and bacterial deposition. Environmental Science & Technology, 36(2): 184-189.
Solovitch, N. et al., 2010. Concurrent Aggregation and Deposition of TiO2 Nanoparticles in a Sandy Porous Media. Environmental Science & Technology, 44(13): 4897-4902.
Sunkara, B. et al., 2010. Nanoscale Zerovalent Iron Supported on Uniform Carbon

Microspheres for the *in situ* Remediation of Chlorinated Hydrocarbons. Acs Applied Materials & Interfaces, 2(10): 2854-2862.
Sunkara, B. et al., 2011. Modifying Metal Nanoparticle Placement on Carbon Supports Using an Aerosol-Based Process, with Application to the Environmental Remediation of Chlorinated Hydrocarbons. Langmuir, 27(12): 7854-7859.
Tiraferri, A. and Sethi, R., 2009. Enhanced transport of zerovalent iron nanoparticles in saturated porous media by guar gum. Journal of Nanoparticle Research, 11(3): 635-645.
Tiraferri, A., Tosco, T. and Sethi, R., 2011. Transport and retention of microparticles in packed sand columns at low and intermediate ionic strengths: experiments and mathematical modeling. Environmental Earth Sciences, 63(4): 847-859.
Tufenkji, N. and Elimelech, M., 2004. Correlation equation for predicting single-collector efficiency in physicochemical filtration in saturated porous media. Environmental Science & Technology, 38(2): 529-536.
Tufenkiji, N. and Elimelech, M. 2005. Breakdown of Filtration Theory: Role of Secondary Energy Minimum and Surface Charge HEterogeneities. Langmuir, 21(3): 841-852.
Wang, D.J. et al., 2011. Transport behavior of humic acid-modified nano-hydroxyapatite in saturated packed column: Effects of Cu, ionic strength, and ionic composition. Journal of Colloid and Interface Science, 360(2): 398-407. Wiesner, M.R. and Bottero, J.-Y., 2007. Environmental Nanotechnology: Applications and Impacts of Nanomaterials. The McGraw-Hill Companies, New York, Chicago, San Francisco, Lisbon, London, Madrid, Mexico City, Milan, New Delhi, San Juan, Seoul, Singapore, Sydney, Toronto.
Yao, K.M., Habibian, M.M. and Omelia, C.R., 1971. Water and Wastewater Filtration - Concenpts and Applications. Environmental Science & Technology, 5(11): 1105.
Zhan, J.J. et al., 2011. Multifunctional Iron-Carbon Nanocomposites through an Aerosol-Based Process for the *in situ* Remediation of Chlorinated Hydrocarbons. Environmental Science & Technology, 45(5): 1949-1954
Zhang, H., Jin, Z.-h., Han, L. and Qin, C.-h., 2006. Synthesis of nanoscale zero-valent iron supported on exfoliated graphite for removal of nitrate. Transactions of Nonferrous Metals Society of China, 16(0): 345-349.
Zhang, W.X., 2003. Nanoscale iron particles for environmental remediation: An overview. Journal of Nanoparticle Research, 5(3-4): 323-332.
Zheng, T.H. et al., 2008. Reactivity characteristics of nanoscale zerovalent iron-silica composites for trichloroethylene remediation. Environmental Science & Technology, 42(12): 4494-4499.
Zhou, D.M., Wang, D.J., Cang, L., Hao, X.Z. and Chu, L.Y., 2011. Transport and re-entrainment of soil colloids in saturated packed column: effects of pH and ionic strength. Journal of Soils and Sediments, 11(3): 491-503.

3. Investigations on mobility of carbon colloid supported nanoscale zero-valent iron (nZVI) in a column experiment and a laboratory 2D-aquifer test system

Article published as J. Busch, T. Meißner, A. Potthoff & S.E. Oswald (2014): Investigations on mobility of carbon colloid supported nanoscale zero-valent iron (nZVI) in a column experiment and a laboratory 2D-aquifer test system Environmental Science & Pollution Research. (21): 10908-10916

3.0.1. Abstract

Nanoscale zerovalent-iron (nZVI) has recently gained great interest in the scientific community as in situ reagent for installation of permeable reactive barriers in aquifer systems, since nZVI is highly reactive with chlorinated compounds and may render them to harmless substances. However, nZVI has a high tendency to agglomerate and sediment; therefore it shows very limited transport ranges. One new approach to overcome the limited transport of nZVI in porous media is using a suited carrier colloid. In this study we tested mobility of a carbon colloid supported nZVI particle "Carbo-Iron Colloids" (CIC) with a mean size of 0.63 µm in a column experiment of 40 cm length and an experiment in a 2D-aquifer test system with dimensions of 110 x 40 x 5 cm. Results show a breakthrough maximum of 82% of the input concentration in the column experiment and 58% in the 2D-aquifer test system. Detected residuals in porous media suggest a strong particle deposition in the first centimeters and few deposition in the porous media in the further travel path. Overall, this suggests a high mobility in porous media which might be a significant enhancement compared to bare or polyanionic stabilized nZVI.

3.1. Introduction

Iron containing nanoparticles are currently under wide investigation to explore their potential for environmental remediation of chlorinated contaminants and heavy metals in soils and aquifers. Especially application of nanoscale zero-valent iron (nZVI) is seem to be a promising approach. This technology can be understood as enhancement of *in situ* permeable reactive barriers using zero-valent iron (ZVI) in granular form for remediation of chlorinated solvent plumes, which is an established technology for almost two decades. First experiments on chemical reduction of chlorinated compounds using ZVI have been published in the early 1990s (Gillham & O'Hannesin 1994, Matheson & Tratnyek 1994) and first field experiments were performed in the late 1990s (McMahon et al. 1999, O'Hannesin & Gillham 1998) are still state-of-the-art technology (Stroo & Ward 2010). These methods for groundwater remediation have shown limited cleaning effectiveness and are expensive (Mueller & Nowack 2010, Savage & Diallo 2005, Stroo 2010). They are not constructible under inaccessible areas. Injection of nZVI slurries into aquifer systems might be able to overcome the technical limitations of established ZVI methods, if they are able to form a permeable reactive barrier for remediation of chlorinated solvents *in situ* (Crane & Scott 2012). The process of reductive dehalogenation of chlorinated carbons follows mainly a beta-elimination pathway (Arnold & Roberts 2000), e. g. Trichlorethylene (TCE) can be reduced to acetylene (Lowry 2007). Additionally, due to surface size effects of nanostructures, the reactivity of nZVI is several orders of magnitude higher than the reactivity of granular ZVI (Mueller & Nowack 2010).

NZVI has been applied successfully to some degree in field experiments, but there is still limitations for its application (Comba et al. 2011). Currently the main limitation of nZVI is fast agglomeration and sedimentation (Phenrat et al. 2007), which results in limited mobility in laboratory (Johnson et al. 2013, Schrick et al. 2004) and in field experiments (He et al. 2010, Quinn et al. 2005). Therefore, remediation processes can only be observed maximally a few meters around the injection well (Zhang 2003), in the best case.

Current research on stabilization of nZVI in aqueous suspensions focuses on two approaches: One way is addition of polyanionic stabilizers, such as carboxymethylcellulose (CMC) (He et al. 2009, He et al. 2010), guar gum (Tiraferri

& Sethi 2009), polyvinyl alcohol-co-vinyl acetate-co-itaconic acid (PV3A), or poly(acrylic acid) (PAA) (Jiemvarangkul et al. 2011), aiming for electrostatic stabilization of colloids. Another approach is based on using a mobile carrier colloid as suggested by Schrick et al. (2004). Following this approach, a suited colloid has to deliver nZVI in a porous medium. Recent approaches are carrier particles made from silica (Zheng et al. 2008), carbon black (Hoch et al. 2008), graphite (Zhang et al. 2006), carbon microspheres (Sunkara et al. 2010, Sunkara et al. 2011, Zhan et al. 2011), or activated carbon (Bleyl et al. 2012, Mackenzie et al. 2012).

In this study we investigate on mobility of nZVI, which is loaded on an activated carbon colloid (Mackenzie et al. 2012). This composite material called "Carbo-Iron© colloids" (CIC) exhibits properties which are favorable for mobility in porous media because (I) the mean particle diameter is in the range for lowest deposition during transport, (II) the density is 1.7 g/cm³ and (III) the composite contains 10 – 25 wt% of nZVI. Production of the material is described in detail by Bleyl et al. (2012): Activated carbon colloids were impregnated with an iron salt, which was immobilized as iron oxide and hydroxide, and dried afterwards. The iron oxide clusters were thermally reduced to nanoscale zero-valent iron clusters of 50 nm size in the pore space of the activated carbon. In a previous study we investigated by column experiments the influence of physicochemical parameters on the mobility of a CIC with a size of 2.4 µm (Busch et al. 2014). In the present study we investigate on smaller sized CIC of 0.63 µm mean diameter. Firstly a sedimentation and column transport experiment is presented to show differences in transport behavior of different particle sizes. Secondly, CIC transport was observed in a 2D-aquifer test system, which includes the effects of lateral and transverse spreading. Quasi 2D laboratory systems can be useful as intermediate step between column experiments and field applications, with the advantage of coming close to real transport behavior, while allowing for detailed investigation and controlled conditions. They have been used for solute transport, reactive transport, two phase flow, and density driven flow, but rarely so far for particle transport. In this study we will present qualitative data on 2D distribution of CIC breakthrough. Furthermore, we will take a closer look on particle retention distribution within the column and the 2D-Aquifer test system and look on particle characteristics of suspensions before and after the 2D-transport experiment.

3.2. Materials and methods

Experiments were made to gain information on transport and retention of CIC. Aiming for that, several experiments have been performed: The first experiment is an experiment on colloid sedimentation in a static suspension. The second experiment is a column transport experiment with detection of a breakthrough curve and a subsequently following investigation on the distribution of particle deposition in the porous medium. The third experiment is an upscaled transport experiment in a 2D-aquifer tank.
Particles were characterized by using a Mastersizer 2000 (Malvern GmbH, Herrenberg, Germany) for detection of particle size distribution by static light scattering (SLS), an ASAP 2010 accelerated surface area and porosimetry analyzer (Micromeritics GmbH, Mönchengladbach, Germany) for measurement of specific surface area (BET method), and a Zetasizer Nano (Malvern GmbH, Herrenberg, Germany) for measurement of zeta potential. Samples for characterization of colloids were obtained by probe sonication using a Branson Sonifier 450 (Branson Ultrasonics Corporation, Danbury, CT, USA). Samples were measured immediately after preparation.
Suspensions for sedimentation and transport experiments were prepared following a previously used procedure (Busch et al. 2014): One litre of deionized water was purged by nitrogen for at least one hour, until oxygen was below detection limit. An amount of 200 mg/l carboxymethylcellulose (CMC) was added into the water for stabilization of colloids and suspended by sonication. Subsequent an amount of 1000 mg/L CIC was added under anaerobic conditions into the solution and dispersed for at least 30 min at 25,000 rpm using an Ultra Turrax (IKA, Staufen, Germany). During transport experiments the speed of the Ultra Turrax was kept at 10,000 rpm in the stock suspension aiming for a constant injection concentration.
For the sedimentation experiment, samples were taken from half height of the glass bottle to observe changes in particle concentration over time. Samples were taken periodically for the duration of two hours. Concentrations were calculated by measuring concentrations and subtracting the background carbon concentration caused by CMC and normalized compared to the initial CIC concentration (n = 3). Detailed information can be found in the previous study (Busch et al. 2014) and data from that study is presented for the sedimentation

and column experiment to evaluate effects of particle size.
For comparability of the experiments, the column experiment was performed using the same equipment and experimental setup as in previous experiments (Busch et al. 2014). Thus, a column of 40 cm length and 2 cm inner diameter (Carl Roth, Karlsruhe, Germany) was used and wet-filled with 125 mL of fine to medium sand (Sand Schulz, Berlin, Germany) to a porosity of 0.39. Sand had a size between 0.1 and 0.5 mm with a rough surface and edgy shape. A background concentration of 200 mg/L CMC was pumped for ten pore volumes before injection of the CIC-suspension to create a constant carbon background concentration. The suspension was pumped vertically against gravity using a speed of 3.4 mL/min. Samples were taken periodically every ten to fifteen minutes by the automatic sampling mechanism of the analyzer. Breakthrough was calculated by subtraction of background carbon concentration and normalization to the CIC concentration in the storage tank. CIC containing suspension was injected also for ten exchanged pore volumes and afterwards the column was flushed again with ten pore volumes of CMC containing background solution. Furthermore five liter of deionized water was pumped through the column to flush out CMC from the porous medium. After the column experiment the remaining water was removed from the column. The column was opened and twenty one samples were taken along the column and dried overnight at 104°C. Via detection of the carbon concentration in these samples it was possible to conclude on the CIC particles remaining in the porous medium.
The two dimensional aquifer test system was designed based on several examples of aquifer test systems reported in literature, e.g. Kanel et al. (2008), Loveland et al. (2003), Phenrat et al. (2010). The aquifer test system consisted of a rectangular container with an inner size of 100 cm length, 40 cm height and 5 cm depth. It was constructed (Polywerk Berlin, Berlin, Germany) to have seven ports on the right and on the left side of the tank for injection and outflow and a pressure release tube on the top of the tank. These ports are numbered from one to seven, with number one being the highest and seven the lowest position. Three porous media were tested (glass beads of 0.3 mm, fine sand of 0.2 mm grain size and coarse sand of 1 – 2 mm grain size). The container was filled with unwashed sand, closed and sand was compacted by vibration, which was performed several times until the container was completely filled

after vibration. The container was flooded by CO_2 and filled with deionized and deoxygenated water. A constant flow of 7.2 mL/min was fed to each port on the left side. After passing the porous medium the fluid left the container on the right side. One set of experiments was using brilliant blue FCF (CI 42090, Dynemic Products ltd., Ahmedabad, India) as ionic tracer because of its clear visibility and a high contrast to soils, low toxicity (food colorant) and weak adsorption in soils. FCF tracer solution was injected for thirty minutes and afterwards flushed with deionized water. Subsequently a following experiment was performed using a CIC-suspension. After CIC injection for 420 minutes the system was flushed with a background concentration of 200 mg/L CMC until no CIC was detected to leave the container anymore. Afterwards the container was flushed with 50 L of deionized water to remove remaining CMC. The container was opened and 69 sand samples were taken and dried at 104° C. Liquid samples from transport experiments were prepared for colloid size measurements by storage in glass bottles, in which they were diluted and measured using the static light scattering device (SLS) and its sonication bath. Samples were approximately two weeks old before measurement of colloid size.

Analysis of liquid samples for carbon concentration was performed using a Vario TOC select carbon analyzer (Elementar, Hanau, Germany) with a high temperature liquid combustion method was used. Details of this method is presented in (Busch et al. 2014). Liquid samples were taken from the column effluent by an automatic sampling system and directly analyzed. Carbon concentrations were measured by subtraction of background carbon concentration from the organic stabilizer CMC and were normalized to the CIC concentration in the stock suspension. CMC-colloid interactions are not considered in this study. CMC attaches to the surface of CIC to an extend of 7% of weight. Surplus CMC is in the liquid phase (Mackenzie et al. 2012). Solid samples were analyzed by weighing in 50 – 200 mg of a sample into a tin capsule. Samples were combusted at 950°C and detected the same way as the liquid samples using nondispersive infrared detection. A previous study investigated the attachment of nZVI to the active carbon carrier particle and showed that detection of carbon concentration directly reflects nZVI transport in column experiments (Mackenzie et al. 2012). Therefore carbon analysis should be sufficient in the experimental setup presented to conclude on CIC transport

including the nZVI part of it.

3.3. Results and Discussion

3.3.1. Particle characterization

Mean particle size, using probe sonication, was determined as 0.63 µm and the surface area was measured to be 600 m^2/g. A TEM bright-field image of thinly sliced CIC samples derived from 0.8 µm activated carbon colloids is shown in Bleyl et al. (2012) and in the supporting information of Mackenzie et al. (2012). In the latter article a microscope image of CIC is presented as well. In the Supporting Material (SM) of this study a SEM image of aged CIC is shown.

3.3.2. Quality assessment and control of analytical data

Experiments were performed to gain information on data quality of the analytical process. In both detection methods calibration with standards (Potassium hydrogen phtalate for liquid samples and standard soil containing 4.1% carbon for solid samples, both provided by Elementar, Hanau, Germany) and CIC reached a R^2 between 0.96 and 0.99 ($n > 5$). Limits of Detection (LOD) and Quantification (LOQ) were calculated by signal-to-noise of three and ten, respectively, and reached 0.02 and 0.05 mg/L C in liquid mode. LOD and LOQ for solid samples from the column experiment were calculated in mass carbon per mass of porous medium to be 0.01 and 0.03 mg/g and respectively 0.09 mg/g and 0.29 mg/g for samples from the 2D-aquifer experiment. Variations in LOD and LOQ result most likely from different sand types and applied cleaning process. Carbon content rates were determined to be 60% carbon in the colloid for liquid samples and 55% carbon from the colloid in solid samples. These recovery ranges are in the expected range given that in the activated carbon there are 20% nZVI and 20% non-carbonaceous material such as iron oxides and ash content (Bleyl et al. 2012). Reproducibility from column experiments is shown in the previous study. Here the column experiment was performed in duplicate and the deviation in the breakthrough maximum reached <1% only.

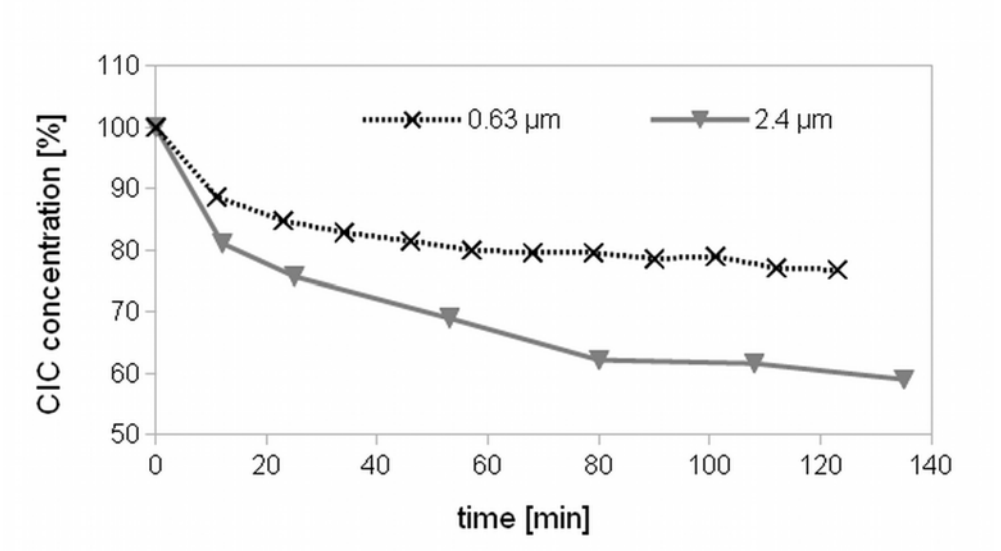

Figure 3.1.: Carbon content curve of a sedimentation experiment. 1000 mg/L CIC and 200 mg/L CMC were dispersed inside a glass bottle. CIC content in suspension is shown in relation to time and describes sedimentation of CIC. Data from 2.4 µm sized particles were taken from a previous study (Busch et al. 2014).

3.3.3. Sedimentation of Carbo-Iron Colloid suspension

Sedimentation in a suspension is a crucial point for injection into an aquifer system. Here CIC concentration was observed for two hours in an unmoved suspension (Fig. 3.1). Half an hour after start of the experiment 83% of the initial concentration remained in the suspension, after one hour the content of CIC had decreased to 80% and furthermore decreased to 77% after two hours, which is relatively stable for nZVI. Therefore, high amounts of CIC remain in suspension for the duration of the transport experiments presented here.
This experiment was performed to compare sedimentation of smaller sized CI colloids of 0.63 µm diameter to bigger sized CIC of 2.4 µm, used before (Busch et al. 2014). In that experiment the concentration of bigger sized CIC decreased within one hour to 65% and within two hours to 60% of the initial concentration, which is less than presented here for the smaller grained colloids, under exactly the same experimental conditions. This shows strong influence of colloid size for sedimentation, which might be explained by agglomeration and gravitational forces. A theoretical sedimentation rate of 0,03 cm/min

can be calculated here for the smaller sized colloids. Sedimentation rates of 2.5 cm/min for unstabilized CIC and 0.046 cm/min for stabilized CIC were calculated according to Stokes law previously for the bigger colloids (Busch et al. 2014). And Bleyl (2012) calculated a theoretical sedimentation rate of 0.17 cm/h for unstabilized CIC with a mean diameter of 0.8 µm, but already mentioned the effect of agglomeration on sedimentation speed. It is reasonable to assume changes of particle distribution characteristics to happen during the sedimentation process and affect sedimentation rates. Compared to sedimentation of pure nZVI and anionic polyelectrolyte stabilized nZVI (Phenrat et al. 2008, Phenrat et al. 2007) both tested sizes of CIC particle show slower sedimentation rates.

3.3.4. Column experiment

By the column experiment performed the breakthrough behavior and retention of CIC in in porous medium could be observed. Breakthrough of CIC started directly after the first pore volume exchanged, reaching 68% relative breakthrough concentration after two exchanged pore volumes, and a rather constant plateau of 78 – 82% after 3.5 exchanged pore volumes (Fig. 3.2). Injection of CIC was stopped after ten exchanged pore volumes, and switched to background solution, for ten more pore volumes. Within two exchanged pore volumes, the effluent concentration fell to 40% of the concentration injected before and after 20 exchanged pore volumes almost no more CIC was found in the effluent. In total 82% of the injected amount of 149 mg CIC was found in the effluent, indicating that less than 18% were retained in the porous medium. Mackenzie et al. (2012) performed a comparable experiment in quartz sand (0.25 – 0.5 mm grain size) and had a comparable, but slightly higher, breakthrough level for 0.8 µm sized CIC in a smaller column of 22 cm length and 1.2 cm diameter at 2 cm min^{-1} pore velocity.
For comparison, previous results made with CIC colloids of a size of 2.4 µm showed under equal conditions only a 36% breakthrough after ten exchanged pore volumes (shown is an average value resulting from six experiments. Having a breakthrough curve maximum of 82% for 0.64 µm sized colloids, the smaller sized CIC shows higher breakthrough than the bigger grained colloids. This result follows the logic of filtration theory which states that here

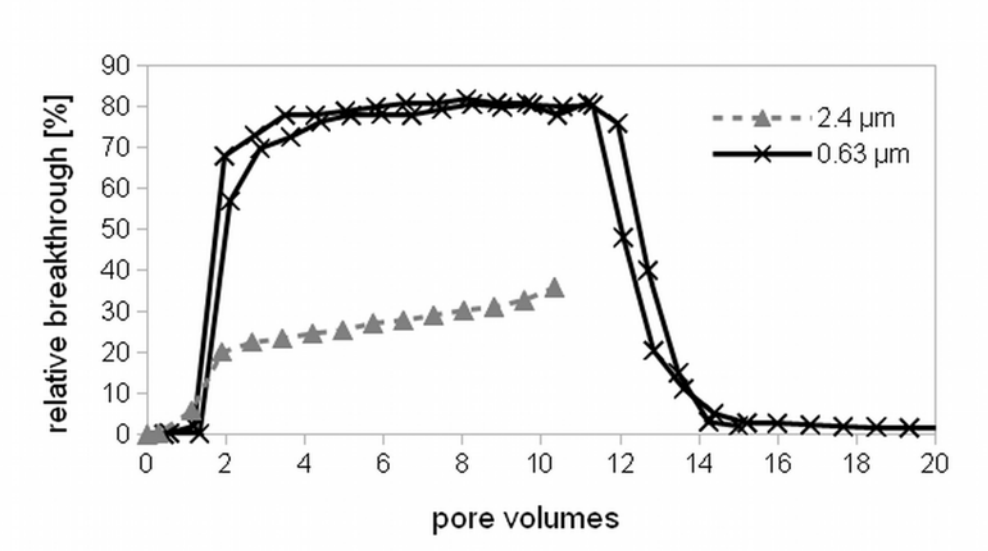

Figure 3.2.: Breakthrough curves for a transport experiment of a CIC suspension of 1000 mg/L CIC and 200 mg/L CMC in a 40 cm glass column filled with medium grained sand. The column was fed for ten exchanged pore volumes with CIC suspension and afterwards with a background solution. The experiment for 0.64 µm sized CIC colloids was performed twice and showed high reproducibility. Additionally, for comparison data for 2.4 µm sized particles are plotted, taken from a previous study (Busch et al. 2014).

the finer grained particles should be more mobile than the coarser grained, due to several possible effects such as different deposition, higher attachment, agglomeration or straining. However, a definite proof for size effects need a broader comparison of differently sized particles in a larger range, e.g. by comparison of several particle sizes between 0.1 and 5 µm.

Breakthrough curves show a slight increase in the slope of the breakthrough curve after the second exchanged pore volume until the end of the experiments for both colloid sizes. This effect has been observed before in column experiments using 1.0 and 3.2 µm sized latex microspheres in sand of different sizes at a Darcy velocity of 0.1 cm min^{-1} in 10 cm long columns (Bradford & Bettahar 2006) and CMC-stabilized nZVI of 70 nm size at a Darcy velocity of 0.445 cm min^{-1} in 9 cm filled columns with sand of 375 µm mean grain size (Raychoudhury et al. 2012). In the study by Bradford & Bettahar (2006), time dependent changes in attachment coefficients are explained to occur from

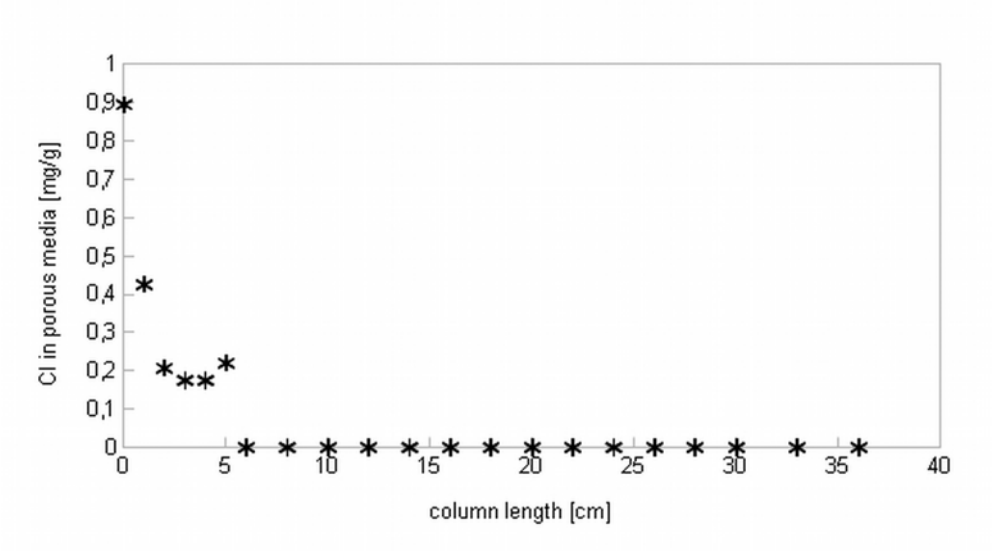

Figure 3.3.: Residuals of CIC in porous media of the column experiment. The column was opened after the transport experiment and samples of the porous medium (sand 0.1 – 0.5 mm) were taken for analysis of CIC residuals. Results are presented in form of CIC permille fraction ($m_{CIC}/m_{sediment}$ [mg/g]).

earlier injected colloids which block favorable deposition sites on the granular porous medium and cause the slight increase of the slope of the breakthrough curve.

Solid samples (n = 21) taken from the porous media were taken to investigate the distribution of CIC after its retention in the porous medium along the flow direction as well as transverse to it. Carbon as indicator for the presence of CIC was only found in samples taken from the first five centimeters of the column (Fig B.3 and Fig. B.4 in SM).

The first sample taken directly from the first millimeters of the column showed the highest CIC concentration with 0.90 mg CIC/g porous medium. The sample taken from 1 cm after the inflow showed a concentration of 0.43 mg/g. Samples taken from 2 – 5 cm showed concentrations of approx. 0.2 mg/g. In the samples further downstream, taken from six or more centimeters no more residuals could be detected. In this case, lack of detection does not completely exclude deposition of CIC, since we observed highly variable blank concentration and reached a high LOD. Anyhow, the results from the column test suggest a strong straining in the beginning of the column, which is reasonable:

Since production of CIC is based on ground activated carbon, there is a considerable range of particle sizes, and therefore a fraction of colloids might be in a size range that is unfavorable for transport. Furthermore, strong attachment in the beginning of a column has been observed for other colloids before, e.g. for latex colloids (Bradford & Bettahar 2006, Bradford et al. 2002). Generally, colloid filtration theory considers exponential or hyperexponential decrease in retention with distance, which means that the major part of deposition has to take place at the beginning of the porous medium (Bradford & Torkzaban 2008).

3.3.5. 2D-aquifer experiment

Tracer tests

Three porous media with hydraulic conductivity in the range of real aquifer materials have been tested in the 2D-aquifer test system, and only the coarse grained sand showed suited characteristics in respect to homogeneity. For fine glass beads and fine sand, based on their lower hydraulic conductivity did not achieve a parallel flow field across our 2D aquifer system. Tracer experiments showed preferential transport along the walls of the container, but no visible transport through the porous medium (Fig. B.5 in SM). However coarse sand (1 – 2 mm grain size) was able to produce a normal flow field without wall effects. For that reason and because its typical grain size for shallow unconsolidated aquifers it was chosen for the subsequent tracer and transport experiment. Three tracer experiments using brilliant blue as ionic tracer were performed under equal conditions to observe flow conditions in the aquifer tank test system. Brilliant blue was injected solely into the middle port 4 on the left side for 30 minutes, while the other ports left-hand-side were fed with deionized water, to create a thin plume allowing transverse dispersion to play a role. The flow was allowed to leave the container at the right-hand-side via all ports. After 30 minutes all injection ports were fed again with deionized water only. Photos were taken regularly to document flow patterns (Fig. B.6 in SM). Results show a first sight of blue color within four minutes after start of the experiment. In the following the tracer plume moved through the coarse sand, initially showing a local upward sidetracking but returning to the central flow path for the rest of the travel distance. The plume shows an

inhomogeneity of the flow field after 30 min, but this is only local and temporal as show the snapshots in SM. After 70 minutes blue color at the middle outflow port 4 was observed for the first time. The replicates from the experiments showed breakthrough after 60 and 65 minutes, respectively. After three hours tracer had been washed out of the aquifer system. Tracer concentration at the outflow was observed mainly at the middle outflow port 4, but the port directly under (port 5) and above (port 3) the middle port showed some light blue effluent. This means there is some slight form of dispersive transport lateral to the mean flow direction. However this transverse plume spreading reaches approximately 15 cm only and is therefore in the expected range of 10% of the length of the main flow direction. More interesting is the shape of the flow path, which seems to be uniform between the left and the right side of the container, except the curved path in the first quarter of the 2D-aquifer test system. This curve reaches its peak almost directly below the safety pressure release tube on top of the container. The porous medium around the opening might have been packed looser during the filling procedure than the rest of porous medium and might explain the local side tracking, though also a slight random variation of permeability by the filling process cannot be excluded. However, when the container was filled again all replicates showed this form of a slightly heterogeneous transport path.

Colloid transport experiment

CIC was observed analogously to the tracer. CIC was injected solely into the middle port 4 on the left side for 420 minutes, while the other ports left-hand-side were fed using water with the same background concentration of CMC as the CIC suspension, creating a thin plume with transverse dispersion playing a role. The flow was allowed to leave the container right-hand-side via all ports. After 420 minutes all injection ports were fed only with deionized water again. Photos were taken regularly to document flow patterns (Fig. 3.4).
Again, a visual observation of transport showed the same shape of the traveling path as tracer and a beginning of breakthrough after 60 minutes. Therefore, gravity effects of CIC seem not to play a role, opposite to another experiment with non-stabilized and poly acrylic acid (PAA) stabilized nZVI particles in a 2D-laboratory system filled with glass beads (Kanel et al. 2008). There, PAA stabilized nZVI showed a gravity driven transport component, which results

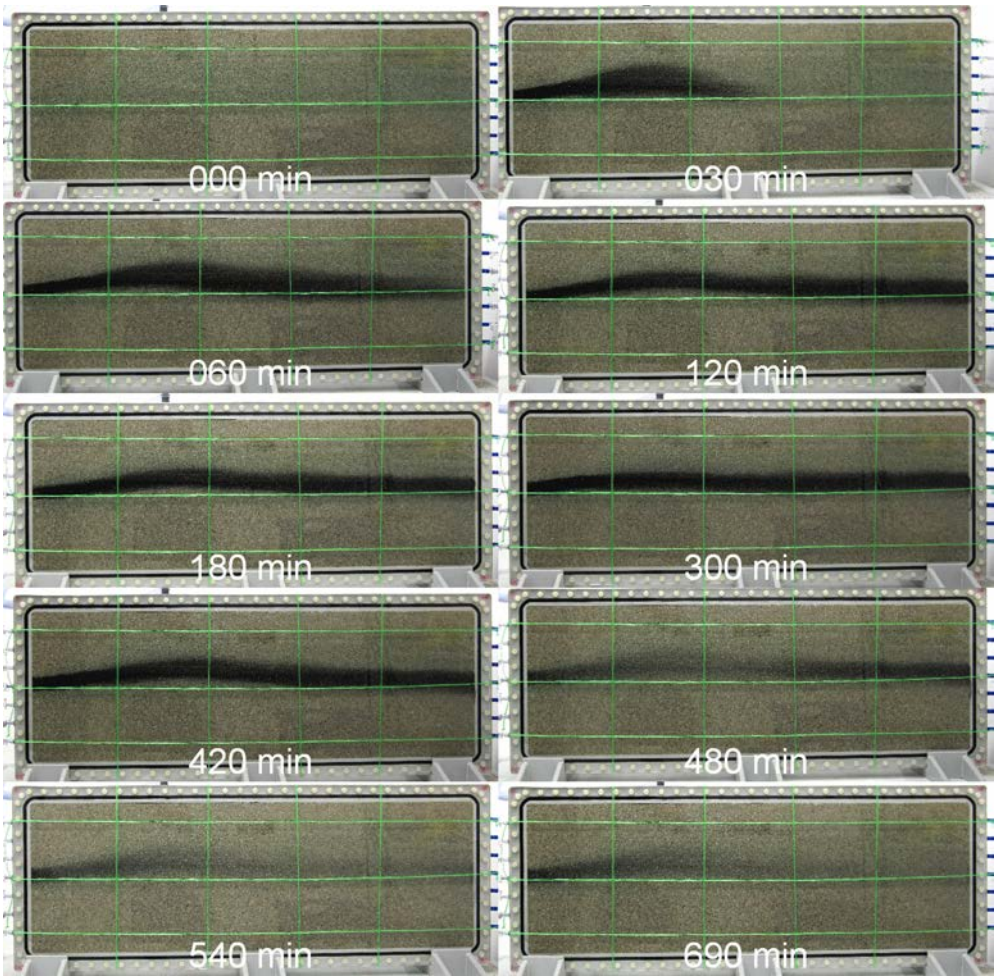

Figure 3.4.: Photos of CIC transport in the 2D-aquifer test system at different time steps during the experiment with a horizontal flow field from left to right. CIC was fed into the middle injection port at the left during the first 420 minutes and observed for 690 minutes. Original images were brightened for better visibility of contrast.

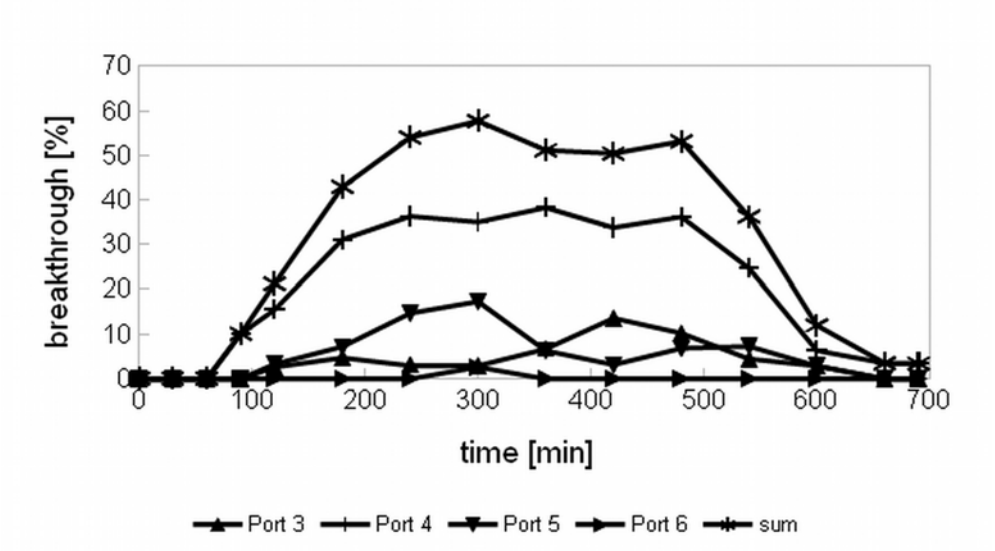

Figure 3.5.: Breakthrough curves of CIC at relevant outflow ports from the 2D-aquifer test system. CIC was injected for 420 minutes at inlet at height of port 4; the other ports were fed with a background solution. After injection of CIC a background solution was injected into all ports.

in a downward flow direction in between horizontal flow direction and vertical direction of gravitational forces.

Breakthrough of CIC was monitored at all seven outflow ports by sampling from all ports every 30 – 60 minutes and subsequent analysis (Fig 3.5).

Breakthrough of CIC was detected in the central ports, i.e. three to six, but not the other ports. Highest CIC concentration in outflow was in port 4 followed by the adjacent ports 5 and 3. Port 6 had only one positive detection of CIC within 15 samples. First detected breakthrough was in the sample taken after 90 minutes from port 4, followed by detections in ports 3 and 5 after 120 minutes.

Concentrations of samples from each port reflect directly on the equivalent amount of CIC. Therefore concentrations can be summed up to conclude on relative breakthrough compared to the injected amount of CIC. Total observed CIC breakthrough maximum after 300 minutes was 58% of the injected amount of CIC, whereas a hypothetical conservative tracer with purely advective transport should show 100%. This is followed by a plateau of more than 50% breakthrough until 480 minutes. After CIC injection was stopped at 420 min-

utes and detected amounts fell within 120 minutes to 36% and leaving a tail of 3% after 180 more minutes.
Differences in visual (60 min) and instrumental (90 min) detection of breakthrough can be explained by detection limits (LOD & LOQ) above the limits of visual cognition of CIC content and sampling rates of liquid samples, which could only determine the beginning of breakthrough to be 90 minutes, even though a sample e.g. taken after 75 minutes at port 4 might have shown positive result in compliance with LOD and LOQ.
The breakthrough curves of port 3 and 5 show a different shape of the breakthrough curve: Detection of CIC in port 5 reaches its peak at similar times than at port 4, but decreased already after 300 minutes, with a slight bouncing back around 480 minutes. This is most likely related to the tubes connected to the outflow. Flow rate of each tube at the outflow was monitored and showed slight, but detectable changes. Overall it looks like small changes in outflow rate at the ports have caused the CIC plume to move downwards towards port 3 and away from port 5 for a limited period between 300 and 480 minutes. Transverse dispersive spreading of the CIC plume was observed visually to rather be smaller than for the tracer experiment. It has been observed earlier that diffusive transport of colloids might be smaller than diffusion driven transport of ions. This might be reasonable, since dissolved ions are subjected more to Brownian motion than colloids (Baumann 2010, Tufenkji & Elimelech 2004).
During the 2D-aquifer experiment samples were taken to determine particle size distributions and zeta potential before and after the passage of the aquifer tank. One sample was taken from the stock suspension and seven samples were taken at port 4 from 90 to 540 min from the beginning of the experiment. Results show a zeta potential of -49 mV in the sample from the stock suspension and -80 mV in the samples taken from port 4. Particle size distribution from the sample taken from the storage tank showed a mean particle size of 2.5 µm after the experiment. Samples from port 4 show a mean diameter of 0.8 µm (Fig. 3.6) and show a smaller mean size than the injected particles.

Given the fact, that a rather big range of colloid sizes exists in a suspension the particle size distribution is not necessarily monodisperse (Busch et al. 2014) and a considerable amount of colloids might be in a size range, which is

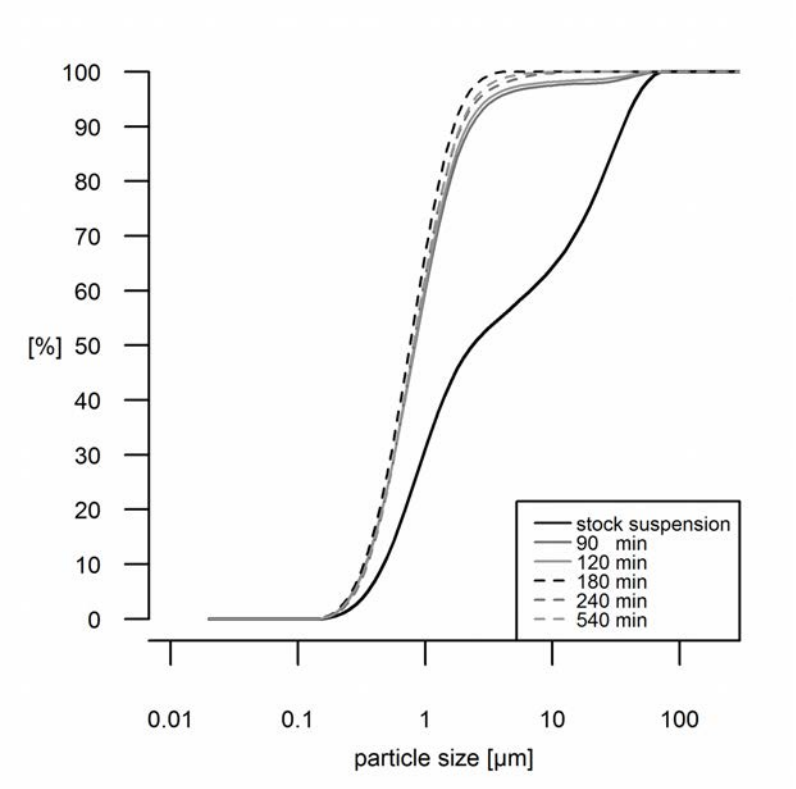

Figure 3.6.: Particle size distribution of CIC suspension in the stock suspension compared to the ones determined from outlet port 4 at different times during the experiment.

unfavorable for transport. Therefore we have to consider that a part of the colloids may not reach the porous medium in column experiments and in the 2D-aquifer experiment, because they might already sediment in the pumps and tubes. However, this should be considered as a general drawback of laboratory experiments in which pumps are used, and also will be there in the case of field application. Results of zeta-potential and particle size distribution measurement show fractionation of particles during the transport experiment towards more favorable properties, which hints on a possible underestimation of transport ranges by calculation of filtration coefficients, since only colloids which are mobile will pass the column and after that passage constitute a suspension with relatively mobile colloids.

Determination of the particle size distribution often gives different particle sizes in between different dispersion methods. Using a Branson Sonifier for preparation, as done for colloid characterization, led to a mean particle size of 0.63 µm. Sample preparations using an Ultra Turrax, storage (samples were stored, send via mail and proceeded after approximately two weeks), and sonication in the SLS device led to a mean size of 2.4 µm. This effect might be explained by aging of the samples and the different energy inputs of the devices, which is transferred into the suspension and has been observed for other colloids before (Meißner et al. 2014). Using a Sonifier gives more energy into the sample and might deagglomerate the sample to smaller colloids than other sonication methods. Between different sonication methods, i.e. using an Ultra Turrax and a sonication bath, the applied energy varies as well. This issue is currently under discussion, especially in toxicological contexts, since laboratory studies might not necessarily reflect on environmental conditions, due to aging and agglomeration of colloids in natural environments (Misra et al. 2012).

However, all results do show that the particle size changes during the transport experiment. Some changes might occur before entrance in the porous medium, such as sedimentation of biggest fraction, or of particles with low zeta potential, if heterogeneity within the colloids is assumed. Anyway, we can assume that a colloid which does not reach the porous medium would not move through porous media anyway. This colloid heterogeneity has been observed before for other particles (Tong & Johnson 2006). It seems reasonable to assume a stronger attachment and sedimentation of bigger colloids. Particles with low

zeta potential should be removed in the porous media as well.
Solid samples from the aquifer taken after the experiment show a CIC concentration of 1.89 mg/g CIC direct at the injection port and somewhat smaller concentrations at the adjunct sampling points (Fig. B.7 in SM). No CIC was found in samples further away than 10 cm from the injection. This result suggests a strong attachment in the beginning and less attachment of particles further away from the injection port. This is comparable to results from the column experiment, as presented above. Here the detected amount of the remaining CIC is larger than in the column experiment, but according to the higher injection speed, coarser porous medium and more injected CIC reasonable.

3.4. Conclusion

In this study transport properties of carbon supported nanoscale zero-valent iron was observed in a column experiment and in a 2D-aquifer test system. Results show breakthrough levels of 82% in a 40 cm column and 58% in the 120 cm long 2D-laboratory test system. The distribution of the CIC was similar in shape to a conservative tracer, but significant amount of retardation and retention of CIC. Nevertheless the flushing without CIC in suspension led to continuous remobilization of CIC and transfer of the major part of CIC to the outlets. Additionally, particle size distribution and surface charge of CIC could be observed for the 2D-aquifer test system. Particle size distribution changed during the transport experiment towards smaller sizes and zeta potential changed to decreased, negative values. Both indicates fractionation of colloids during the transport experiment. The concept of carbon supported nanoscale zero-valent iron shows promising characteristics to be able to create *in situ* a permeable reactive barrier, for sorptive retention and removal of chlorinated solvents in sandy aquifers.

3.5. Acknowledgments

This study was supported by the German Ministry for Education and Research (Bundesministerium für Bildung und Forschung, BMBF) in the project Fe-NANOSIT (Iron based nanoparticles and nano-composite structures for

remediation of ground- and wastewater). We want to thank Stefan Scholz from the department Bioanalytical Ecotoxicology and the staff of the department Environmental Engineering from the Helmholtz-Centre for Environmental Research UFZ (Leipzig, Germany) for provision of particles and technical support.

3.6. Literature

Arnold WA, Roberts AL (2000): Pathways and Kinetics of Chlorinated Ethylene and Chlorinated Acetylene Reaction with Fe(0) Particles. Environ. Sci. Technol. 34, 1794-1805

Baumann T (2010): Nanoparticles in Groundwater – Occurrence and Applications. In: Frimmel FH , Niessner R (Editors), Nanoparticles in the Water Cycle. Springer Berlin Heidelberg, pp. 23-34

Bleyl S, Kopinke F-D, Mackenzie K (2012): Carbo-Iron® Synthesis and stabilization of Fe(0)-doped colloidal activated carbon for *in situ* groundwater treatment. Chemical Engineering Journal 191, 588-595

Bradford SA, Yates SR, Bettahar M, Simunek J (2002): Physical factors affecting the transport and fate of colloids in saturated porous media. Water Resources Research 38

Bradford SA, Bettahar M (2006): Concentration dependent transport of colloids in saturated porous media. Journal of Contaminant Hydrology 82, 99-117

Bradford SA, Torkzaban S (2008): Colloid Transport and Retention in Unsaturated Porous Media: A Review of Interface-, Collector-, and Pore-Scale Processes and Models. Vadose Zone J. 7, 667-681

Busch J, Meissner T, Potthoff A, Oswald SE (2014): Transport of carbon colloid supported nanoscale zero-valent iron in saturated porous media. submitted

Comba S, Di Molfetta A, Sethi R (2011): A Comparison Between Field Applications of Nano-, Micro-, and Millimetric Zero-Valent Iron for the Remediation of Contaminated Aquifers. Water Air Soil Pollut. 215, 595-607

Crane RA, Scott TB (2012): Nanoscale zero-valent iron: Future prospects for an emerging water treatment technology. Journal of Hazardous Materials 211–212, 112-125

Gillham RW, O'Hannesin SF (1994): Enhanced Degradation of Halogenated Aliphatics by Zero-Valent Iron. Ground Water 32, 958-967

He F, Zhang M, Qian T, Zhao D (2009): Transport of carboxymethyl cellulose stabilized iron nanoparticles in porous media: Column experiments and modeling. J. Colloid Interface Sci. 334, 96-102

He F, Zhao D, Paul C (2010): Field assessment of carboxymethyl cellulose stabilized iron nanoparticles for *in situ* destruction of chlorinated solvents in source zones. Water Res. 44, 2360-2370

Hoch LB, Mack EJ, Hydutsky BW, Hershman JM, Skluzacek JM, Mallouk TE (2008): Carbothermal synthesis of carbon-supported nanoscale zero-valent iron particles for the remediation of hexavalent chromium. Environ. Sci. Technol. 42, 2600-2605

Jiemvarangkul P, Zhang WX, Lien HL (2011): Enhanced transport of polyelectrolyte stabilized nanoscale zero-valent iron (nZVI) in porous media. Chemical Engineering Journal 170, 482-491

Johnson RL, Nurmi JT, O'Brien Johnson GS, Fan D, O'Brien Johnson RL, Shi Z, Salter-

Blanc AJ, Tratnyek PG, Lowry GV (2013): Field-Scale Transport and Transformation of Carboxymethyl-
cellulose Stabilized Nano Zero-Valent Iron. Environ. Sci. Technol. 47, 1573-1580
Kanel SR, Goswami RR, Clement TP, Barnett MO, Zhao D (2008): Two dimensional transport characteristics of surface stabilized zero-valent iron nanoparticles in porous media. Environ. Sci. Technol. 42, 896-900
Loveland JP, Bhattacharjee S, Ryan JN, Elimelech M (2003): Colloid transport in a geochemically heterogeneous porous medium: aquifer tank experiment and modeling. Journal of Contaminant Hydrology 65, 161-182
Lowry GV (2007): Nanomaterials for Groundwater Remediation. In: Wiesner MR , Bottero JY (Editors), Environmental Nanotechnology. Applications and Impacts of Nanomaterials. McGraw-Hill, New York, pp. 297-336
Mackenzie K, Bleyl S, Georgi A, Kopinke F-D (2012): Carbo-Iron An Fe/AC composite As alternative to nano-iron for groundwater treatment. Water Res. 46, 3817-3826
Matheson LJ, Tratnyek PG (1994): Reductive dehalogenation of chlorinated methanes by iron metal. Environ. Sci. Technol. 28, 2045-2053
McMahon PB, Dennehy KF, Sandstrom MW (1999): Hydraulic and geochemical performance of a permeable reactive barrier containing zero-valent iron, Denver Federal Center. Ground Water 37, 396-404
Meißner T, Oelschlägel K, Potthoff A (2014): Dispersion of nanomaterials used in toxicological studies: a comparison of sonication approaches demonstrated on TiO2 P25. J. Nanopart. Res. 16, 1-13
Misra SK, Dybowska A, Berhanu D, Luoma SN, Valsami-Jones E (2012): The complexity of nanoparticle dissolution and its importance in nanotoxicological studies. Science of The Total Environment 438, 225-232
Mueller NC, Nowack B (2010): Nanoparticles for Remediation: Solving Big Problems with Little Particles. Elements 6, 395-400
O'Hannesin SF, Gillham RW (1998): Long-term performance of an *in situ* "iron wall" for remediation of VOCs. Ground Water 36, 164-170
Phenrat T, Saleh N, Sirk K, Tilton RD, Lowry GV (2007): Aggregation and sedimentation of aqueous nanoscale zerovalent iron dispersions. Environ. Sci. Technol. 41, 284-290
Phenrat T, Saleh N, Sirk K, Kim HJ, Tilton RD, Lowry GV (2008): Stabilization of aqueous nanoscale zerovalent iron dispersions by anionic polyelectrolytes: adsorbed anionic polyelectrolyte layer properties and their effect on aggregation and sedimentation. J. Nanopart. Res. 10, 795-814
Phenrat T, Cihan A, Kim HJ, Mital M, Illangasekare T, Lowry GV (2010): Transport and Deposition of Polymer-Modified Fe-0 Nanoparticles in 2-D Heterogeneous Porous Media: Effects of Particle Concentration, Fe-0 Content, and Coatings. Environ. Sci. Technol. 44, 9086-9093
Quinn J, Geiger C, Clausen C, Brooks K, Coon C, O'Hara S, Krug T, Major D, Yoon W-S, Gavaskar A, Holdsworth T (2005): Field Demonstration of DNAPL Dehalogenation Using Emulsified Zero-Valent Iron. Environ. Sci. Technol. 39, 1309-1318
Raychoudhury T, Tufenkji N, Ghoshal S (2012): Aggregation and deposition kinetics of carboxymethyl cellulose-modified zero-valent iron nanoparticles in porous media. Water Res. 46, 1735-1744
Savage N, Diallo MS (2005): Nanomaterials and water purification: Opportunities and challenges. J. Nanopart. Res. 7, 331-342
Schrick B, Hydutsky BW, Blough JL, Mallouk TE (2004): Delivery vehicles for zerova-

lent metal nanoparticles in soil and groundwater. Chem. Mat. 16, 2187-2193
Stroo HF (2010): Remedial Technology Selection for Chlorinated Solvent Plumes. In: Stroo HF , Ward CH (Editors), *in situ* Remediation of Chlorinated Solvent Plumes. Springer Science + Business Media, New York, Heidelberg, Dordrecht, London
Stroo HF, Ward CH (2010): *In situ* Remediation of Chlorinated Solvent Plumes. Springer Science + Business Media, New York, Heidelberg, Dordrecht, London
Sunkara B, Zhan JJ, He JB, McPherson GL, Piringer G, John VT (2010): Nanoscale Zerovalent Iron Supported on Uniform Carbon Microspheres for the *in situ* Remediation of Chlorinated Hydrocarbons. ACS Appl. Mater. Interfaces 2, 2854-2862
Sunkara B, Zhan JJ, Kolesnichenko I, Wang YQ, He JB, Holland JE, McPherson GL, John VT (2011): Modifying Metal Nanoparticle Placement on Carbon Supports Using an Aerosol-Based Process, with Application to the Environmental Remediation of Chlorinated Hydrocarbons. Langmuir 27, 7854-7859
Tiraferri A, Sethi R (2009): Enhanced transport of zerovalent iron nanoparticles in saturated porous media by guar gum. J. Nanopart. Res. 11, 635-645
Tong M, Johnson WP (2006): Colloid Population Heterogeneity Drives Hyperexponential Deviation from Classic Filtration Theory. Environ. Sci. Technol. 41, 493-499
Tufenkji N, Elimelech M (2004): Correlation equation for predicting single-collector efficiency in physicochemical filtration in saturated porous media. Environ. Sci. Technol. 38, 529-536
Zhan JJ, Kolesnichenko I, Sunkara B, He JB, McPherson GL, Piringer G, John VT (2011): Multifunctional Iron-Carbon Nanocomposites through an Aerosol-Based Process for the *in situ* Remediation of Chlorinated Hydrocarbons. Environ. Sci. Technol. 45, 1949-1954
Zhang H, Jin Z-h, Han L, Qin C-h (2006): Synthesis of nanoscale zero-valent iron supported on exfoliated graphite for removal of nitrate. Transactions of Nonferrous Metals Society of China 16, 345-349
Zhang WX (2003): Nanoscale iron particles for environmental remediation: An overview. J. Nanopart. Res. 5, 323-332
Zheng TH, Zhan JJ, He JB, Day C, Lu YF, McPherson GL, Piringer G, John VT (2008): Reactivity characteristics of nanoscale zerovalent iron-silica composites for trichloroethylene remediation. Environ. Sci. Technol. 42, 4494-4499

4. A field investigation on the mobility of carbon supported nanoscale zero-valent iron (nZVI) in groundwater

Article submitted as J. Busch, Meißner, T., Potthoff, Bleyl, S., A, Georgi, A., Mackenzie, K., Trabitzsch, R., Werban, U., Oswald, S. E. (in review since November 30, 2014): A field investigation on the mobility of carbon supported nanoscale zero-valent iron (nZVI) in groundwater. Journal of Contaminant Hydrology[1]

4.0.1. Abstract

Application of nanoscale zero-valent iron (nZVI) for subsurface remediation of groundwater contaminants is a promising new technology, which can be understood as a development continuing the permeable reactive barrier technique using granular iron. Studies have shown promising results for dechlorination of organic contaminants by zero-valent iron. Currently, a main limitation for its widespread application is fast aggregation and sedimentation of nZVI in colloidal suspensions, even more when in soils and sediments, which limits the applicability for applicability for treatment of sources and plumes of contamination. Colloid-supported nZVI shows promising characteristics to overcome these limitations. Carbo-Iron Colloids (CIC) – a newly developed composite material, based on finely ground activated carbon as carrier for nZVI, was tested in a field application for its mobility. In this study, we established a horizontal dipole flow field between two wells with a distance of 5.3 m in a confined, natural aquifer. The injection- and extraction rate was 500 L/h. Approximately 1.2 kg of CIC was dispersed and brought in suspension with the polyanionic stabilizer carboxymethyl cellulose. The suspension was introduced into the aquifer via the injection well and the breakthrough curve of CIC was observed at the extraction

[1]This article is now accepted and published online in revised form since April 3rd 2015, with identifier doi:10.1016/j.jconhyd.2015.03.009 .

well. Filtration of water samples revealed a particle breakthrough of about 12% of the amount introduced. This result illustrates high mobility of CIC particles and supports the applicability of CIC as a special form of nZVI for construction of broad plume treatment zones in contaminated aquifers.

4.1. Introduction

For remediation of chlorinated organic compounds, zero-valent iron (ZVI) has proven to be a useful reactive agent (Gillham and O'Hannesin, 1994; Matheson and Tratnyek, 1994; Orth and Gillham, 1995). Iron reductively dechlorinates contaminants such as chlorinated ethenes to less harmful substances such as ethane and ethene, while in a first step the reaction often follows a beta elimination forming ethylene (Arnold and Roberts, 2000). Field-scale applications of granular ZVI have been applied successfully since the mid '90s and were mostly constructed as funnel-and-gate systems (McMahon et al., 1999; O'Hannesin and Gillham, 1998; Vogan et al., 1999; Wilkin et al., 2003). These applications are still state-of-the-art technology (Stroo and Ward, 2010), but application of granular ZVI has limitations in application, since this technology requires extensive in construction work and is practically not deployable under sealed areas. A recent approach to extend the applicability of conventional permeable reactive barriers (PRBs) is the injection of nanoscale zero-valent iron (nZVI) suspensions into contaminated aquifers to *in situ* build permeable treatment zones (Quinn, J. et al., 2005; Henn and Waddill, 2006; Cai et al., 2006; Baumann, 2010). Nanoscale iron particles are attractive not only by the possibility to inject them into overbuilt and deep aquifers but also due to their higher reactivity compared to granular iron (Grieger et al., 2010).
The main limitation for application of nZVI is the fast agglomeration and thus sedimentation due to iron's magnetic attraction forces (Phenrat et al., 2007), which results in limited mobility. Studies estimate transport ranges of centimeters (Schrick et al., 2004) to few meters (Johnson et al., 2013; Laumann et al., 2013; Tiraferri and Sethi, 2009). In field experiments, also transport distances in the lower meter range have been observed (Tab. 4.1), but not farer than that. Consequently, chemical evidence of contaminant degradation could only be observed in close proximity around the injection wells (Zhang, 2003).
Current approaches for improvement of subsurface transport of nZVI follow strategies such as coating and surface functionalization. Meanwhile, these measures are common tools for minimizing nZVI aggregation. Increasing the surface charge (electrostatic stabilization) and coating the particles with sterically demanding stabilizers enhances steric repulsion forces (steric stabilization) or a combination of both (electrosteric stabilization). The materials

Transport range	Application	Soil characteristics	Source
4.5 m	Recirculation of bimetallic doted nZVI. Recirculation for two days. Injection of 1.7 kg. Concentrations of 20 – 30 mg/L were found at the observation wells.	Hydraulic conductivity (K) = 0.2 cm/s Porosity = 0.25	Elliot & Zhang, 2001
Close to injection wells	Visual evidence of nZVI transport in soil cores close to injection wells	Medium to coarse grained sand	Quinn et al. 2005
1.5 - 3 m	Pd doted nZVI ,70% normalized to tracer after 1.5 m. After 3 m almost no recovery.	Silty clay with sand and gravel	He et al., 2010
1.06 m	Observation of colored water, recirculation of Pd-doted nZVI slurry	Clayey sand or silty very fine-to-fine sand	Henn and Wadilll, 2006
3 m	Gravity injection of approx. 40 kg nZVI with small traces of palladium	Medium to coarse sand and few silt	Wei at al., 2010
0.54 – 1.3 m	Injection and observation, push-pull-test	Holocene and Pleistocene alluvial sediments, predominantly silts and clays, and coarse grained sediment deposits along ancient stream beds	Bennett et al., 2010

Table 4.1.: Compilation of studies investigating on the mobility of nZVI in field studies.

used for coating nZVI can be divided into three classes: polyelectrolytes, surfactants and polymers. Most often polyanionic stabilizer, among them carboxymethyl cellulose (CMC) and polyacrylic acid (He et al., 2009; He et al., 2010) are used as suspension stabilizers. Alternatively, application of a suitable carrier colloid, such as silica (Zheng et al., 2008), carbon black (Hoch et al., 2008), graphite (Zhang et al., 2006), carbon microspheres (Sunkara et al., 2010; Sunkara et al., 2011; Zhan et al., 2011), or activated carbon (Bleyl et al., 2013; Bleyl et al., 2012; Mackenzie et al., 2012) followed the aim to i) finely disperse the metal, ii) hold the single iron species apart from each other (spacer effect) and iii) positively combine the properties of iron and support material in regard to remediation.
One of the new materials designed for improved subsurface transport, the so called "Carbo-Iron colloids" (CIC), is a composite of colloidal activated carbon particles with a d_{50}-size of 0.8 µm, which contains nZVI within the porous carbon grains. They are characterized by a mean effective density of 1.7 g/cm^3 and a nZVI content of approx. 20 wt-% (Mackenzie et al., 2012). In laboratory experiments CIC has already shown to be mobile (Busch et al., 2014a; Busch et al., 2014b) and to be able to reduce trichloroethylene (TCE) to chlorine-free hydrocarbons (Mackenzie et al., 2012). In this study we present the results from a field experiment on mobility of CIC in a confined natural aquifer as investigation of a key question for the applicability of CIC for field-scale remediation of groundwater contamination.

4.2. Materials and methods

4.2.1. Site description

The selected site is located near the city of Leuna, Saxony-Anhalt, Germany. The test site is downstream of a large industrial area, which was established before more than 100 years. In this area, chemical plants and refineries are still operated. Former spills and leakages contaminated the surrounding soil and groundwater to a severe level, leading also to investigations of contaminant plumes and natural attenuation at this site (Martienssen et al., 2006). Typically groundwater there is mainly contaminated with benzene (20 mg/L), MTBE (3.9 mg/L) and ammonium (55 mg/L) but also other contaminants

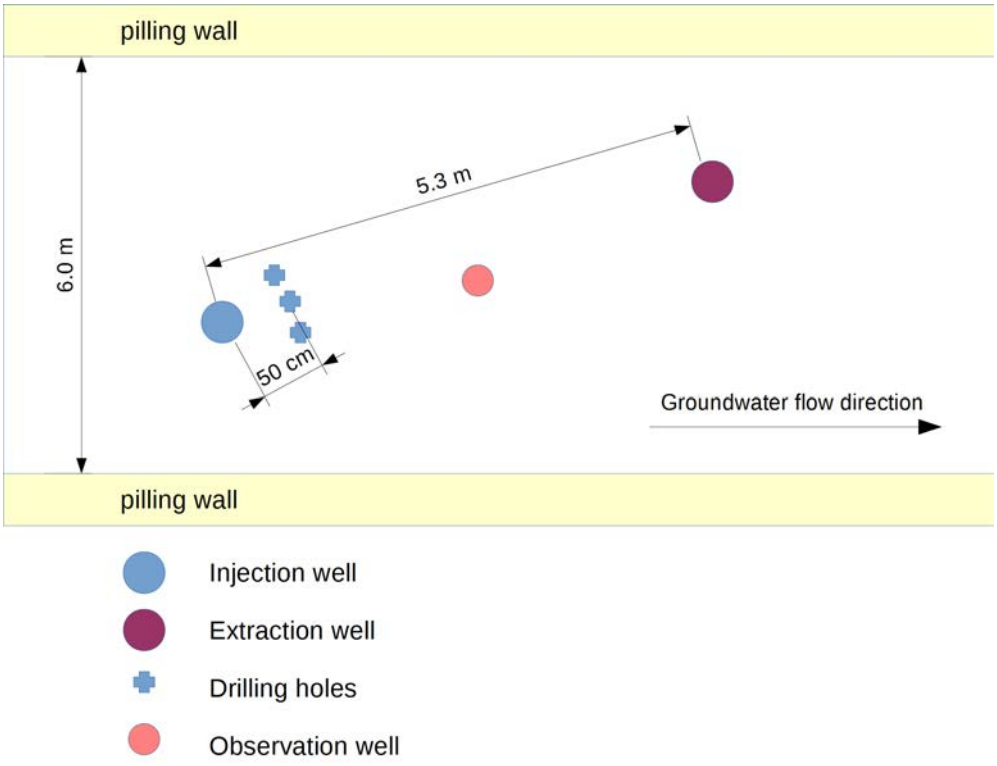

Figure 4.1.: Sketch of the field site.

(De Biase et al., 2011; Jechalke et al., 2010). Though, CIC would only target these contaminants by sorption but not by degradation, for mobility studies the site offers developed experimental aquifers and realistic field conditions for a contaminated site. The spot selected for the experiment has been used within the SAFIRA II project (Rügner et al., 2007), where groundwater is well characterized (De Biase et al., 2011) and sheet-pile walls have been installed in groundwater flow direction. The aquifer strip between two pile walls used for our experiment was 6 m wide. Within the selected aquifer strip two wells had been installed in 5.3 m distance, now to be used as injection and extraction well. Additionally, an observation well was installed in the middle between injection and extraction well, with an offset of 30 cm from the direct line between injection and extraction well. Core analysis data were available for the extraction well (see SM).

The slow well screen of the injection well was situated between a depth of 3.04 and 6.04 m below surface. The well construction had been completed

with horizons of sand (0 – 1.64 m below surface), a clay barrier (1.64 – 3.34 m), gravel (3.34 – 6.04 m) and another clay barrier 40 cm underneath. An additional feature of the aquifer strip used is that it was hydraulically separated by pile-sheets from the aquifer in the environment and a continuous clay formation at the aquifer bottom from underlying aquifers. Therefore, an undesired release to the environment outside the aquifer strip could be excluded. A background flux of water to simulate natural groundwater flux was 1 m^3/d in the separated aquifer strip.
Injection of tracer and particles occurred in a depth between 3.34 – 6.04 m into sand and gravel, according to the well screen, measured water table elevation and location of the confining layer. Transport of tracer and colloids presumably has mainly taken place in the gravel layer, since its hydraulic conductivity and transmissivity was the largest.

4.2.2. Additional site characterization

4.2.3. Tracer experiment

A tracer test using fluorescein has been performed in order to study the hydrodynamic properties of the aquifer at the test site. The injection well was fed with 500 L/h of tap water and the same amount of water was removed from the extraction well using a MP1 pump (Eijkelkamp, Giesbeek, Netherlands). After adjustment of constant flow rates and monitoring for several hours, 5 g of tracer were diluted in 200 L (25 mg/L) of tap water, and this solution was injected into the well with the above injection rate, i.e. during about 24 minutes. Afterwards, the well was fed again with tap water to maintain the forced groundwater flow field. The pump at the extraction well was connected to an automatic sampling system that extracted samples every hour and stored them in 1 L glass bottles. The bottles were covered with aluminum foil to avoid photolytic degradation of fluorescein.
Samples were measured using a field fluorescence photometer (MKT-2, Sommer, Austria). Since the fluorescence intensity of the tracer depends on physicochemical parameters of the water, the measurement of the tracer via its fluorescence was calibrated several times using local groundwater, local tap water, and deionized water. All samples were measured once as taken and once after pH adaptations using small amounts of NaOH (max. 0.5 mL of

2M NaOH added into one liter of sample) in order to adjust to a pH of 11. In additional to the automated hourly sampling, samples were taken by hand for control and as retain sample.

4.2.4. Sediment samples

Sonic core samples were taken after the experiment at a distance of 0.5 m downstream from the injection well from a depth of 4 – 8 m covering the sand and gravel layer in the aquifer. These samples were used for characterization of the investigation site. Visual changes by CIC deposition on the sediment comparable to a previous study using NZVI (Quinn et al., 2005), were not expected taking the mass of CIC injected and its high mobility into account (i.e. travel distances >1 m in previous studies).

4.2.5. Colloid transport experiment

Particle characterization

Colloids were characterized by using a Mastersizer 2000 (Malvern Instruments GmbH, Herrenberg, Germany) for detection of particle size distribution by static light scattering (SLS). Each sample was prepared by dissolution of 300 mg/L CMC and approx. 2 g of CIC from the delivery vessel. The sample was subsequently dispersed for 30 min with an Ultra Turrax at 24,000 rpm for 30 min. Samples were sent to an external laboratory and were not more than two weeks old when being analyzed. All samples were analyzed three times applying different methods. SLS was used (i) after shaking, (ii) after shaking and sonication for five minutes in the SLS device with the internal sonication method and (iii) after sonication (five minutes at 50% amplitude) of a 40 mL sample using a Branson Sonifier 450 (Branson Ultrasonics Corporation, Danbury, CT, USA).

Preparation of colloids

In preparation for the experiment, three containers with the volume of 1 m^3 were filled with tap water. Then 1 kg of carboxymethyl cellulose (CMC, Carl Roth GmbH, Karlsruhe, Germany) was dissolved in each container (final CMC

concentration 1 g/L). One container was purged with nitrogen in order to remove dissolved oxygen. CIC with a zero-valent iron content of 15% by weight was delivered to the site in a 60 liter container, where CIC was stored in 40 L of water (CIC concentration 200 g/L) under a nitrogen atmosphere.
1.2 kg of this concentrated CIC slurry was batch-wise dispersed in two 5 L containers for 30 min per batch in a 1:3 dilution with tap water, using two Ultra-Turrax (T25D, IKA, Stauffenberg, Germany) devices. For dilution of CIC, deoxygenated CMC-containing water from the storage tank was taken. The suspensions with dispersed CIC were stored in a nitrogen-flushed container until all batches of CIC were treated. The final CIC and CMC concentrations in the suspension for injection were 1 g/L and approximately 1.2 g/L, respectively. Since laboratory tests had shown that sedimentation in well-dispersed suspensions was slow, the content of the container was not agitated further than by the nitrogen purging. However, sedimentation did occur in the container at the field site.
For injection, 200 L of CMC-containing water were injected prior to the injection of 850 L of CIC-containing suspension. After particle injection, 1.5 m^3 of CMC-containing solution were used to rinse the system, followed by tap water, all at a rate of 500 L/h. The initial suspension in the storage tank had an electrical conductivity of 1.1 µS/cm, a pH of 9.83 and oxygen below detection limit.

Colloid and groundwater sample treatment

Samples from the groundwater were taken regularly every hour by an automatic sampling system. Additionally, samples were manually taken in 30 min intervals. Colloid concentrations were analyzed after vacuum filtration using 0.2 µm filters. Samples were thoroughly shaken and a 10 mL aliquot was taken and mixed with 10 mL of concentrated hydrochloric acid. The so-treated water sample was shaken overnight and afterwards filtrated with a 0.45 µm PTFE filter. Instrumental analysis was performed by Inductively Coupled Plasma Spectroscopy (ICP-OES). Additionally, some samples were sent to an external analytical laboratory for iron-concentration measurements.

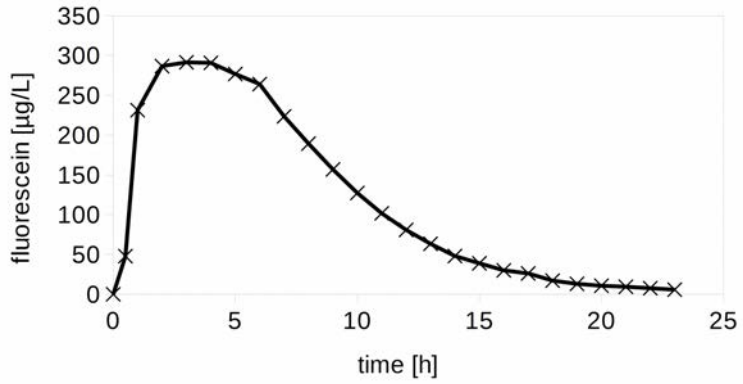

Figure 4.2.: Tracer breakthrough curve for the breakthrough experiment at the field site using tracer (tracer = fluorescein; m_{tracer} = 5 g; distance between injection and extraction well = 5.3 m; Vfeed = 500 L/h).

4.3. Results and discussion

4.3.1. Tracer experiment

Fluorescein is a well-known and frequently used tracer in hydrological experiments, but it is also well-known to be sensitive towards environmental conditions. To address the issue, several calibration series applying various water types were performed and reached in all cases a linearity of R^2 = 0.98 or higher. However, calibration using local groundwater from the test site resulted in reduced signal intensity by a factor between 1.7 and 2.3 compared to tap water, whereas calibration using deionized water and tap water and pH adjustment from field conditions (pH = 7.5) to pH = 8 (and higher) showed negligible effects on signal intensity. Therefore, tracer recovery in the field experiment is expected to be lower than achieved in the calibration tests due to mixing of tap water based tracer solution and adjacent local ground water. To estimate this effect, a calibration was conducted using water from the extraction well, after establishing the flow field and taken directly before injection of the fluorescein solution, and adding 5 g of tracer, which resulted in a recovery of 63 wt-%. Tracer was detected already one hour after injection at the extraction well (Fig. 4.2). The peak maximum was occurring after three hours. The peak form showed a plateau-like maximum from two to six hours, before it

declined with a long tailing. This behavior is mainly a result of transport in the dipole flow field where tracer exhibits short quick flow paths as well as long and slow flow paths before reaching the extraction well. Nevertheless, tracer breakthrough is faster than expected for a homogeneous sand and gravel aquifer, compared to a pre-test numerical modelling exercise to estimate suited tracer solution volumes and test durations (data not shown). This suggests that heterogeneous conditions and preferential flow paths are present, which is not unusual in aquifers (Beven and Germann, 2013). Thus, conditions as being present here may indeed be typical for sand and gravel aquifers, as often used for groundwater exploitation.

4.3.2. Aquifer sampling

Sediment samples were taken after the experiment at a distance of 0.5 m downstream from the injection well for a depth of 4 – 8 m covering the sand and gravel layer in the aquifer. These samples were used primarily for site characterization. Visual changes by CIC deposition on the sediment at this location were not expected, other than in a previous study using nZVI (Quinn et al., 2005), but taking into account the mass of CIC injected and its high mobility (i.e. travel distances >1 m in previous studies, e.g. Busch et al., 2014b).

An interesting observation was made: soil samples which were taken from the same gravel layer, as shown in Fig. 4.3, showed remarkably different characteristics. The soil sample taken from the direct line between injection- and extraction well showed a gravel layer with sand and clay fraction inside. The core had a grayish color. The sample taken 30 cm southwards of the direct line showed a higher ratio of fine sand and clay compared to the sample before. The color was rather yellow than gray. The third sample, which was taken 30 cm off northwards, showed almost no sand and clay content at all. Changes in color and composition of soil samples from the gravel-containing layer varied in all other samples taken, even though all samples were taken within a few square meters. This supports the assumption that preferential flow paths in this aquifer can be present between the two wells, formed by parts of the gravel layer having a really high conductivity.

Figure 4.3.: Soil samples taken with a sonic drilling approach. The samples were all taken in a distance of approx. 50 cm downstream from the injection well. The middle image shows a sample taken in direct line from injection to extraction well. The other two images were taken 30 cm left and right from the middle sample position. All images show the core area from the gravel layer.

4.3.3. Colloid transport experiment

Particle characterization

The retention of CIC in suspension strongly depends on CIC agglomeration. There the (nominal) particle size was determined as indicator for presence and size of aggregated CIC. Samples for particle characterization were directly taken from the CIC suspension used in the field experiment, stored in a bottle and aliquots sent to an external laboratory. Samples were approximately two weeks old when being analyzed. When no sonication was done before measurement, the volume-weighted particle size distribution showed a medium size of 4.4 µm with a d_{10} of 0.7 µm and a d_{90} of 15.4 µm. After sonication of the sample in the sonication bath of the SLS measurement device, the mean size determined was 1.6 µm, d_{10} = 0.6 µm and d_{90} = 7.5 µm. After sonication with a Branson Sonifier, the mean particle size was similar to the originally introduced carbon precursor: d_{50} = 1.01 µm, d_{10} = 0.4 µm and d_{90} = 2.7 µm. Different sample treatment methods lead to clearly different results in particle size distribution, i.e. different by a factor of maximal 4.4. This has already been observed in previous studies on CIC (Busch et al., 2014a; Busch et al., 2014b). However, the mean effective particle size varied from 1.0 µm to 4.4 µm, depending on the aging time and the dispersion method. The particle (i.e. agglomerate) size to be assumed as the true one in the field test will be between these two values, as has been found in pre-tests with quantitative evaluation of the sonication methods.

Water characteristic throughout the transport experiment

Dissolved oxygen, electrical conductivity and pH were measured in the suspension storage tanks and in water samples from the extraction well. The CIC-containing container had an electrical conductivity of 1.1 µS/cm, a pH value of 9.8 and the dissolved oxygen content was below the detection limit. The CMC-containing solution in the storage tank had an electrical conductivity of 0.9 µS/cm, a pH value of 10.4 and an oxygen content of 8.55 mg/L.
In water samples from the extraction well, the pH value remained constant at 7.5 ± 0.1 with a maximum of 7.8 and a minimum of 7.45 without any significant trend during time. Electrical conductivity showed a value of 2.03 µS/cm at the start of the experiment, reaching a peak of 2.25 µS/cm after 4 h and then a

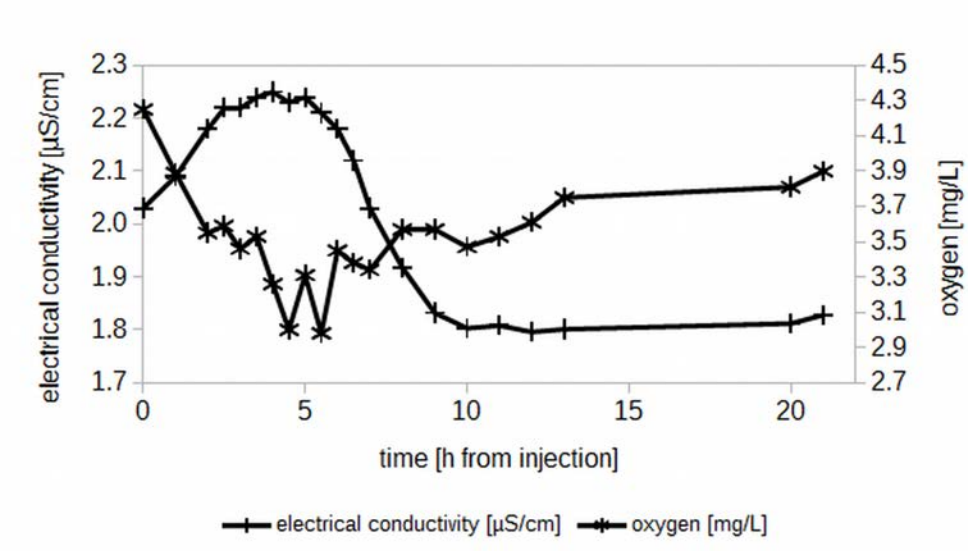

Figure 4.4.: Influence of the injection event on the electrical conductivity and the oxygen concentration in the test aquifer (samples taken from the extraction well).

falling trend stabilizing at 1.8 µS/cm for the rest of the experiment duration. The oxygen content decreased from its initial value of 4.25 mg/L, reached a minimum with about 3.0 mg O_2/L after 5.5 h and then recovering slowly. The peak minimum of oxygen concentration and maximum of electrical conductivity occur similar to the peak arrival time of the tracer in the previous experiment (see Fig. 4.4).

The behavior of both can well be explained by the CIC injection: the oxygen content decreased due to the injection of oxygen-free water from the storage tank, which on one hand may mix with oxygen containing background water and, on the other hand, constitutes only a fraction of the water arriving at one time at the extraction well via the dipole flow field. The increase in electrical conductivity might follow from parallel reactions in the aquifer after injection, either due to the change in aqueous-phase pH during injection of the slightly alkaline CIC suspension and CMC solution or due to reactions of nZVI. Thus, we have indications of CIC reactivity, though this study exclusively focuses on transport issues of CIC, but not reactivity. Nevertheless, it is a clear advantage in respect to comparability that the experiment was done with reactive CIC particles as could be used for remediation.

Figure 4.5.: Image of samples from the field experiment. The bottles in the upper line show images of samples taken every 30 minutes for the first five hours of the experiment (with increasing time from left to right). Beyond five hours the water samples start to lose the black color of the CIC until they are clear again (samples not shown here).

Colloid transport

Colloid transport was observed in the first instance by visual control. The color change to the typical activated-carbon black could be seen in the water samples from the extraction when CIC breakthrough was expected. Fig. 4.5 shows an image of samples taken from the extraction well in 30 minute time intervals after injection of CIC. A clear change in color in the bottles is visible.
In order to quantify the CIC content, the water samples were filtered and the dried remainder was weighted. In Fig. 4.6 the filters are shown that were received by this process. The photos show that at first only a background concentration of particulate sediment matter is trapped in the filter, which can be noticed as a slight grey film on the filter. This was taken as background to be subtracted from the following samples in respect to CIC mass. One hour after injection, a first sign of CIC particle breakthrough is observable by black residuals on the filter. Two hours after the beginning of the experiment the filter is already coated by a black deposit. After that the residuals of CIC blocked the filters for water samples, so the amount of water filtrated had to be decreased.
These images show that there are substantial CIC residues on the filter and therefore it can be concluded that breakthrough was taking place. In Fig. 4.7 the breakthrough curve of CIC as determined from the weight of residues on these filters is presented, as an approximate quantification of CIC breakthrough behavior.
The weight of residues was normalized to 1 L of filtrated water sample. The

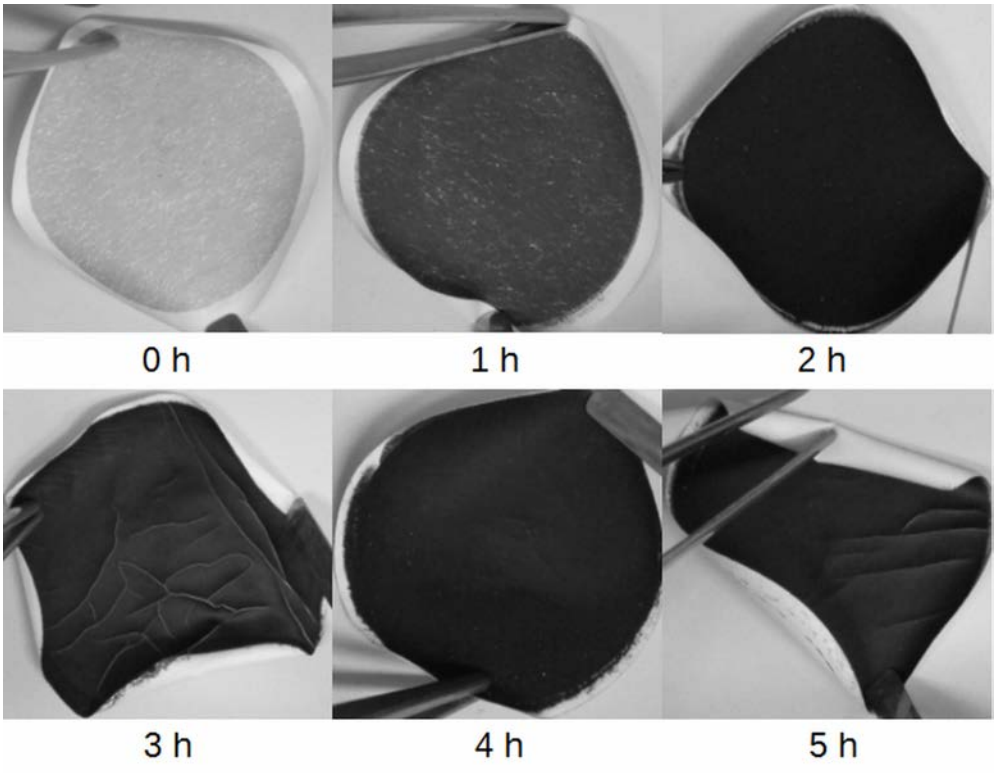

Figure 4.6.: Images of filters taken from hourly samples from one hour before injection of CIC until five hours after injection. Beyond five hours the samples showed declining CIC concentration until the color of the filter was the same as in the beginning.

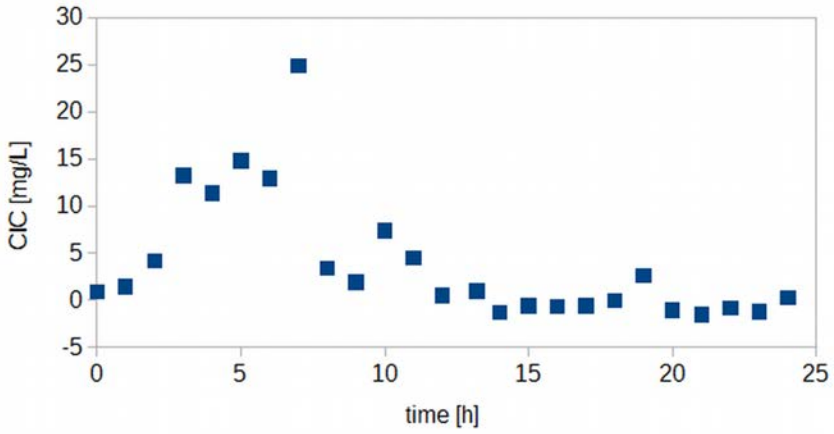

Figure 4.7.: Particle concentration at the extraction well measured as normalized filter residue of water samples taken from the CIC transport experiment. Samples were filtrated through a 0.2 µm mesh filter. Weights were off-set by subtraction of background and filter weight and then normalized to a 1 L sample volume. Shown are samples taken every full hour.

curve starts to increase within one hour after injection and reaches the highest point after seven hours before falling to about zero CIC concentration after twelve hours. The observed trend in measured weight of particulate matter goes along well with the observed color change of the water samples. The peak height corresponds to a CIC concentration of 15 – 25 mg/L.

The calculation of a CIC mass balance between injected and recovered CIC particle mass at the extraction well was attempted by using the complete data set of CIC mass found in the water samples. In sum a mass of 125.3 g CIC was found, which is approx. 12.5% of the nominal amount of CIC injected. However, this value might be underestimating the real recovery rate because the concentration of CIC in the injection suspension was lower than the nominal one due to sedimentation as observed in the CIC tank.

Measured iron concentrations showed a background concentration below the detection limit (0.1 mg/L). A maximum of 0.74 mg/L was reached at 180 minutes, however, with a gap in the iron content data before that. The concentration decreased after that until the measured concentration fell to the detection limit again (Fig. 4.8).

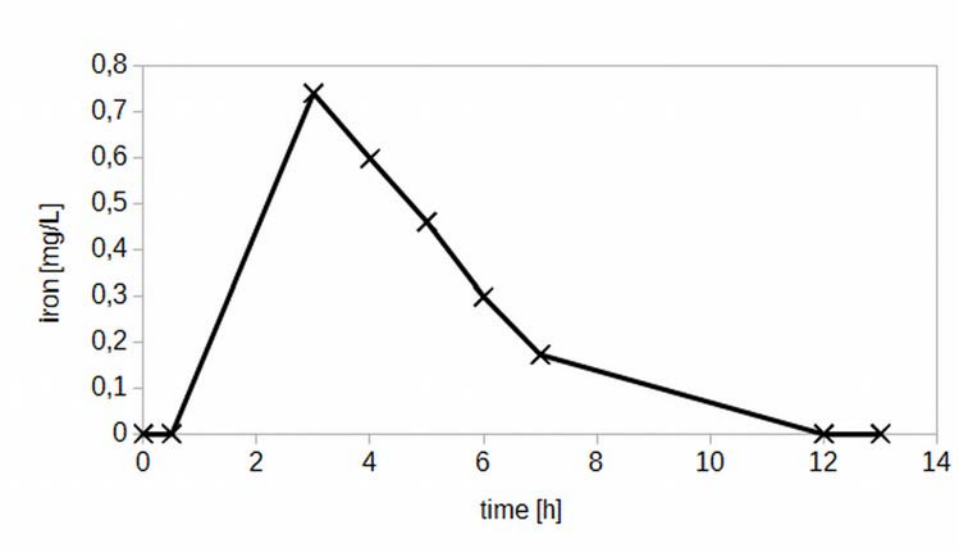

Figure 4.8.: Concentration of total iron detected in water samples taken from the extraction well starting with CIC injection.

The highest iron concentration found nominally corresponds to a CIC colloid concentration of 5 mg/L. This is 3-5 times less than the CIC concentration determined by filtration. There are two possible explanations for the lower amount: firstly, a fractionation of colloids during transport based on iron loading of colloids may take place. A certain fractionation by particle size was already observed in our previous studies on CIC transport, where changes in particle size distribution and colloid surface charge between the original CIC and effluent samples of column experiments and a 2D-laboratory scale experiment were observed (Busch et al., 2014a; Busch et al., 2014b). Secondly, a strong attachment of colloids to the glass walls in the storage bottle could have occurred, where shaking of the sample bottle prior to sampling and even sonication in a sonication bath and stirring with an Ultra-Turrax device is not sufficient for detachment. And indeed we have observed such an effect in our retain samples. Therefore we can conclude on existence of breakthrough of CIC by increased iron loads compared to background concentrations, but without a full quantification based on iron loads in the samples. Nevertheless, also the iron content data support the order of magnitude of CIC arriving at the extraction well. Further lab-scale experiments with mass balance calculations are needed in order to obtain detailed information on the influence of iron

content on CIC particle mobility

4.4. Conclusion

4.4.1. CIC transport

Overall, based on colloid concentrations determined by filtration and iron loads in samples a CIC breakthrough over more than five meters was indisputably found in the natural aquifer. The timing and shape of breakthrough curves of CIC also correspond well with the ones observed of an inert tracer, oxygen content and electrical conductivity of water samples measured in parallel at the extraction well. In general, at least two different scenarios for CIC transport are to be considered: I) the injection period which is characterized by high seepage velocities and high particle and stabilizer concentrations and II) groundwater flow conditions after the end of the injection which are determined by lower seepage velocities (typically in the range of 0.1 - 1 m/d), and dilution of the injected suspension with groundwater leading to a decrease in particle concentration as well as desorption of stabilizer. The conditions applied in the presented field test are representative of the injection period, applying a high seepage velocity and a high concentration of the suspension stabilizer CMC. Further transport of particles under typical groundwater flow conditions, i.e. after infiltration or extraction stopped, will be limited to much lower distances.
Further detailed lab-scale column experiments including the cascading column approach (Comba and Braun, 2012) as well as a field application are needed to study transport and reactivity of CIC and evaluate the optimal applicability in *in situ* remediation, and such are scheduled within the EU-funded NanoRem project (http://www.nanorem.eu) . In respect to reactivity we would like to mention a first field test of CIC performed at a site contaminated with tetrachloroethene (PCE). There preliminary results on CIC reactivity are promising in respect to actual remediation (as part of the FE-NANOSIT-project, http://www.nanopartikel.info/en/projects/completed-projects/fe-nanosit. For example, the concentration of chlorinated hydrocarbons (e.g. PCE, TCE) has been reduced from several ppm to trace levels (ppb) within few days after injection of CIC and formation of C2-hydrocarbons (acetylene to ethane)

confirmed a complete reduction to occur. The lifetime of the injected CIC material for the chemical reaction was estimated to be larger than 2 months (Mackenzie et al., 2014). An advantage for achieving high degradation rates with low amount of nZVI is that the design of CIC offers additionally to the improved transport the sorptive enrichment of pollutants in the neighborhood of the reactive iron centers which can drastically increase the efficient utilization of the iron (Bleyl et al., 2013; Bleyl et al., 2012).
Our study has proven the sufficient spatial coverage achieved for a field application by injection of CIC, since the possible transport ranges are at least in the upper end of the transport ranges demonstrated for pure and nZVI stabilized by polyanionic additives. This leads the way to CIC being applicable for aquifer remediation accounting for CIC reactivity, as demonstrated already in the laboratory (Bleyl et al., 2013; Bleyl et al., 2012) and investigated by ongoing studies in the field (as discussed above).

4.4.2. Methodology of injection

The methodological approach for colloid dispersion seems crucial and should be discussed for an integrated conclusion we made from the observations: two disperser devices Ultra Turrax T25 D were used in 5 L buckets with rather high concentrations of CIC. Since the Ultra-Turrax device is designed for volumes from 1 – 2000 mL. This might not sufficient for complete dispersion of colloids. Here is a high potential for optimization of suspension stability during the injection process. For future experiments we therefore recommend the use of bigger devices integrated into the suspension feed. Also, nitrogen injection rates higher than applied here could produce stronger turbidity, which might have an additional stabilizing effect on the colloid suspension.

4.4.3. Overall conclusions

In this study we observed transport of CIC in a field experiment. Transport was observed between two wells in 5.30 m distance from each other. Independently of amounts of breakthrough, which were quantified to be around 12% of the dispersed amount, transport of a mobile CIC fraction was observed for a distance of 5.30 m in a natural aquifer system. This CIC mobility is representative for injection conditions since the seepage velocity of water was in the range

of 2 m/h. The transport distance found in this study can be regarded as high when compared to those of approaches with nZVI stabilized by polyanionic suspension stabilizers. Therefore, an approach using a carrier particle properly designed with respect to particle size and density, as it has been realized by CIC, might be suitable for further optimization of nZVI delivery for *in situ* groundwater remediation. Also in respect to ecotoxicological impacts the CIC applied here seems to be acceptable. On one hand parallel investigations of CIC toxicity to different organisms indicate low or no toxicity for concentrations realistic in the environment outside the remediation site. And on the other hand from our field experiment it is also possible to conclude that a substantial portion of the applied CIC does not travel beyond the scale of several meters. Thus, the transport properties of CIC in shallow, quaternary aquifers seems to be just in the right range to be essentially limited to a remediation site but also to be able to cover several cubic meters of aquifer with one injection.

4.5. Acknowledgments

This study was supported financially by the German Ministry for Education and Research (Bundesministerium für Bildung und Forschung, BMBF) in the project Fe-NANOSIT (Iron based nanoparticles and nano-composite structures for remediation of ground- and wastewater, FKZ 03X0082). We want to thank Stefan Scholz, Ronald Krieg, Jörg Ahlheim, and Peter Mosig from the Helmholtz Centre for Environmental Research – UFZ, Leipzig, as well as Eyk Hasselwander from G.U.T., Merseburg, Germany, for technical support.

4.6. Literature

Arnold, W.A. and Roberts, A.L., 2000. Pathways and Kinetics of Chlorinated Ethylene and Chlorinated Acetylene Reaction with Fe(0) Particles. Environmental Science & Technology, 34(9): 1794-1805.

Bennett, P., He, F., Zhao, D.Y., Aiken, B. and Feldman, L., 2010. *In situ* testing of metallic iron nanoparticle mobility and reactivity in a shallow granular aquifer. Journal of Contaminant Hydrology, 116(1-4): 35-46.

Beven, K. and Germann, P., 2013. Macropores and water flow in soils revisited. Water Resources Research, 49(6): 3071-3092.

Bleyl, S., Kopinke, F.-D., Georgi, A. and Mackenzie, K., 2013. Carbo-Iron – ein maßgeschneidertes Reagenz zur In-situ-Grundwassersanierung. Carbo-Iron – A Tailored Reagent for *in situ* Groundwater Remediation. Chemie Ingenieur Technik, 85(8):

1302-1311.
Bleyl, S., Kopinke, F.-D. and Mackenzie, K., 2012. Carbo-Iron ® Synthesis and stabilization of Fe(0)-doped colloidal activated carbon for *in situ* groundwater treatment. Chemical Engineering Journal, 191: 588-595.
Busch, J., Meißner, T., Potthoff, A. and Oswald, S., 2014a. Investigations on mobility of carbon colloid supported nanoscale zero-valent iron (nZVI) in a column experiment and a laboratory 2D-aquifer test system. Environmental Science and Pollution Research(21): 10908-10916.
Busch, J., Meißner, T., Potthoff, A. and Oswald, S.E., 2014b. Transport of carbon colloid supported nanoscale zero-valent iron in saturated porous media. Journal of Contaminant Hydrology, 164: 25-34.
Comba, S. and Braun, J., 2012. A new physical model based on cascading column experiments to reproduce the radial flow and transport of micro-iron particles. Journal of Contaminant Hydrology, 140–141(0): 1-11.
De Biase, C. et al., 2011. Treatment of volatile organic contaminants in a vertical flow filter: Relevance of different removal processes. Ecological Engineering, 37(9): 1292-1303.
Elliott, D.W. and Zhang, W.X., 2001. Field assessment of nanoscale biometallic particles for groundwater treatment. Environmental Science & Technology, 35(24): 4922-4926.
Gillham, R.W. and O'Hannesin, S.F., 1994. Enhanced Degradation of Halogenated Aliphatics by Zero-Valent Iron. Ground Water, 32(6): 958-967.
Grieger, K.D. et al., 2010. Environmental benefits and risks of zero-valent iron nanoparticles (nZVI) for *in situ* remediation: Risk mitigation or trade-off? Journal of Contaminant Hydrology, 118(3-4): 165-183.
He, F., Zhang, M., Qian, T. and Zhao, D., 2009. Transport of carboxymethyl cellulose stabilized iron nanoparticles in porous media: Column experiments and modeling. Journal of Colloid and Interface Science, 334(1): 96-102.
He, F., Zhao, D. and Paul, C., 2010. Field assessment of carboxymethyl cellulose stabilized iron nanoparticles for *in situ* destruction of chlorinated solvents in source zones. Water Research, 44(7): 2360-2370.
Henn, K.W. and Waddill, D.W., 2006. Utilization of nanoscale zero-valent iron for source remediation—A case study. Remediation Journal, 16(2): 57-77.
Hoch, L.B. et al., 2008. Carbothermal synthesis of carbon-supported nanoscale zero-valent iron particles for the remediation of hexavalent chromium. Environmental Science & Technology, 42(7): 2600-2605.
Jechalke, S. et al., 2010. Aerated treatment pond technology with biofilm promoting mats for the bioremediation of benzene, MTBE and ammonium contaminated groundwater. Water Research, 44(6): 1785-1796.
Johnson, R.L. et al., 2013. Field-Scale Transport and Transformation of Carboxymethylcellulose-Stabilized Nano Zero-Valent Iron. Environmental Science & Technology, 47(3): 1573-1580.
Laumann, S., Micić, V., Lowry, G.V. and Hofmann, T., 2013. Carbonate minerals in porous media decrease mobility of polyacrylic acid modified zero-valent iron nanoparticles used for groundwater remediation. Environmental Pollution, 179: 53-60.
Mackenzie, K., Bleyl, S., Georgi, A. and Kopinke, F.-D., 2012. Carbo-Iron An Fe/AC composite As alternative to nano-iron for groundwater treatment. Water Research, 46(12): 3817-3826.
Mackenzie, K., Bleyl, S., Kopinke, F.-D., Doose, H. and Bruns, J., 2014. Tailoring of Carbo-Iron as Alternative to Nanoiron: From Laboratory Design to the First Field -

The Concept and Its Implementation., 9th international conference on remediation of chlorinated and recalcitrated compounds. May 19 – 22, 2014, Monterey, California, USA.
Martienssen, M. et al., 2006. Determination of naturally occurring MTBE biodegradation by analysing metabolites and biodegradation by-products. Journal of Contaminant Hydrology, 87(1–2): 37-53.
Matheson, L.J. and Tratnyek, P.G., 1994. Reductive dehalogenation of chlorinated methanes by iron metal. Environmental Science & Technology, 28(12): 2045-2053.
McMahon, P.B., Dennehy, K.F. and Sandstrom, M.W., 1999. Hydraulic and geochemical performance of a permeable reactive barrier containing zero-valent iron, Denver Federal Center. Ground Water, 37(3): 396-404.
O'Hannesin, S.F. and Gillham, R.W., 1998. Long-term performance of an *in situ* "iron wall" for remediation of VOCs. Ground Water, 36(1): 164-170.
Orth, W.S. and Gillham, R.W., 1995. Dechlorination of Trichloroethene in Aqueous Solution Using Fe0. Environmental Science & Technology, 30(1): 66-71.
Phenrat, T., Saleh, N., Sirk, K., Tilton, R.D. and Lowry, G.V., 2007. Aggregation and sedimentation of aqueous nanoscale zerovalent iron dispersions. Environmental Science & Technology, 41(1): 284-290.
Quinn, J. et al., 2005. Field Demonstration of DNAPL Dehalogenation Using Emulsified Zero-Valent Iron. Environmental Science & Technology, 39(5): 1309-1318.
Rügner, H. et al., 2007. SAFIRA II – Revitalisierungskonzepte für großskalige Boden- und Grundwasserverunreinigungen. Altlasten Spektrum(1/2007): 7-12.
Schrick, B., Hydutsky, B.W., Blough, J.L. and Mallouk, T.E., 2004. Delivery vehicles for zerovalent metal nanoparticles in soil and groundwater. Chemistry of Materials, 16(11): 2187-2193.
Stroo, H.F. and Ward, C.H., 2010. *In situ* Remediation of Chlorinated Solvent Plumes. Springer Science + Business Media, New York, Heidelberg, Dordrecht, London.
Sunkara, B. et al., 2010. Nanoscale Zerovalent Iron Supported on Uniform Carbon Microspheres for the *in situ* Remediation of Chlorinated Hydrocarbons. Acs Applied Materials & Interfaces, 2(10): 2854-2862.
Sunkara, B. et al., 2011. Modifying Metal Nanoparticle Placement on Carbon Supports Using an Aerosol-Based Process, with Application to the Environmental Remediation of Chlorinated Hydrocarbons. Langmuir, 27(12): 7854-7859.
Tiraferri, A. and Sethi, R., 2009. Enhanced transport of zerovalent iron nanoparticles in saturated porous media by guar gum. Journal of Nanoparticle Research, 11(3): 635-645.
Vogan, J.L., Focht, R.M., Clark, D.K. and Graham, S.L., 1999. Performance evaluation of a permeable reactive barrier for remediation of dissolved chlorinated solvents in groundwater. Journal of Hazardous Materials, 68(1-2): 97-108.
Wei, Y.-T. et al., 2010. Influence of nanoscale zero-valent iron on geochemical properties of groundwater and vinyl chloride degradation: A field case study. Water Research, 44(1): 131-140.
Wilkin, R.T., Puls, R.W. and Sewell, G.W., 2003. Long-term performance of permeable reactive barriers using zero-valent iron: Geochemical and microbiological effects. Ground Water, 41(4): 493-503.
Zhan, J.J. et al., 2011. Multifunctional Iron-Carbon Nanocomposites through an Aerosol-Based Process for the *in situ* Remediation of Chlorinated Hydrocarbons. Environmental Science & Technology, 45(5): 1949-1954.
Zhang, H., Jin, Z.-h., Han, L. and Qin, C.-h., 2006. Synthesis of nanoscale zero-valent

iron supported on exfoliated graphite for removal of nitrate. Transactions of Nonferrous Metals Society of China, 16(0): 345-349.
Zhang, W.X., 2003. Nanoscale iron particles for environmental remediation: An overview. Journal of Nanoparticle Research, 5(3-4): 323-332.
Zheng, T.H. et al., 2008. Reactivity characteristics of nanoscale zerovalent iron-silica composites for trichloroethylene remediation. Environmental Science & Technology, 42(12): 4494-4499.

5. Tomographic investigations on mobility of carbon supported nanoscale zerovalent iron (nZVI)

5.0.1. Abstract

Recent developments in tomographic imaging methods have made them an emerging asset in a geoscientific context. Especially three-dimensional imaging technologies, such as X-ray and synchrotron approaches or magnet resonance imaging (MRI), might lead to a deeper understanding of processes in situ, without destruction of samples. Two approaches, synchrotron tomography and MRI, were applied in this study to investigate transport of carbon supported nanoscale zero-valent iron (c-nZVI). C-nZVI was developed as nano-composite material for environmental remediation. Our studies aims for gaining new information on transport behavior of these colloids. Results of an experiment using MRI suggests a strong straining in the beginning of the column and results of an experiment with synchrotron imaging suggests straining of the bigger sized fraction of colloids at pore throats. Comparison with previous experiments showed potential good applicability of these two methods: In previous studies, strong straining in column experiments was observed using carbon detection methods in a column experiment and a 2D-aquifer test system. Visualization of transport using MRI could reproduce these results with an iron sensitive measurement and therefore confirms the results independently from the detection method. Additionally it was shown in previous studies that colloid size distribution changes towards smaller particles in column experiments. Results from synchrotron imaging were able to explain this change in colloid size distribution by filtration at pore throats. Therefore tomographic methods were able to add new information to the existing knowledge on c-nZVI transport.

5.1. Introduction

Advantages in imaging technologies have recently led to numerous successful applications in soil and plant sciences: Those were made using X-ray computed tomography, synchrotron microtomography, neutron imaging, magnetic resonance imaging, geophysical imaging tools, and other tomography techniques (Anderson and Hopmans, 2013). Several reviews are available and present today's possibilities and possible future developments of imaging technologies in geoscientific contexts (Bayer et al., 2010; Nestle et al., 2002; Werth et al., 2010). Three-dimensional imaging technologies seem to be of special interest, because they might lead to deeper understanding of *in situ* processes without sample destruction.

5.1.1. Synchrotron observation

X-Ray technologies have been used for several decades in geoscientific contexts. Wildenschild et al. (2002) presented three usable X-ray systems in geoscientific contexts: Industrial tube X-ray which rotates the sample in front of the beam and produces slices of 0.4 mm thickness. Secondly, usable systems are medical X-ray scanner, which can produce highest resolution between 100 and 500 µm at energy ranges of 85 to 130 keV. Horizontal slides are bigger and can produce a slice thickness of 1 to 2 mm. The third possible system is the application of synchrotron X-ray systems, which can offer resolutions in the low µm range. Ketcham and Carlson (2001) have classified X-ray technologies by the scale of observation and resolution (Tab 5.1).

Type	Scale of observation	Scale of resolution
Conventional	m	mm
High resolution	dm	100 µm
Ultra-high resolution	cm	10 µm
Microtomography	mm	µm

Table 5.1.: Classification of X-ray technologies in terms of scale and resolution according to Ketcham and Carlson (2001).

The application of x-ray tomographic (microtomographic) imaging based on synchrotron radiation is applied in this study. Reviews with detailed physical background information on synchrotron technologies are available from

Kinney and Nichols (1992) and Margaritondo et al. (2008). In geosciences, the most used synchrotron technology is the radiologic approach: X-rays are send through an object and morphology of an object is revealed by the different adsorption rates of various materials (Margaritondo et al., 2008).
Synchrotron radiation has been used for material description of building materials and for quantification of pores (Bentz et al., 2000), for specification of silver and zinc oxide nanoparticles (Scheckel et al., 2010), observation of air-water interfaces in sandy porous media (Costanza-Robinson et al., 2008), pore level imaging of fluid transport (Coles et al., 1998) and the observation of the evolution of pore geometry which derived from colloid transport (Chen et al., 2009).

5.1.2. Magnet resonance imaging (MRI]

Magnet resonance Imaging is based on observation of nuclear spins and their interaction with surrounding media via their magnetic moment under the influence of a magnetic field and radiofrequency impulses.
In medicine, proton MRI has been used for several decades. The information is based on contrast between tissues resulting from differences in relaxation times of proton spins. Paramagnetic contrast agents can produce and enhanced signal. MRI was also used already to observe iron concentrations, e.g. for iron loads in heart tissue (Anderson et al., 2001), liver tissue (Gandon et al., 2004), other tissue (Brittenham and Badman, 2003; Kim et al., 2001), or for observation of iron oxide nanoparticles as MRI contrast agent (Babes et al., 1999). In a geoscientific context, MRI has been used since the 1970ies (Gummerson et al., 1979; Prebble and Currie, 1970). It was used to observe analysis of nickel concentrations around plant roots (Moradi et al., 2010) or in porous media (Moradi et al., 2008). Water flow has been observed in glass bead or sand filled column experiments (Deurer et al., 2002; Herrmann et al., 2002), and iron release from sand into pore water (MitreiTer et al., 2010), or flow from water with different tracers, e.g. salt, gadolinium or model contaminants (Chen et al., 2002; Haber-Pohlmeier et al., 2010; Nestle et al., 2008; Oswald et al., 2002; Simpson et al., 2007). Furthermore, there are studies on sorption and release of heavy metals (Nestle et al., 2003), but the number of studies on colloid transport is still very limited.

For observation of colloid transport, it could be interesting, whether the iron in CIC can be observed and agglomerations can be found. One study by Ramanan et al. (2011) already observed transport of medical nanoparticles in heterogeneous porous geological media, in this case quartz with a mean diameter of 3.5 mm grain size. Another interesting study using MRI for observation of transport was performed by Amitay-Rosen (2005), in which 12 µm sized PFTE colloids were pumped through a column filled with monodisperse polystyrene beads. Straining, deposition, and detachment of colloids were observed; additionally, changes in porosity and pore water velocity were observed in relation to time.

5.1.3. Objects of study

In this study carbon supported nanoscale zero-valent iron (c-nZVI), a novel nanocomposite material for environmental remediation, is subject of investigation. Application of nanoscale zero-valent iron (nZVI) has been proven to be a useful tool for environmental remediation (Comba et al., 2011). Currently, the main limitation for application of this technology is fast agglomeration and sedimentation, which results in limited mobility (Johnson et al., 2013; Laumann et al., 2013; Phenrat et al., 2007; Schrick et al., 2004). According to filtration theory, bigger colloids with a size around 1 µm might be more mobile than nanoscale ZVI in environmental aquifer systems (Tufenkji and Elimelech, 2004; Yao et al., 1971). C-nZVI has been developed for this reason; the material consists of a carbon carrier colloid, which contains nZVI (Bleyl et al., 2013; Bleyl et al., 2012; Mackenzie et al., 2012) and is most likely more mobile than nZVI (Busch et al., 2014a; Busch et al., 2014b; Busch et al., 2014c).
Aim of this study is the application of synchrotron tomography for visualization of colloid deposition in porous media and furthermore the development of a detection and quantification method for c-nZVI using MRI. Furthermore, this study aims for observation of transport processes in a column experiment. Results from the measurements are compared qualitatively to previous column experiments with an alternative detection method.

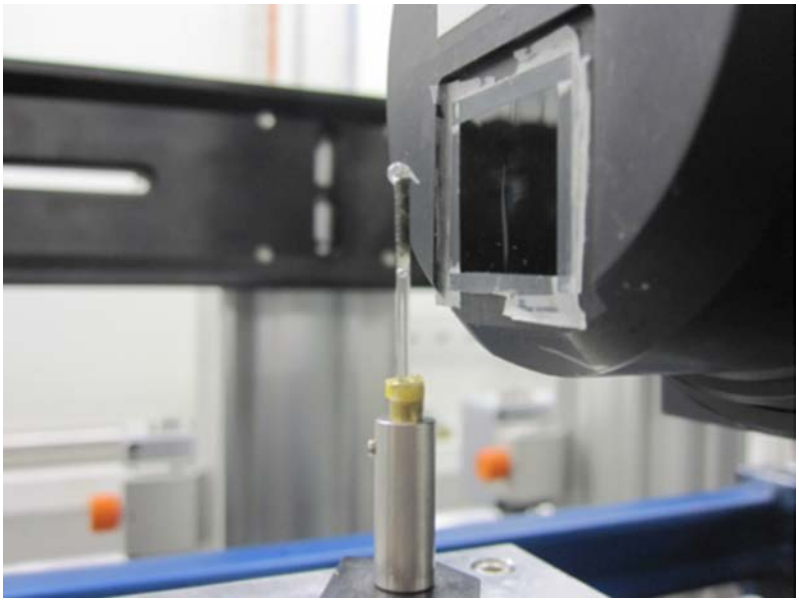

Figure 5.1.: Image of a sample positioned at the sample holder in front of the camera. The image was taken from an experiment within the set of experiments, where the presented results were obtained.

5.2. Materials and Methods

5.2.1. Synchrotron observation

Samples were prepared by filling the tip of a pipette with sand of 0.3 mm grain size or glass beads. A sample of aged Carbo-Iron colloids, the same charge as presented in a study by Busch et al. (2011) was prepared as follows: Carboxymethyl cellulose (CMC) was diluted in deionized water by sonication in an sonication bath, and afterwards 100 mg c-nZVI was added and diluted by sonication for 30 min. 500 to 600 mL of the suspension was pumped with a peristaltic pump through the pipette at a pumping rate of approx. 3 mL/min. After reaching the needed pumping volume (approximately 500 mL), the needle tip was closed by hot glue and was removed from the pipette. After that, the open end was closed, as well. The sample was glued to a sample holder and put into the position for obtaining images (Fig. 5.1).
All experiments were performed at the TOMCAT (TOmographic Microscopy and Coherent rAdiology experimentTs) beamline at the Paul Scherrer Institute (Villingen, Switzerland). This beamline offers adsorption and phase contrast

imaging with a voxel size range from 0.16 up to 14.8 microns at field of views between 0.42x0.35 mm^2 and 30x30 mm^2, respectively, at an energy level between 8 and 45 keV (http://www.psi.ch/sls/tomcat/, Stampanoni et al. (2006)).
Basic settings were obtaining 1501 images per run. 180° of sample rotation was used for reconstruction. 100 flat images and 10 darks were taken before a projection. A LAG (Lutetium Aluminum Garnet) of 20 mm was used. The coating was mono stripe ruthenium/carbon plating, which is recommended for energy levels smaller than 21 keV. 10 times magnification was used. Within this setup energy levels between 13 and 21 keV can be applied. Energy levels and exposure time were varied for evaluation of the optimal energy for highest contrast between porous medium and colloid. Image post processing was performed using the open source software ImageJ (http://rsb.info.nih.gov/ij/).

5.2.2. MRI

Experiments were performed in order to assess mobility of CIC in a laboratory sized transport experiment using MRI-technology with the aim of being able to observe and reconstruct transport in a three-dimensional way.
Preparation of c-nZVI suspensions was performed the same way as in previous studies (Busch et al., 2014a): Deionized and deoxygenized water was used to dissolve a defined amount of 200 mg/L carboxymethyl cellulose (CMC). Defined amounts between 10 mg/L and 1000 mg/L of CIC with a mean diameter of 2.4 µm were added and dispersed by an Ultra-Turrax T 25 digital (IKA, Staufen, Germany) at 24,000 rpm for 30 minutes. Samples for calibration and the transport experiment were prepared in the laboratory and brought to the external laboratory for measurements.
Several porous media including various kinds of glass beads and different sands were tested for applicability. Glass was used as delivered by the manufacturer, sand was washed with acid and base washing as done in previous experiment (Busch et al., 2014b) and afterwards cleaned with magnetic sieving, similar as Nestle et al. (2003) have done it in their study. A 1.2 Tesla magnet was used to remove magnetic particles present in the porous medium by pouring dry sand over the surface of the magnet.
For calibration one blank sample and six samples of c-nZVI suspensions with concentrations between 10 mg/L and 1000 mg/L were stored in a 250 mL

PU-HD bottle (60 mm diameter and 125 mm height) and filled with porous media similar to the filling of columns in the previous experiment.
The transport experiment was performed in a 250 mL PU-HD bottle, which was prepared with a tube inlet at the bottom of the bottle and another in the head end cap. The bottle was filled with deionized and degassed water and closed. In the transport experiment, the bottle was put in a holder and c-nZVI suspension was pumped through the container from bottom to top, similar to column experiments in the previous study.
Samples were brought to a MRI-laboratory in a local hospital (Ernst von Bergmann Klinik, Potsdam, Germany) and measured with a Magnetom Avato 1.5 Tesla MRI device from Siemens (Siemens Healthcare Diagnostics GmbH, Eschborn, Germany). Several methods including HASTE (Half Fourier Acquisition Single Shot Turbo Spin Echo), TSE (Turbo Spin Echo), SWI (3D) (Susceptibility Weighted Imaging), FLASH (Fast Low Angle Shot) and several configurations of the localizer method (a fast default methods to check correct positioning) were tested as techniques for obtaining images from the samples. Images were given from the MRI device in the DICOM (Digital Imaging and Communications in Medicine) format, which is a standardized container format for meta information and the original image in a format, which is technically similar to .TIFF, if uncompressed, or .JPG, if compressed, standards. Images were organized with the programs MicroDicom (http://www.microdicom.com/) and syngo fast view (http://www.healthcare.siemens.com). Image processing was performed in ImageJ and FIJI and the additional "TUDOR Dicom package for Dicom view and manipulation" in ImageJ and FIJI (http://fiji.sc/Fiji). Image processing was performed in several steps. At first the images were calibrated according to the results of the calibration series, then the image contrast was increased (calibration was not touched during this process). After that, the image was adjusted in size and at last a different color palette was chosen to change from gray values to a color palette for better visibility differences in signal intensity.

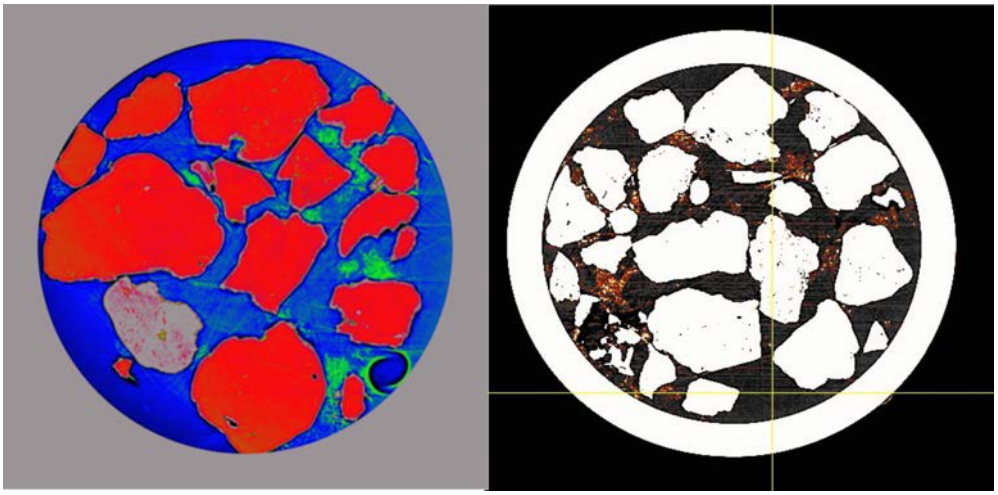

Figure 5.2.: Horizontal slices through the tomographies of two samples. In one image, the sand grains forming the porous medium are visible in red and show a well-defined surface. Water in the pore space is represented by blue color in the first image. Colloids are in green color. An imaging reconstruction artefact is visible at the lower right side of the image. The glass body of the pipette has been cut out of the image. In the second image, sand grains and glass walls are colored white and c-nZVI Colloids are colored in yellow and red. Water is colored black in the column. In both images the image size is 1 mm in each direction.

5.3. Results and discussion

5.3.1. Synchrotron radiation

From all tested energy levels and exposition times, best results in contrast were obtained at the lowest possible energy level of 13 keV and for an exposure time of 180 ms. Several porous media were tested and sand grains showed best properties for the experimental set-up. Blank experiments were performed for quality control to ensure identification of iron in the images. In comparison to blank images, iron loads could be identified by different contrast to porous media and the absence of typical structures in the blank images.
Figures 5.2 and 5.3 show slices through the datasets, which were obtained after image processing and recoloring. Iron is visible in some of the pore spaces in between the sand grains. This can be approved in 3D view, as well. This result suggests that a share of the colloids, which were sent through the column, was

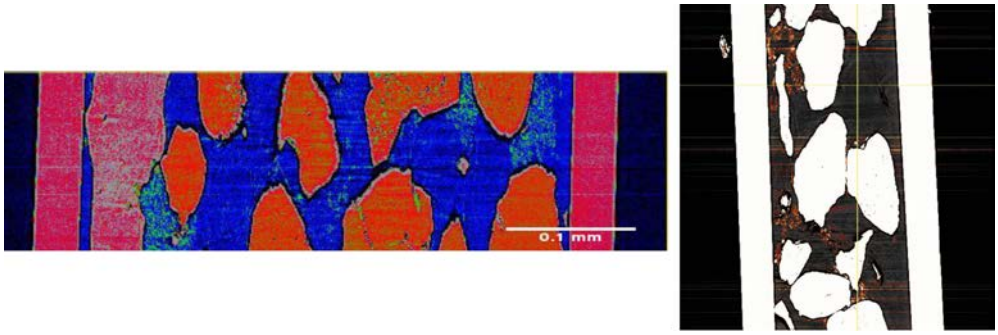

Figure 5.3.: Two horizontal slices through a layer of images from two samples. In one image, porous media is visible in red and shows sand grains. Water in the pore space is represented by blue color. Colloids are in green color. The glass body of the pipette is visible as the left and right border. In the second image, sand grains and glass is colored white, c-nZVI colloids are colored and water is black in the column.

retained at pore throats as larger c-nZVI agglomerates.

If particles were retained at pore throats, it can be assumed, that they are too big for passing them. This mechanism gives a better explanation than other factors, which lead to colloid retention, as discussed in the introduction of this thesis.

Previous studies (Busch et al., 2014a; Busch et al., 2014b) have already shown that particle size distribution of c-nZVI changes during transport experiments in columns and 2D-aquifer tank experiments. These studies showed, that all colloids, which exceed a certain size were filtrated and were not in the column effluent anymore. This could be the same here in this study. These results are according to colloid filtration theory (Tufenkji and Elimelech, 2004; Yao et al., 1971), which states, that colloids with a size above a certain limit are not mobile in porous media.

Results from this study are not progressed enough to determine definitely, which fraction of the colloids remain in the porous media and which pass through the porous media. However, the results suggest that results from the previous studies in column experiments and a 2D aquifer experiment, which were derived with other methods, could be supported by application of this method e.g. for observation of filtration of the biggest fraction of colloids, which remains at the pore throats of a porous medium.

5.3.2. MRI

Several methods were tested and the best signal for a c-nZVI suspension in porous media was found with a Low Flip Angle MRI sequence. Within this sequence, the best contrast was derived in sand (0.1-0.5 mm grain size) with a repetition time (TR) of 7.0 ms, an echo time (TE) of 2.95 ms and a flip angle of 20°. The TE and TR times of the measurement were limited by the MRI device; both times were the shortest possible. Based on the properties of the iron, shorter TR and TE might increase the contrast. In Fig. 5.4 the visual output of a calibration series is shown in a recolored image.
The signal intensity was given by the MRI device in terms of gray values in the images. Regions of interest (ROI) were defined in the images and mean values were determined. Calibration from mean values is shown in Fig. 5.5. The gray value from the highest concentration standard is very close to the gray values from the area outside the bottles. Hence, this concentration was not taken into account for calibration, even though the value behaves linear with the other (lower) values.
Random noise was present within the ROI. This random noise is inherent to the experimental setup: The pixels are in a size range, where the porous medium cannot be optically dissolved and distinguished clearly from pore space. Therefore every pixel represents a mixture of grains of the porous medium and pore space, which is filled with c-nZVI suspension. Noise varies between 2% and 23% of the average value in the ROI.
A breakthrough experiment was performed in sand as porous medium. Here, a c-nZVI suspension was pumped vertically against gravity into the column-like bottle. Transport was observed by MRI imaging every ten minutes for the duration of one hour. Images were taken lateral and transversal to the standing bottle. In Fig. 5.6 results from a breakthrough experiment are shown.
Spreading of c-nZVI into the porous medium is visible in this compilation of images. After ten minutes a relatively small blue patch is visible at the lower end of the bottle. The blue patch gets bigger and darker while the experiment progresses.
According to the calibration, this means that c-nZVI, which was injected into the bottle, fills the area close to the inlet. To investigate the signal intensity distribution, signal intensities were plotted along two defined lines, horizon-

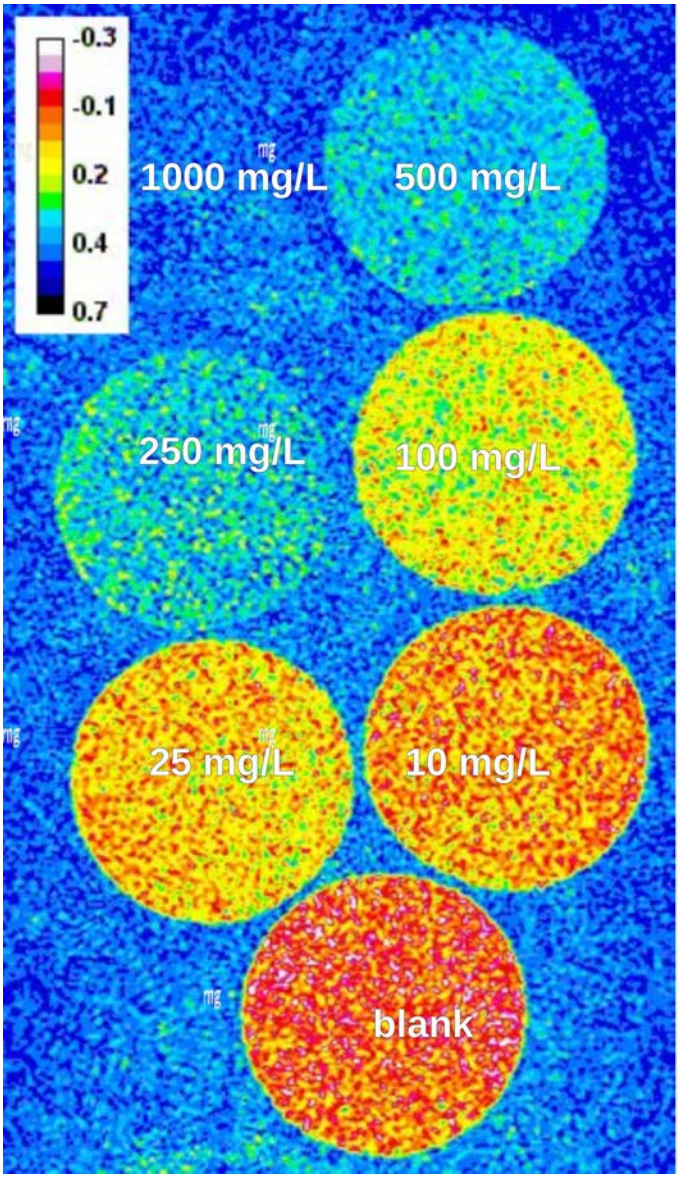

Figure 5.4.: Calibrated and recolored image of a calibration series with c-nZVI concentration ranging from 0 to 1000 mg/l using a Low Flip Angle MRI sequence. The legend shows linear calibration of c-nZVI concentrations [mg/L] using gray values within the auto calibrate function of the image processing tool ImageJ. Concentrations were obtained from a calibration suspension (with the concentrations used for calibration), which was filled in a bottle and afterwards filled up with porous media. Therefore the concentrations reflect on suspension concentration in the pore space.

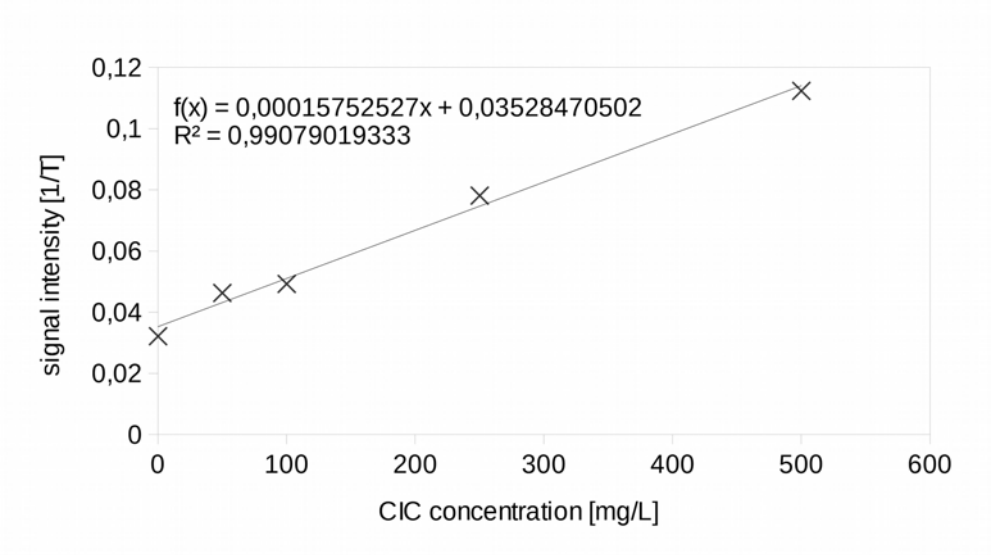

Figure 5.5.: Calibration of the MRI signal. Gray values of MRI images from calibration samples are correlating inverse to the concentration of c-nZVI colloids in the pore space of a porous medium.

tally (Fig. 5.7) and vertically (Fig. 5.8) through the image of the bottle, which taken after 60 minutes. These profiles were put through the dark blue patch, representing the highest c-nZVI concentration in the image.
Results confirm the information from Fig. 5.6, but additionally reflect on noise in signal intensity. Especially in Fig. 5.7 the calculated concentration varies highly between pixels, which are close to each other in the area of highest concentration. Therefore a method for noise reduction should be found in future applications.
In this study, the c-nZVI distribution in the bottle was limited to close to the inlet of the column. Concentrations decreased with distance from the inlet. This could lead to the interpretation that c-nZVI remains in the first centimeters of the column. In previous studies (Busch et al., 2014a; Busch et al., 2014b), we observed c-nZVI transport in glass columns, which were filled with the same sand. After the experiment, the glass column was opened and distribution of carbon content, and by that the distribution of c-nZVI, was measured. In these studies residuals of c-nZVI were only observed within the first centimeters of the column. This confirms the observation made using MRI. In the previous experiments carbon analysis was used to determine c-nZVI concentration dis-

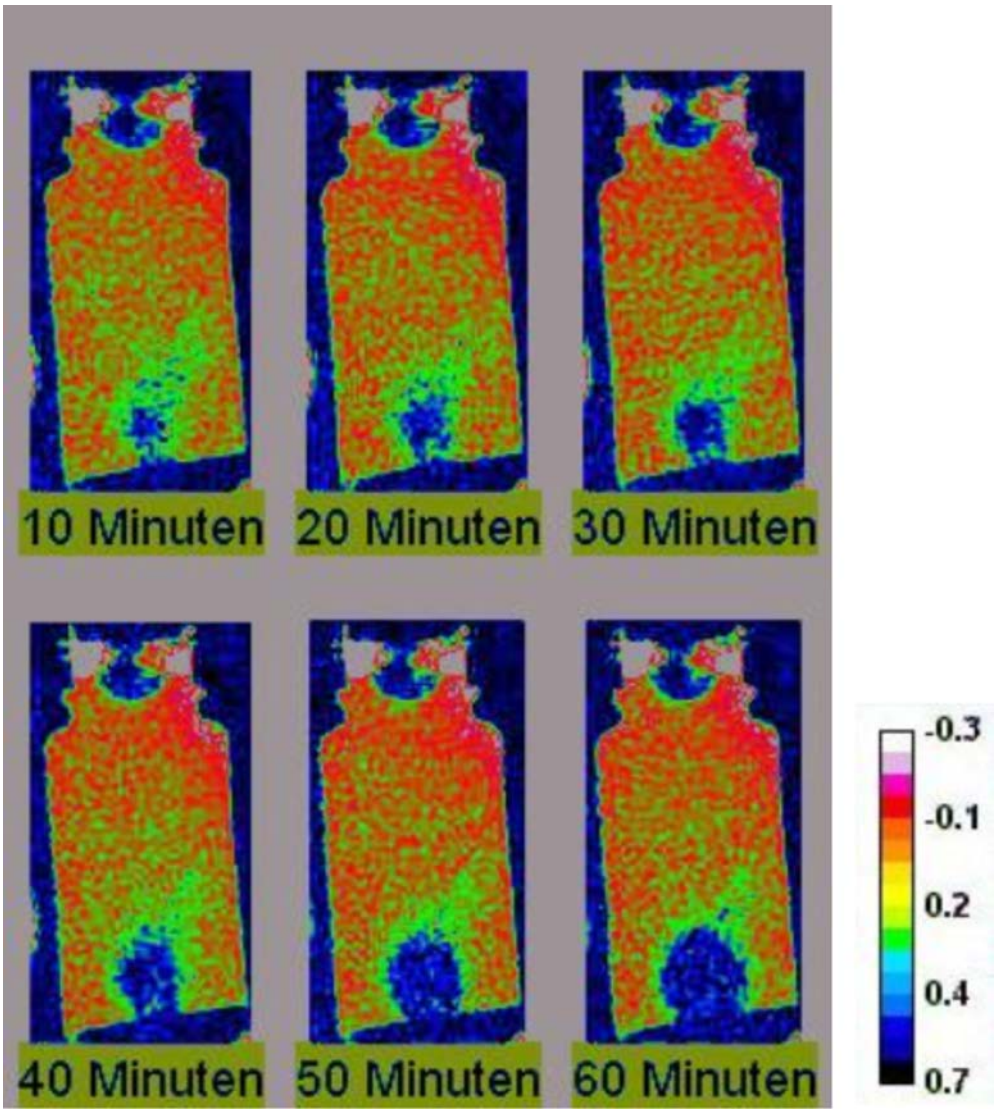

Figure 5.6.: MRI images during a transport experiment. Images were taken every ten minutes. Concentrations are created by the auto calibrate function of ImageJ. All concentrations are in mg/L in the suspension in the pore space.

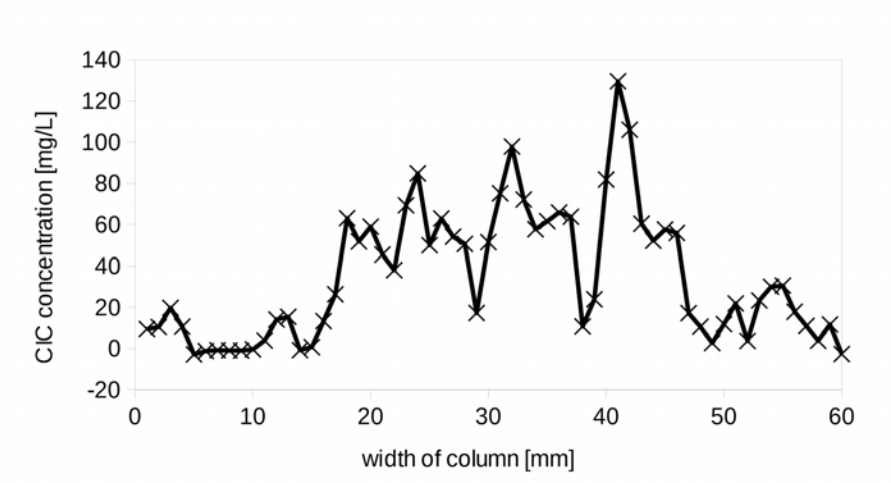

Figure 5.7.: A horizontal line was layed through the highest concentration area of the image "60 minutes" taken from Fig 5.6. The values were calculated by the inverse linear calibration using the values obtained from Fig. 5.4. All values are in mg/L. The concentration in the middle (20 – 45 mm length) of the column is higher than on the left and right side of the main flow path. High variations in the middle of the flow field reflect on noise between the pixels.

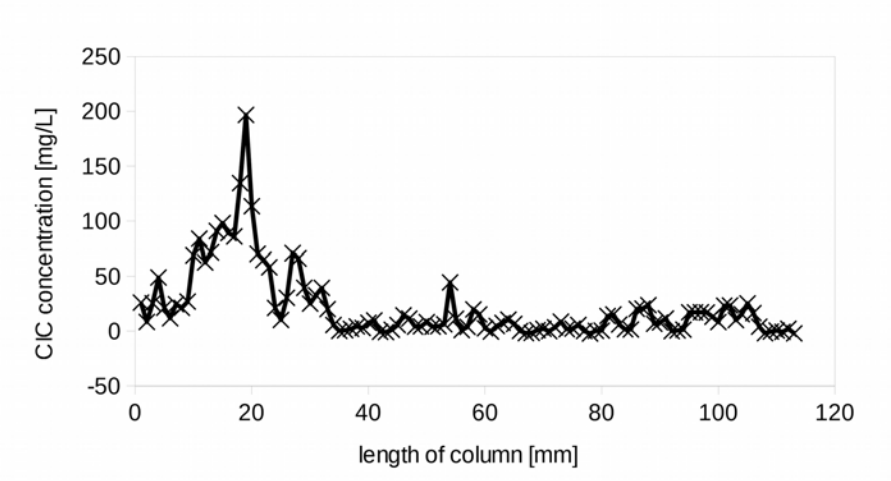

Figure 5.8.: A vertical cut through the highest concentration area of the image "60 minutes" taken from Fig 5.6 vertically through range. The values were calculated by the inverse linear calibration using the values obtained from Fig. 5.4. All values are in mg/L. High variations from one pixel to the next pixel reflect on noise between the pixels.

tribution. Here in this experiment a MRI measurement was used to determine c-nZVI concentrations in a porous medium. Since MRI is sensitive to iron content, a comparison between the detection methods can be made. Results suggest that both detection methods lead to similar results in c-nZVI values and distribution observation. According to that, it can be concluded, that the carbon measurement method, as performed in earlier studies, can directly reflect on the iron concentration and the iron distribution. This could be expected, because the nZVI should be attached strongly to the carbon containing composite material (Mackenzie et al., 2012), and therefore should have been an adequate proxy.

However, a quantitative interpretation of the MRI experiment, as performed and presented here, should be interpreted cautiously for the following reasons: The c-nZVI suspension was prepared in the laboratory and afterwards it was transported to the hospital where the MRI device was located. This leads to uncontrolled agglomeration and sedimentation of the particles during transport and waiting time in hospital. Moreover, agglomeration was never determined in dependence of time. Therefore, we probably might observe retention of colloids that are bigger than the size which was determined. This again would lead to higher filtration due to size effects (Tufenkji and Elimelech, 2004; Yao et al., 1971).

For possible future research several changes and further developments have to be done. At first there is the need to find a way to deagglomerate c-nZVI shortly before the experiment. In the MRI room high frequency technology is not allowed, therefore deagglomeration is neither possible to be performed shortly before the experiment nor during the injection in the transport experiment. Another next investigation, which should be performed, is to assess the influence of the magnetic field of the MRI on particle transport. One could expect that the magnetic field of the MRI may have an influence on transport because of the ferromagnetic properties of the iron in the c-nZVI. An example for such a comparing experiment is to perform a breakthrough experiment in the laboratory for a defined time period, then append a MRI investigation, and at least performing it in the magnetic field of the MRI during a time period of same length. Additionally, the experimental setup could be changed from observation of residuals towards observation of a plume obtained from a impulse injection, instead of injection of a continuous concentration.

5.4. Conclusion and outlook

In this study, transport and retention of c-nZVI colloids has been observed using synchrotron and MRI technology. Colloid transport and retention was observed in column experiments and the results were compared to results from previous studies using carbon analysis. The results from this study show that the applied imaging methods can lead to a better understanding of c-nZVI transport processes and make it feasible to gain information, which might not be reachable with other techniques. Therefore it might be useful to explore the full potential of both methods in the future.

5.5. Acknowledgments

This study was supported by the German Ministry for Education and Research (Bundesministerium für Bildung und Forschung, BMBF) in the project Fe-Nanosit (Iron based nanoparticles and nano-composite structures for remediation of ground- and wastewater). We want to thank the staff from the Helmholtz Centre for Environmental Research (UFZ, Leipzig, Germany) for provision of particles and technical support. Special thanks to Federica Marone and the team of the TOMCAT Beamline at PSI for technical support and help in image postprocessing. Special thanks to Martin Küper and the staff of the radiology department of the Ernst-von-Bergmann Klinik (Potsdam, Germany) for technical support and time at the MRI scanner.

5.6. Literature

Amitay-Rosen, T., Cortis, A. and Berkowitz, B., 2005. Magnetic resonance imaging and quantitative analysis of particle deposition in porous media. Environmental Science & Technology, 39(18): 7208-7216.
Anderson, L.J. et al., 2001. Cardiovascular T2-star (T2*) magnetic resonance for the early diagnosis of myocardial iron overload. European Heart Journal, 22(23): 2171-2179.
Anderson, S.H. and Hopmans, J.W., 2013. Soil-Water-Root Processes: Advances in Tomography and Imaging. Madison, Wi: Soil Science Society of America.
Babes, L. et al., 1999. Synthesis of Iron Oxide Nanoparticles Used as MRI Contrast Agents: A Parametric Study. Journal of Colloid and Interface Science, 212(2): 474-482.
Bayer, J.V., Jaeger, F. and Schaumann, G.E., 2010. Proton Nuclear Magnetic Resonance (NMR) Relaxometry in Soil Science Applications. The Open Magnetic Resonance Journal, 3: 15-26.

Bentz, D.P. et al., 2000. Microstructure and transport properties of porous building materials. II: Three-dimensional X-ray tomographic studies. Materials and Structures, 33(3): 147-153.
Bleyl, S., Kopinke, F.-D., Georgi, A. and Mackenzie, K., 2013. Carbo-Iron – ein maßgeschneidertes Reagenz zur In-situ-Grundwassersanierung. Carbo-Iron – A Tailored Reagent for *In situ* Groundwater Remediation. Chemie Ingenieur Technik, 85(8): 1302-1311.
Bleyl, S., Kopinke, F.-D. and Mackenzie, K., 2012. Carbo-Iron ® Synthesis and stabilization of Fe(0)-doped colloidal activated carbon for *in situ* groundwater treatment. Chemical Engineering Journal, 191: 588-595.
Brittenham, G.M. and Badman, D.G., 2003. Noninvasive measurement of iron: report of an NIDDK workshop. Blood, 101(1): 15-19.
Busch, J., Meißner, T., Potthoff, A. and Oswald, S., 2014a. Investigations on mobility of carbon colloid supported nanoscale zero-valent iron (nZVI) in a column experiment and a laboratory 2D-aquifer test system. Environmental Science and Pollution Research(21): 10908-10916.
Busch, J., Meissner, T., Potthoff, A. and Oswald, S., 2011. Plating of nano zero-valent iron on activated carbon. A fast delivery method of iron for source remediation? Geohydro 2011, Quebec, Canada, August 28-31 2011.
Busch, J., Meißner, T., Potthoff, A. and Oswald, S.E., 2014b. Transport of carbon colloid supported nanoscale zero-valent iron in saturated porous media. Journal of Contaminant Hydrology, 164: 25-34.
J. Busch, Meißner, T., Potthoff, Bleyl, S., A, Georgi, A., Mackenzie, K., Trabitzsch, R., Werban, U., Oswald, S. E., 2014c. A field investigation on the mobility of carbon supported nanoscale zero-valent iron (nZVI) in groundwater. Journal of Contaminant Hydrology (submitted).
Chen, C., Lau, B.L.T., Gaillard, J.-F. and Packman, A.I., 2009. Temporal evolution of pore geometry, fluid flow, and solute transport resulting from colloid deposition. Water Resources Research, 45(6): W06416.
Chen, Q., Kinzelbach, W. and Oswald, S., 2002. Nuclear Magnetic Resonance Imaging for Studies of Flow and Transport in Porous Media. Journal of Environmental Quality, 31(2): 477-486.
Coles, M.E. et al., 1998. Pore level imaging of fluid transport using synchrotron X-ray microtomography. Journal of Petroleum Science and Engineering, 19(1–2): 55-63.
Comba, S., Di Molfetta, A. and Sethi, R., 2011. A Comparison Between Field Applications of Nano-, Micro-, and Millimetric Zero-Valent Iron for the Remediation of Contaminated Aquifers. Water Air and Soil Pollution, 215(1-4): 595-607.
Costanza-Robinson, M.S., Harrold, K.H. and Lieb-Lappen, R.M. 2008. X-Ray Microtomography Determination of Air-Water Interfacial Area-Water Saturation Relationships in Sandy Porous Media. Environmental Science & Technology, 42(8): 2949-2956.
Deurer, M., Vogeler, I., Khrapitchev, A. and Scotter, D., 2002. Imaging of Water Flow in Porous Media by Magnetic Resonance Imaging Microscopy. Journal of Environmental Quality, 31(2): 487-493.
Gandon, Y. et al., 2004. Non-invasive assessment of hepatic iron stores by MRI. The Lancet, 363(9406): 357-362.
Gummerson, R.J. et al., 1979. Unsaturated water flow within porous materials observed by NMR imaging. Nature, 281(5726): 56-57.
Haber-Pohlmeier, S., Bechtold, M., Stapf, S. and Pohlmeier, A., 2010. Water Flow Monitored by Tracer Transport in Natural Porous Media Using Magnetic Resonance

Imaging. Vadose Zone Journal, 9(4): 835-845.
Herrmann, K.-H., Pohlmeier, A., Gembris, D. and Vereecken, H., 2002. Three-dimensional imaging of pore water diffusion and motion in porous media by nuclear magnetic resonance imaging. Journal of Hydrology, 267(3–4): 244-257.
Johnson, R.L. et al., 2013. Field-Scale Transport and Transformation of Carboxymethylcellulose-Stabilized Nano Zero-Valent Iron. Environmental Science & Technology, 47(3): 1573-1580.
Ketcham, R.A. and Carlson, W.D., 2001. Acquisition, optimization and interpretation of X-ray computed tomographic imagery: applications to the geosciences. Comput. Geosci., 27(4): 381-400.
Kim, D.K. et al., 2001. Characterization and MRI study of surfactant-coated superparamagnetic nanoparticles administered into the rat brain. Journal of Magnetism and Magnetic Materials, 225(1–2): 256-261.
Kinney, J.H. and Nichols, M.C., 1992. X-Ray tomographic mictroscopy (XTM) using synchrotron radiation. Annual Review of Materials Science, 22: 121-152.
Laumann, S., Micić, V., Lowry, G.V. and Hofmann, T., 2013. Carbonate minerals in porous media decrease mobility of polyacrylic acid modified zero-valent iron nanoparticles used for groundwater remediation. Environmental Pollution, 179: 53-60.
Mackenzie, K., Bleyl, S., Georgi, A. and Kopinke, F.-D., 2012. Carbo-Iron An Fe/AC composite As alternative to nano-iron for groundwater treatment. Water Research, 46(12): 3817-3826.
Margaritondo, G., Hwu, Y. and Je, J.H., 2008. Nondestructive Characterization by Advanced Synchrotron Light Techniques: Spectromicroscopy and Coherent Radiology. Sensors(8): 8378-8400.
Mitreiter, I., Oswald, S.E. and Stallmach, F., 2010. Investigation of Iron(III)-Release in the Pore Water of Natural Sands by NMR Relaxometry. The Open Magnetic Resonance Journal, 3(1): 46-51.
Moradi, A.B. et al., 2008. Magnetic resonance imaging methods to reveal the real-time distribution of nickel in porous media. European Journal of Soil Science, 59(3): 476-485.
Moradi, A.B. et al., 2010. Analysis of nickel concentration profiles around the roots of the hyperaccumulator plant Berkheya coddii using MRI and numerical simulations. Plant and Soil, 328(1-2): 291-302.
Nestle, N., Baumann, T. and Niessner, R., 2002. Peer Reviewed: Magnetic Resonance Imaging in Environmental Science. Environmental Science & Technology, 36(7): 154A-160A.
Nestle, N., Baumann, T., Wunderlich, A. and Niessner, R., 2003. MRI observation of heavy metal transport in aquifer matrices down to sub-mg quantities. Magnetic Resonance Imaging, 21(3): 345-349.
Nestle, N., Wunderlich, A. and Baumann, T., 2008. MRI studies of flow and dislocation of model NAPL in saturated and unsaturated sediments. European Journal of Soil Science, 59(3): 559-571.
Oswald, S., Scheidegger, M. and Kinzelbach, W., 2002. Time-Dependent Measurement of Strongly Density-Dependent Flow in a Porous Medium via Nuclear Magnetic Resonance Imaging. Transport in Porous Media, 47(2): 169-193.
Phenrat, T., Saleh, N., Sirk, K., Tilton, R.D. and Lowry, G.V., 2007. Aggregation and sedimentation of aqueous nanoscale zerovalent iron dispersions. Environmental Science & Technology, 41(1): 284-290.
Prebble, R.E. and Currie, J.A., 1970. Soil Water Measurement by a Low-Resolution

Nuclear Magnetic Resonance Technique. Journal of Soil Science, 21(2): 273-288.
Ramanan, B., Holmes, W.M., Sloan, W.T. and Phoenix, V.R., 2011. Investigation of Nanoparticle Transport Inside Coarse-Grained Geological Media Using Magnetic Resonance Imaging. Environmental Science & Technology.
Scheckel, K.G., Luxton, T.P., El Badawy, A.M., Impellitteri, C.A. and Tolaymat, T.M., 2010. Synchrotron Speciation of Silver and Zinc Oxide Nanoparticles Aged in a Kaolin Suspension. Environmental Science & Technology, 44(4): 1307-1312.
Schrick, B., Hydutsky, B.W., Blough, J.L. and Mallouk, T.E., 2004. Delivery vehicles for zerovalent metal nanoparticles in soil and groundwater. Chemistry of Materials, 16(11): 2187-2193.
Simpson, M.J., Simpson, A.J., Gross, D., Spraul, M. and Kingery, W.L., 2007. 1H and 19F nuclear magnetic resonance microimaging of water and chemical distribution in soil columns. Environmental Toxicology and Chemistry, 26(7): 1340-1348.
Stampanoni, M. et al., 2006. Trends in synchrotron-based tomographic imaging: the SLS experience, Proc. SPIE.
Tufenkiji, N. and Elimelech, M., 2004. Correlation equation for predicting single-collector efficiency in physicochemical filtration in saturated porous media. Environmental Science & Technology, 38(2): 529-536.
Werth, C.J., Zhang, C., Brusseau, M.L., Oostrom, M. and Baumann, T., 2010. A review of non-invasive imaging methods and applications in contaminant hydrogeology research. Journal of Contaminant Hydrology, 113(1–4): 1-24.
Wildenschild, D., Vaz, C.M.P., Rivers, M.L., Rikard, D. and Christensen, B.S.B., 2002. Using X-ray computed tomography in hydrology: systems, resolutions, and limitations. Journal of Hydrology, 267(3–4): 285-297.
Yao, K.M., Habibian, M.M. and Omelia, C.R., 1971. Water and Wastewater Filtration - Concenpts and Applications. Environmental Science & Technology, 5(11): 1105.

6. General discussion and final conclusions

6.1. Summary of the achievements

The aim of this work was to investigate the mobility of a newly developed colloid for environmental remediation. The material consists of activated carbon that acts as mobile carrier for nZVI. Application of nZVI is currently under investigation as reactive agent for *in situ* remediation of chlorinated compounds in aquifer systems, but nZVI is limited in its applicability by fast agglomeration and sedimentation, which leads to insufficient mobility and distribution in aquifer systems. To overcome these limitations, two major categories of approaches have been suggested in scientific literature: the first approach is coating of the particles with a polyanionic surface, and the other approach is transport of nZVI by a more mobile carrier colloid. In this thesis, the mobility of carbon-colloid supported nZVI was investigated.

The scientific contribution of this dissertation is to investigate and evaluate the mobility of Carbo-Iron, a newly developed nano-composite material consisting of a mobile carrier colloid, which is doped with nZVI. There has been no sound scientific evaluation of mobility of the concept of carbon-supported nZVI, except one published column experiment (Mackenzie et al., 2012). Thus, the scientific progress derived in this dissertation is a survey of mobility of this newly developed material under different conditions in various experimental set-ups. The results allow an integrated evaluation, whether this material is applicable in terms of mobility for *in situ* remediation of chlorinated hydrocarbons.

The research was carried out in several steps. First, proper methods have been identified to perform this task. Several possible methods for detection of carbon-supported nZVI were identified. These methods were detection of single compounds of the material (either detection of carbon or iron via classical chemical methods), separation by material-specific properties (filtration

and weighting of filters and visual observation via colour), or methods based on physical properties of the compound iron (magnetic properties of iron via MRI observation and X-ray radiation radiation via synchrotron tomography). Furthermore, adequate experimental set-ups for experiments were determined. Applicable methods were several column experiments in various sizes, a 2D laboratory aquifer experiment, and finally a field experiment.
The reasoned order of experiments followed from the scale of experimental set-up. Column experiments are the smallest possible set-up for experiments, which were, after successful application, followed by a bigger-scaled laboratory experiment in a 2D laboratory tank experiment set-up. It could be shown that mobility is given under a wide range of physicochemical conditions from smallest to biggest-possible scaled laboratory experiments; therefore a field experiment was performed at last to observe transport under environmental conditions, which was successfully applied. Parallel to these experiments non-invasive methods were applied to observe transport in small-scale column experiments. These results were able to provide additional insight in column-scale experimental set-ups by observation of retention and deposition of colloids. These experiments were able to help to explain the results from the other experiments in this thesis.
Column experiments are capable of investigating the influence of single experimental conditions, as done here with several different porous media and varying physicochemical conditions. This set-up does not allow to draw the final conclusion, as to whether carbon-supported nZVI is applicable for *in situ* remediation, but one can learn which conditions reduce or exclude potential applicability. If there had been no observation of mobility, or very limited mobility, column experiments could at least hint at the problems which need to be solved before further application. However, the general conclusion from these experiments was that this approach shows potential for *in situ* delivery of ZVI. This potential was furthermore investigated in the 2D laboratory aquifer set-up. Next to the observation of a transport distance of more than 1.2 m, no gravitational influence on transport was observed. This is quite an important feature, since otherwise stabilised nZVI is hampered by this characteristic. Based on breakthrough and transport distances which were achieved in laboratory experiments, the next logical step was to apply the newly developed material in a field experiment, which was needed for definitive proof of poten-

tial applicability in terms of *in situ* iron delivery. While the first three studies focused on transport observation, the fourth study was able to give further insight on the previous results. Particle deposition was observed in column experiments via carbon detection and visual observation. MRT experiments were able to repeat these findings based on an iron-sensitive method. Here, the result of high deposition at the beginning of a column was independently approved by a different method. Application of synchrotron-based detection gave a hint at the reason for deposition: since the carrier colloid is based on crushed activated carbon, there is a considerable range in particle size distribution, and immobile colloids were retained at pore throats, which might have led to strong deposition of a rather immobile fraction of colloids at the beginning of the filter section in column and 2D laboratory experiments.
The overall conclusion of this study is that carbon-supported nZVI seems to be mobile under environmental conditions for several meters. Therefore the concept of carbon-colloid supported nZVI seems to be very promising for environmental application in terms of mobility.

6.2. Outlook

Research can only be understood as work in progress and most research opens up more questions than the answers achieved. Therefore this work could be continued with several interesting research questions.
This could begin with additional small-scale laboratory experiments, from basic knowledge on physicochemical interactions to more column experiments on transport with other boundary conditions, more experiments on non-invasive methods, a full-scale field remediation or work on other carrier materials or applications.
The first limitation of the laboratory-scaled experiments which were performed was the application of carbon detection as the method for evaluation of transport. Even though the colloids do substantially consist of carbon, the aim of the colloids is to transport iron. Within this project, it has been proven that carbon and iron are strongly connected (Mackenzie et al., 2012) and one study in this thesis confirmed the result by MRI observation. Since the iron was not measured in the laboratory experiment and for the field experiment only in stored samples, iron-sensitive methods should be applied in future

work to confirm the experiments. Furthermore, more information should be gained on colloid-stabiliser interactions, since there is hardly any information, which hints at behaviour under field conditions. Knowledge on interaction is crucial to learn about environmental behaviour *in situ* and to estimate whether the colloids remain mobile in natural groundwater fluxes or are only mobile during injection. The colloids used in this thesis were synthesised by batch production which led to very individual results of each batch in particle size and hence mobility. Reproducibility in production, and following from that in mobility, should be investigated.

As a methodological continuation of this work, non-invasive measurement technology should be further pursued. Not only new insights on transport of carbon-colloid supported nZVI are possible, but also the full potential of this technology should be explored. Furthermore, it should be attempted to apply this technology in bigger-scaled laboratory experiments for observation of carbon-supported nZVI.

The field experiment in this study was performed with a rather small amount of material. Field-scale remediation would need greater amounts of engineered colloids. Greater amounts could lead to pore clogging, and following from that redirection of groundwater fluxes.

Several approaches for possible carrier colloids have been presented in scientific literature, but there is a big lack in understanding transport properties of these materials. If the class of engineered colloids shows successful applications in the subsurface environment there are many more approaches to test, and new ones which could be developed further.

7. Literature

Adeleye, A., Keller, A., Miller, R. and Lenihan, H., 2013. Persistence of commercial nanoscaled zero-valent iron (nZVI) and by-products. Journal of Nanoparticle Research, 15(1): 1-18.
Aiken, G.R., Hsu-Kim, H. and Ryan, J.N., 2011. Influence of Dissolved Organic Matter on the Environmental Fate of Metals, Nanoparticles, and Colloids. Environmental Science & Technology, 45(8): 3196-3201.
Arnold, W.A. and Roberts, A.L., 2000. Pathways and Kinetics of Chlorinated Ethylene and Chlorinated Acetylene Reaction with Fe(0) Particles. Environmental Science & Technology, 34(9): 1794-1805.
ASTM, 2006. Standard E 2456-06: Terminology for Nanotechnology, West Conshohocken, USA.
Baumann, T., 2010. Nanoparticles in Groundwater – Occurrence and Applications. In: F.H. Frimmel and R. Niessner (Editors), Nanoparticles in the Water Cycle. Springer Berlin Heidelberg, pp. 23-34.
BBodSchG, B.-B., 1998. Gesetz zum Schutz vor schaedlichen Bodenveraenderungen und zur Sanierung von Altlasten. In: B. Deutschland (Editor).
BBodSchV, 1999. Bundes-Bodenschutz- und Altlastenverordnung. In: B. Deutschland (Editor).
Bennett, P., He, F., Zhao, D.Y., Aiken, B. and Feldman, L., 2010. *In situ* testing of metallic iron nanoparticle mobility and reactivity in a shallow granular aquifer. Journal of Contaminant Hydrology, 116(1-4): 35-46.
Birke, V., Ebert, M., Finkel, M., Rosenau, D. and Schad, H., 2006. Anwendungen von durchstroemten Reinigungswaenden zur Sanierung von Altlasten. Teil 1, Universität Lueneburg, Fakultät III (Umwelt und Technik), Campus Suderburg, Suderburg.
Bleyl, S., Kopinke, F.-D., Georgi, A. and Mackenzie, K., 2013. Carbo-Iron – ein maßgeschneidertes Reagenz zur In-situ-Grundwassersanierung. Carbo-Iron – A Tailored Reagent for *in situ* Groundwater Remediation. Chemie Ingenieur Technik, 85(8): 1302-1311.
Bleyl, S., Kopinke, F.-D. and Mackenzie, K., 2012. Carbo-Iron ® Synthesis and stabilization of Fe(0)-doped colloidal activated carbon for *in situ* groundwater treatment. Chemical Engineering Journal, 191: 588-595.
Brant, J., Labille, J., Bottero, J.Y. and Wiesner, M.R., 2007. Nanoparticle Transport, Aggregation, and Deposition. In: M.R. Wiesner and J.Y. Bottero (Editors), Environmental Nanotechnology: Applications and Impacts of Nanomaterials. The McGraw-Hill Companies, Wiesner, M.R., Bottero, J.-Y., 2007. Environmental Nanotechnology: Applications and Impacts of Nanomaterials. The McGraw-Hill Companies, New York, Chicago, San Francisco, Lisbon, London, Madrid, Mexico City, Milan, New Delhi, San Juan, Seoul, Singapore, Sydney, Toronto.
Busch, J., Meißner, T., Potthoff, A. and Oswald, S., 2014a. Investigations on mobility of carbon colloid supported nanoscale zero-valent iron (nZVI) in a column experiment

and a laboratory 2D-aquifer test system. Environmental Science and Pollution Research(21): 10908-10916.
Busch, J., Meißner, T., Potthoff, A. and Oswald, S.E., 2014b. Transport of carbon colloid supported nanoscale zero-valent iron in saturated porous media. Journal of Contaminant Hydrology, 164: 25-34.
Busch, J., Meissner, T., Potthoff, A., Bleyl, S. Georgi, A., Mackenzie, K., Trabitzsch, R., Werban, U., and Oswald, S.E., 2014c. A field investigation on the mobility of carbon supported nanoscale zero-valent iron (nZVI) in groundwater. submitted.
Cai, Z.S., Thomson, N.R., Wilson, R.D. and Oswald, S.E., 2006. A lumped parameter approach to model the treatment of organic contaminants by a granular iron filled fracture. Advances in Water Resources, 29(4): 624-638.
Cantrell, K. and Kaplan, D., 1997. Zero-Valent Iron Colloid Emplacement in Sand Columns. Journal of Environmental Engineering, 123(5): 499-505.
Chen, Z. et al., 2013. Multifunctional kaolinite-supported nanoscale zero-valent iron used for the adsorption and degradation of crystal violet in aqueous solution. Journal of Colloid and Interface Science, 398(0): 59-66.
Cirtiu, C.M., Raychoudhury, T., Ghoshal, S. and Moores, A., 2011. Systematic comparison of the size, surface characteristics and colloidal stability of zero valent iron nanoparticles pre- and post-grafted with common polymers. Colloids and Surfaces A: Physicochemical and Engineering Aspects, 390(1–3): 95-104.
Comba, S., Di Molfetta, A. and Sethi, R., 2011. A Comparison Between Field Applications of Nano-, Micro-, and Millimetric Zero-Valent Iron for the Remediation of Contaminated Aquifers. Water Air and Soil Pollution, 215(1-4): 595-607.
Cook, S., 2009. Assessing the Use and Application of Zero-Valent Nanoparticle Technology for Remediation at Contaminated Sites, U.S. Environmental Protection Agency, Office of Solid Waste and Emergency Response, Washington SC.
Crane, R.A. and Scott, T.B., 2012. Nanoscale zero-valent iron: Future prospects for an emerging water treatment technology. Journal of Hazardous Materials, 211–212(0): 112-125.
Domenico, P.A. and Schwartz, F.W., 1990. Physical and Chemical Hydrogeology. John Wiley & Sons, New York.
Elliott, D.W. and Zhang, W.X., 2001. Field assessment of nanoscale biometallic particles for groundwater treatment. Environmental Science & Technology, 35(24): 4922-4926.
Elschenbroich, C., 2006. Organometallics. Wiley-VCH, Weinheim. Entemann, W., 1998. Hydrogeologische Untersuchungsmethoden von Altlasten. Springer, Berlin, Heidelberg.
European Union, 2011. Comission Recomendation of 18 October 2011 on the definition of nanomaterial [2011/696/EU].
Fleischauer, W. and Falkenhain, G., 1996. Angewandte Umwelttechnik: ein einfuehrender Ueberblick fuer Techniker in Ausbildung und Praxis. Cornelsen Verlag, Berlin.
Foerstner, U., 2008. Umweltschutztechnik. Springer, Berlin, Heidelberg. Franchi, A. and O'Melia, C.R., 2003. Effects of natural organic matter and solution chemistry on the deposition and reentrainment of colloids in porous media. Environmental Science & Technology, 37(6): 1122-1129.
Frimmel, F. and Delay, M., 2010. Introducing the "Nano-world". In: F.H. Frimmel and R. Niessner (Editors), Nanoparticles in the Water Cycle. Springer Berlin Heidelberg, pp. 1-11.
Gilham, R.W., Vogan, J., Gui, L., Ducheme, M. and Son, J., 2010. Iron Barrier Walls for Chlorinated Solvent Removal. In: H.F. Stroo and C.H. Ward (Editors), *In situ*

Remediation of Chlorinated Solvent Plumes. Springer Science + Business Media, New York, Heidelberg, Dordrecht, London.
Gillham, R.W. and O'Hannesin, S.F., 1994. Enhanced Degradation of Halogenated Aliphatics by Zero-Valent Iron. Ground Water, 32(6): 958-967.
Grieger, K.D. et al., 2010. Environmental benefits and risks of zero-valent iron nanoparticles (nZVI) for *in situ* remediation: Risk mitigation or trade-off? Journal of Contaminant Hydrology, 118(3-4): 165-183.
He, F., Zhang, M., Qian, T. and Zhao, D., 2009. Transport of carboxymethyl cellulose stabilized iron nanoparticles in porous media: Column experiments and modeling. Journal of Colloid and Interface Science, 334(1): 96-102.
He, F., Zhao, D. and Paul, C., 2010. Field assessment of carboxymethyl cellulose stabilized iron nanoparticles for *in situ* destruction of chlorinated solvents in source zones. Water Research, 44(7): 2360-2370.
Henn, K.W. and Waddill, D.W., 2006. Utilization of nanoscale zero-valent iron for source remediation—A case study. Remediation Journal, 16(2): 57-77.
Hoch, L.B. et al., 2008. Carbothermal synthesis of carbon-supported nanoscale zero-valent iron particles for the remediation of hexavalent chromium. Environmental Science & Technology, 42(7): 2600-2605.
International Organization for Standardization, 2010. ISO 14887:2000. Sample preparation - dispersing procedures for powders in liquids. ISO, 2008. ISO/TS 27687:2008.
Jiemvarangkul, P., Zhang, W.X. and Lien, H.L., 2011. Enhanced transport of polyelectrolyte stabilized nanoscale zero-valent iron (nZVI) in porous media. Chemical Engineering Journal, 170(2-3): 482-491.
Johnson, R.L., Johnson, G.O.B., Nurmi, J.T. and Tratnyek, P.G., 2009. Natural Organic Matter Enhanced Mobility of Nano Zerovalent Iron. Environmental Science & Technology, 43(14): 5455-5460.
Johnson, R.L. et al., 2013. Field-Scale Transport and Transformation of Carboxymethylcellulose-Stabilized Nano Zero-Valent Iron. Environmental Science & Technology, 47(3): 1573-1580.
Kanel, S.R., Goswami, R.R., Clement, T.P., Barnett, M.O. and Zhao, D., 2008. Two dimensional transport characteristics of surface stabilized zero-valent iron nanoparticles in porous media. Environmental Science & Technology, 42(3): 896-900.
Kanti Sen, T. and Khilar, K.C., 2006. Review on subsurface colloids and colloid-associated contaminant transport in saturated porous media. Advances in colloid and interface science, 119(2-3): 71-96.
Keane, E., 2010. Fate, Transport and Toxicity of nanoscale zero-valent Iron (nZVI) used during superfund remediation. Duke University.
Kobus, H., 1996. The Role of Large-Scale Experiments in Groundwater and Subsurface Remediation Research: The VEGAS Concept and Approach. In: H. Kobus, B. Barczewski and H.-P. Koschitzky (Editors), Groundwater and Subsurface Remediation. Environmental Engineering. Springer Berlin Heidelberg, pp. 1-18.
Koschitzky, H.-P., 2010. Was steckt in den innovative in-situ-Sanierugnsverfahren? Das neue ITVA-Arbeitshilfe gibt auskunft und Hilfestellung. ITVA Fachausschuss H1: Technologien und Verfahren. Arbeitskreis Innovative In-situ-Sanierungsverfahren, GAB - Altlastensymposium 2010 30.06.-01.07.2013, Ingolstadt.
Laumann, S., Micić, V., Lowry, G.V. and Hofmann, T., 2013. Carbonate minerals in porous media decrease mobility of polyacrylic acid modified zero-valent iron nanoparticles used for groundwater remediation. Environmental Pollution, 179: 53-60.
Li, Z., Greden, K., Alvarez, P.J.J., Gregory, K.B. and Lowry, G.V., 2010. Adsorbed

Polymer and NOM Limits Adhesion and Toxicity of Nano Scale Zerovalent Iron to E. coli. Environmental Science & Technology, 44(9): 3462-3467.
Lowry, G.V., 2007. Nanomaterials for Groundwater Remediation. In: M.R. Wiesner and J.Y. Bottero (Editors), Environmental Nanotechnology. Applications and Impacts of Nanomaterials. McGraw-Hill, New York, pp. 297-336.
Lutterodt, G., Basnet, M., Foppen, J.W.A. and Uhlenbrook, S., 2009. The effect of surface characteristics on the transport of multiple Escherichia coli isolates in large scale columns of quartz sand. Water Research, 43(3): 595-604.
Macé, C. et al., 2006. Nanotechnology and groundwater remediation: A step forward in technology understanding. Remediation Journal, 16(2): 23-33.
Mackenzie, K., Bleyl, S., Georgi, A. and Kopinke, F.-D., 2012. Carbo-Iron an Fe/AC composite As alternative to nano-iron for groundwater treatment. Water Research, 46(12): 3817-3826.
Marcus, D.L. and Bonds, C., 1999. Results of the reactant sand-fracking pilot test and implications for the *in situ* remediation of chlorinated VOCs and metals in deep and fractured bedrock aquifers. Journal of Hazardous Materials, 68(1-2): 125-153.
Matheson, L.J. and Tratnyek, P.G., 1994. Reductive dehalogenation of chlorinated methanes by iron metal. Environmental Science & Technology, 28(12): 2045-2053.
McCarthy, P., 2010. Groundwater Contamination by Chlorinated Solvents: History, Remediation Technologies and Strategies In: H.F. Stroo and C.H. Ward (Editors), *In situ* Remediation of Chlorinated Solvent Plumes. Springer Science + Business Media, New York, Heidelberg, Dordrecht, London.
McMahon, P.B., Dennehy, K.F. and Sandstrom, M.W., 1999. Hydraulic and geochemical performance of a permeable reactive barrier containing zero-valent iron, Denver Federal Center. Ground Water, 37(3): 396-404.
Morris, B.L. et al., 2003. Groundwater and its Susceptibility to Degradation. A Global Assessment of the Problem and Options for Management, United Nations Environment Programme, Nairobi, Kenya.
Mueller, N.C. et al., 2012. Application of nanoscale zero valent iron (NZVI) for groundwater remediation in Europe. Environmental Science and Pollution Research, 19(2): 550-558.
Nowack, B. and Bucheli, T.D., 2007. Occurrence, behavior and effects of nanoparticles in the environment. Environmental Pollution, 150(1): 5-22.
Nyer, E.K. and Vance, D.B., 2001. Nano-Scale Iron for Dehalogenation. Ground Water Monitoring & Remediation, 21(2): 41-46.
O'Hannesin, S.F. and Gillham, R.W., 1998. Long-term performance of an *in situ* "iron wall" for remediation of VOCs. Ground Water, 36(1): 164-170.
Odensass, M. and Schroers, S., 2002. Durchstroemte Reinigungswaende - aktueller Kentnisstand. In: L. NRW (Editor). Landesumweltamt NRW, Duesseldorf.
Orth, W.S. and Gillham, R.W., 1995. Dechlorination of Trichloroethene in Aqueous Solution Using Fe^0. Environmental Science & Technology, 30(1): 66-71.
Pelley, A.J. and Tufenkji, N., 2008. Effect of particle size and natural organic matter on the migration of nano- and microscale latex particles in saturated porous media. Journal of Colloid and Interface Science, 321(1): 74-83.
Petosa, A.R., Jaisi, D.P., Quevedo, I.R., Elimelech, M. and Tufenkji, N., 2010. Aggregation and Deposition of Engineered Nanomaterials in Aquatic Environments: Role of Physicochemical Interactions. Environmental Science & Technology, 44(17): 6532-6549.
Phenrat, T. et al., 2010. Transport and Deposition of Polymer-Modified Fe-0 Nanoparticles in 2-D Heterogeneous Porous Media: Effects of Particle Concentration, Fe-0

Content, and Coatings. Environmental Science & Technology, 44(23): 9086-9093.
Phenrat, T., Fagerlund, F., Illangasekare, T., Lowry, G.V. and Tilton, R.D., 2011. Polymer-Modified Fe^0 Nanoparticles Target Entrapped NAPL in Two Dimensional Porous Media: Effect of Particle Concentration, NAPL Saturation, and Injection Strategy. Environmental Science & Technology, 45(14): 6102-6109.
Phenrat, T. et al., 2009. Particle Size Distribution, Concentration, and Magnetic Attraction Affect Transport of Polymer-Modified Fe^0 Nanoparticles in Sand Columns. Environmental Science & Technology, 43(13): 5079-5085.
Phenrat, T., Saleh, N., Sirk, K., Tilton, R.D. and Lowry, G.V., 2007. Aggregation and sedimentation of aqueous nanoscale zerovalent iron dispersions. Environmental Science & Technology, 41(1): 284-290.
Prokop, G. and Schamann, M., 2000. Mamagement of Contaminated sites in Europe, European Environmental Agency, Kopenhagen.
Quinn, J. et al., 2005. Field Demonstration of DNAPL Dehalogenation Using Emulsified Zero-Valent Iron. Environmental Science & Technology, 39(5): 1309-1318.
Raychoudhury, T., Tufenkji, N. and Ghoshal, S., 2012. Aggregation and deposition kinetics of carboxymethyl cellulose-modified zero-valent iron nanoparticles in porous media. Water Research, 46(6): 1735-1744.
Ryan, J.N. and Elimelech, M., 1996. Colloid mobilization and transport in groundwater. Colloids and Surfaces a-Physicochemical and Engineering Aspects, 107: 1-56.
Saleh, N. et al., 2008. Ionic strength and composition affect the mobility of surface-modified Fe-0 nanoparticles in water-saturated sand columns. Environmental Science & Technology, 42(9): 3349-3355.
Schaefer, D., Koeber, R. and Dahmke, A., 2003. Competing TCE and cis-DCE degradation kinetics by zero-valent iron—experimental results and numerical simulation. Journal of Contaminant Hydrology, 65(3–4).
Schrick, B., Hydutsky, B.W., Blough, J.L. and Mallouk, T.E., 2004. Delivery vehicles for zerovalent metal nanoparticles in soil and groundwater. Chemistry of Materials, 16(11): 2187-2193.
Schwister, K., 2010. Taschenbuch der Umwelttechnik. Carl Hanser Verlag, München.
Shellenberger, K. and Logan, B.E., 2002. Effect of molecular scale roughness of glass beads on colloidal and bacterial deposition. Environmental Science & Technology, 36(2): 184-189.
Shi, L.-n., Zhang, X. and Chen, Z.-l., 2011. Removal of Chromium (VI) from wastewater using bentonite-supported nanoscale zero-valent iron. Water Research, 45(2): 886-892.
Shiklomanov, I.A. and Rodda, J.C., 2004. World Water Resources at the Beginning of the Twenty-First Century (International Hydrology Series). International Hydrology Series. Cambridge University Press.
Sohn, K., Kang, S.W., Ahn, S., Woo, M. and Yang, S.-K., 2006. Fe^0 Nanoparticles for Nitrate Reduction: Stability, Reactivity, and Transformation. Environmental Science & Technology, 40(17): 5514-5519.
Stroo, H.F., 2010. Remedial Technology Selection for Chlorinated Solvent Plumes. In: H.F. Stroo and C.H. Ward (Editors), *In situ* Remediation of Chlorinated Solvent Plumes. Springer Science + Business Media, New York, Heidelberg, Dordrecht, London.
Stroo, H.F. and Ward, C.H., 2010. *In situ* Remediation of Chlorinated Solvent Plumes. Springer Science + Business Media, New York, Heidelberg, Dordrecht, London.
Sunkara, B. et al., 2010. Nanoscale Zerovalent Iron Supported on Uniform Carbon Microspheres for the *in situ* Remediation of Chlorinated Hydrocarbons. Acs Applied

Materials & Interfaces, 2(10): 2854-2862.
Sunkara, B. et al., 2011. Modifying Metal Nanoparticle Placement on Carbon Supports Using an Aerosol-Based Process, with Application to the Environmental Remediation of Chlorinated Hydrocarbons. Langmuir, 27(12): 7854-7859.
Swartjes, F.A., 2011. Dealing with Contaminated Sites. Springer, Dordrecht, Heidelberg, London, New York.
Tiraferri, A. and Sethi, R., 2009. Enhanced transport of zerovalent iron nanoparticles in saturated porous media by guar gum. Journal of Nanoparticle Research, 11(3): 635-645.
Tratnyek, P.G., Scherer, M.M., Deng, B. and Hu, S., 2001. Effects of Natural Organic Matter, Anthropogenic Surfactants, and Model Quinones on the Reduction of Contaminants by Zero-Valent Iron. Water Research, 35(18): 4435-4443.
Tufenkji, N. and Elimelech, M., 2004. Correlation equation for predicting single-collector efficiency in physicochemical filtration in saturated porous media. Environmental Science & Technology, 38(2): 529-536.
UBA, 2010a. Stand und Perspektiven des Nachsorgenden Bodenschutzes, Umweltbundesamt, Dessau.
UBA, 2010b. Wasserwirtschaft in Deutschland - Teil 1 Grundlagen. Umweltbundesamt, Dessau-Roslau.
UBA, 2012. Einsatz von Nanoeisen beider Sanierung von Grundwasserschaeden, Umweltbundesamt, Dessau-Roslau.
UNEP, 2006. WWDR2: Water a Shared Responsibility. United Nations World Water Development Report 2, Paris, France.
US House of Representatives, 1980. The Comprehensive Environmental Response, Compensation, and Liability Act (CERCLA). US House of Representatives.
US House of Representatives, 1986. The Superfund Amendments and Reauthorization Act (SARA).
USEPA, 2008. Brownfield and Land Revitaization Programms: Changing American Land and Lives. EPA 560-F-09-519, Solid Waste and Emergency Response, USEPA.
USEPA, 2012. A Citizen's Guide to Permeable Reactive Barriers. EPA Document Number 542-F-12-017, U.S. EPA.
Vogan, J.L., Focht, R.M., Clark, D.K. and Graham, S.L., 1999. Performance evaluation of a permeable reactive barrier for remediation of dissolved chlorinated solvents in groundwater. Journal of Hazardous Materials, 68(1-2): 97-108.
Wei, Y.-T. et al., 2010. Influence of nanoscale zero-valent iron on geochemical properties of groundwater and vinyl chloride degradation: A field case study. Water Research, 44(1): 131-140.
Wilkin, R.T., Puls, R.W. and Sewell, G.W., 2003. Long-term performance of permeable reactive barriers using zero-valent iron: Geochemical and microbiological effects. Ground Water, 41(4): 493-503.
Yao, K.M., Habibian, M.M. and Omelia, C.R., 1971. Water and Wastewater Filtration - Concenpts and Applications. Environmental Science & Technology, 5(11): 1105.
Zhan, J.J. et al., 2011. Multifunctional Iron-Carbon Nanocomposites through an Aerosol-Based Process for the *In situ* Remediation of Chlorinated Hydrocarbons. Environmental Science & Technology, 45(5): 1949-1954.
Zhan, J.J. et al., 2008. Transport Characteristics of Nanoscale Functional Zerovalent Iron/Silica Composites for *in situ* Remediation of Trichloroethylene. Environmental Science & Technology, 42(23): 8871-8876.
Zhang, H., Jin, Z.-h., Han, L. and Qin, C.-h., 2006. Synthesis of nanoscale zero-valent

iron supported on exfoliated graphite for removal of nitrate. Transactions of Nonferrous Metals Society of China, 16(0): 345-349.
Zhang, W.X., 2003. Nanoscale iron particles for environmental remediation: An overview. Journal of Nanoparticle Research, 5(3-4): 323-332.
Zheng, T.H. et al., 2008. Reactivity characteristics of nanoscale zerovalent iron-silica composites for trichloroethylene remediation. Environmental Science & Technology, 42(12): 4494-4499.
Zhuang, Y. et al., 2011. Dehalogenation of Polybrominated Diphenyl Ethers and Polychlorinated Biphenyl by Bimetallic, Impregnated, and Nanoscale Zerovalent Iron. Environmental Science & Technology, 45(11): 4896-4903.

List of Figures

1.1. Different natural and artificial particles and colloids which appear in aqueous systems. The figure was taken from Frimmel and Delay (2010). 8
1.2. Transport mechanisms of colloids according to Yao et al. (1971). 11
1.3. Mechanisms of attachment of colloids and their influence on colloids of different size (Yao et al., 1971). Next to physicochemical drivers such as surface charges, the influence of the mechanisms diffusion, interception and sedimentation are relevant to different extents, depending on colloid size. 12
1.4. Collector efficiency as function of particle size according to (Tufenkji and Elimelech, 2004). Here, an example for a numerical interpretation for collector efficiencies depending on colloid size is presented. 13
1.5. Transport of tracer, stabilised iron nanoparticles and pristine iron nanoparticles in a 2D aquifer container filled with glass beads (Kanel et al., 2008). In this example a vertical flow field from the right to the left side is applied. While transport of tracer (a) follows the flow of water, stabilised nZVI (b) is mobile, but underlies a strong influence of gravity. Unstabilised nZVI (c) is hardly mobile at all under these experimental conditions. . 20
1.6. Comparison of iron and carbon concentration in a CIC transport experiment according to Mackenzie et al. (2012). Iron and Carbon breakthrough curves show the same shape, therefore it can be assumed that CIC is a stable material. 23

2.1. Zeta potential of c-nZVI suspension in the presence of different amounts of CMC. The amount of CMC is described as percentual content related to the c-nZVI Content of 100 mg/L. Average standard deviation is 1.43 mV (See Supporting Material). The experiment was performed at pH 10. 34
2.2. Relative c-nZVI concentration in a sedimentation experiment in dependence to time after the beginning of the experiment. The experiment was performed once without a polyanionic stabilizer and once using a background concentration of 200 mg/L of CMC and contained 1000 mg/L c-nZVI. Duplicates are not presented. 35

2.3. Panel a shows four selected breakthrough curves for a c-nZVI (500 mg/L) suspension containing different amounts of CMC (0, 0.5, 1, 5, and 20% related to 500 mg/l c-nZVI). Panel b shows breakthrough level of c-nZVI after ten exchanged pore volumes of c-nZVI (500 mg/L) in porous medium B1 in relation to the addition of the polyanionic stabilizer CMC. 38

2.4. Particle size distribution of a c-nZVI suspension of a sample from the storage tank, before injection, and samples taken from the column outlet. The sample from the storage tank represents 100% of the concentration, while the samples taken after one and two pore volumes represent a concentration of 8% and 18% at this time in the outflow, and the other samples represent 25 – 36% of the injected concentration. 39

2.5. Breakthrough curves for c-nZVI in different porous media under identical experimental conditions (500 mg/L c-nZVI, 100 mg/L CMC. Used sand types are quartz sand (A: 1-2mm grain size, B1: 0.1-0.5, B2:0.2-1) Aquifer samples (C: 0.2-0.63, D1: 0.2-0.63, D2: 0.63-2) and glass beads (E1: 0.25-0.51, E2 0.75-1mm, see table 1 for detailed information). Sand “B1” is the same sample as sample “20%” in Fig. 2.3. 41

2.6. Breakthrough curves of c-nZVI (1000 mg/L) with a background concentration of CMC (200 mg/L) in the presence of different amounts of NaCl. Sample “0 mM” equals sample “20%” in Fig. 2.3, and “B1” in Fig. 2.5. 43

2.7. Breakthrough curves of c-nZVI (1000 mg/L) with a background concentration of CMC (200 mg/L) in the presence of different amounts of $CaCl_2$. Sample “0 mM” equals sample “0 mM” in Fig. 2.6, “20%” in Fig. 2.3, and “B1” in Fig. 2.5. 44

2.8. Breakthrough curves of c-nZVI (1000mg/L) with a background concentration of CMC (200 mg/L) in porous medium B1 at different pH values. Sample “pH 10” equals sample “0 mM” in Fig. 2.5 and 2.6, “20%” in Fig. 2.3, and “B1” in Fig. 2.5. 45

3.1. Carbon content curve of a sedimentation experiment. 1000 mg/L CIC and 200 mg/L CMC were dispersed inside a glass bottle. CIC content in suspension is shown in relation to time and describes sedimentation of CIC. Data from 2.4 µm sized particles were taken from a previous study (Busch et al. 2014). . 58

3.2. Breakthrough curves for a transport experiment of a CIC suspension of 1000 mg/L CIC and 200 mg/L CMC in a 40 cm glass column filled with medium grained sand. The column was fed for ten exchanged pore volumes with CIC suspension and afterwards with a background solution. The experiment for 0.64 µm sized CIC colloids was performed twice and showed high reproducibility. Additionally, for comparison data for 2.4 µm sized particles are plotted, taken from a previous study (Busch et al. 2014). 60
3.3. Residuals of CIC in porous media of the column experiment. The column was opened after the transport experiment and samples of the porous medium (sand 0.1 – 0.5 mm) were taken for analysis of CIC residuals. Results are presented in form of CIC permille fraction ($m_{CIC}/m_{sediment}$ [mg/g]). 61
3.4. Photos of CIC transport in the 2D-aquifer test system at different time steps during the experiment with a horizontal flow field from left to right. CIC was fed into the middle injection port at the left during the first 420 minutes and observed for 690 minutes. Original images were brightened for better visibility of contrast. 64
3.5. Breakthrough curves of CIC at relevant outflow ports from the 2D-aquifer test system. CIC was injected for 420 minutes at inlet at height of port 4; the other ports were fed with a background solution. After injection of CIC a background solution was injected into all ports. 65
3.6. Particle size distribution of CIC suspension in the stock suspension compared to the ones determined from outlet port 4 at different times during the experiment. 67

4.1. Sketch of the field site. 78
4.2. Tracer breakthrough curve for the breakthrough experiment at the field site using tracer (tracer = fluorescein; m_{tracer} = 5 g; distance between injection and extraction well = 5.3 m; Vfeed = 500 L/h). 82
4.3. Soil samples taken with a sonic drilling approach. The samples were all taken in a distance of approx. 50 cm downstream from the injection well. The middle image shows a sample taken in direct line from injection to extraction well. The other two images were taken 30 cm left and right from the middle sample position. All images show the core area from the gravel layer. . 84
4.4. Influence of the injection event on the electrical conductivity and the oxygen concentration in the test aquifer (samples taken from the extraction well). 86

4.5. Image of samples from the field experiment. The bottles in the upper line show images of samples taken every 30 minutes for the first five hours of the experiment (with increasing time from left to right). Beyond five hours the water samples start to lose the black color of the CIC until they are clear again (samples not shown here). 87

4.6. Images of filters taken from hourly samples from one hour before injection of CIC until five hours after injection. Beyond five hours the samples showed declining CIC concentration until the color of the filter was the same as in the beginning. . . 88

4.7. Particle concentration at the extraction well measured as normalized filter residue of water samples taken from the CIC transport experiment. Samples were filtrated through a 0.2 µm mesh filter. Weights were off-set by subtraction of background and filter weight and then normalized to a 1 L sample volume. Shown are samples taken every full hour. 89

4.8. Concentration of total iron detected in water samples taken from the extraction well starting with CIC injection. 90

5.1. Image of a sample positioned at the sample holder in front of the camera. The image was taken from an experiment within the set of experiments, where the presented results were obtained. 101

5.2. Horizontal slices through the tomographies of two samples. In one image, the sand grains forming the porous medium are visible in red and show a well-defined surface. Water in the pore space is represented by blue color in the first image. Colloids are in green color. An imaging reconstruction artefact is visible at the lower right side of the image. The glass body of the pipette has been cut out of the image. In the second image, sand grains and glass walls are colored white and c-nZVI Colloids are colored in yellow and red. Water is colored black in the column. In both images the image size is 1 mm in each direction. 104

5.3. Two horizontal slices through a layer of images from two samples. In one image, porous media is visible in red and shows sand grains. Water in the pore space is represented by blue color. Colloids are in green color. The glass body of the pipette is visible as the left and right border. In the second image, sand grains and glass is colored white, c-nZVI colloids are colored and water is black in the column. 105

5.4. Calibrated and recolored image of a calibration series with c-nZVI concentration ranging from 0 to 1000 mg/l using a Low Flip Angle MRI sequence. The legend shows linear calibration of c-nZVI concentrations [mg/L] using gray values within the auto calibrate function of the image processing tool ImageJ. Concentrations were obtained from a calibration suspension (with the concentrations used for calibration), which was filled in a bottle and afterwards filled up with porous media. Therefore the concentrations reflect on suspension concentration in the pore space. 107

5.5. Calibration of the MRI signal. Gray values of MRI images from calibration samples are correlating inverse to the concentration of c-nZVI colloids in the pore space of a porous medium. 108

5.6. MRI images during a transport experiment. Images were taken every ten minutes. Concentrations are created by the auto calibrate function of ImageJ. All concentrations are in mg/L in the suspension in the pore space. 109

5.7. A horizontal line was layed through the highest concentration area of the image "60 minutes" taken from Fig 5.6. The values were calculated by the inverse linear calibration using the values obtained from Fig. 5.4. All values are in mg/L. The concentration in the middle (20 – 45 mm length) of the column is higher than on the left and right side of the main flow path. High variations in the middle of the flow field reflect on noise between the pixels. 110

5.8. A vertical cut through the highest concentration area of the image "60 minutes" taken from Fig 5.6 vertically through range. The values were calculated by the inverse linear calibration using the values obtained from Fig. 5.4. All values are in mg/L. High variations from one pixel to the next pixel reflect on noise between the pixels. 110

A.1. Breakthrough curves from a reproducibility experiment. A breakthrough experiment was performed in sand B1 six times under identical conditions (1000 mg/L c-nZVI, 200 mg/L CMC). Mean breakthrough level after ten exchanged pore volumes was 32.5%, standard deviation 4.6 (14%), highest breakthrough value was 37.6%, lowest value 26.4%. XXI

A.2. Carbon content distribution in the porous medium (sand B1) after ten exchanged pore volumes of a 1000 mg/L c-nZVI suspension with 200 mg/L CMC. After injection of c-nZVI suspension the column was washed with CMC containing solution and deionized water for ten pore volumes. Measurement was with a method for solid samples. Result shows strong attachment of colloids in the first centimeter of the column. XXIII
A.3. Particle size distribution of a sample from the stock suspension. Particle size distribution does not follow a Gaussian distribution. In samples from the column effluent, the distribution follows a Gaussian shape. XXIV

B.1. Side view on the 2D-aquifer test system. The numbers of the ports are beginning at the highest port at number 1 and ends with the lowest port at number 7. XXV
B.2. Side view on the 2D-aquifer test system with connected tubes. . XXVI
B.3. Image of the opened column. On the left side, residues of c-nZVI are visible (black color). XXVI
B.4. Residuals of Carbo-Iron in porous media of the column experiment. The column was opened after the transport experiment and samples of the porous media (Sand 0.1 – 0.5 mm) were taken for analysis of CIC residuals. Results represent loading of CIC on porous media ($m_{CIC}/m_{sediment}$ [g/g]). XXVII
B.5. Image from a transport experiment of color tracer with a preferential flow path, which does not cross the porous medium. Here the porous medium is glass beads. XXVIII
B.6. Photos of tracer breakthrough in the 2D-aquifer test system at different time steps during the experiment. Color tracer was fed into the middle injection port for thirty minutes and observed for two hours. Horizontal gridlines were placed along between between the ports on the left and right side at ports 1, 4, and 7. . XXIX
B.7. Residuals of CIC in porous medium of the 2D-aquifer test system.XXIX
B.8. Additional photos on CIC breakthrough. This additional figure was shown originally as figure B.6 in the submitted version of this PhD thesis, but replaced then by the appropriate diagram and caption, as remarked by a review comment. XXX

C.1. Geographical position of Leuna in Germany. Original image taken from http://www.weltkarte.com/uploads/pics/umrisskarte-deutschland.png XXXI
C.2. View on the field site (Foto: Punctum GmbH, 2010). XXXII
C.3. View on the field site (Source: UFZ). XXXIII
C.4. Soil classification of the extraction well. XXXIV

C.5. Residues in all filters. Here values for all filters are shown. In the manuscript only values from each full hour are presented. . XXXIV
C.6. An additional image of samples from the extraction well. The tree bottles on the left side represent samples from one hour before the injection to one hour after injection. The samples on the right side represent samples taken after two hours. XXXV
C.7. Image of the extraction well during the experiment. XXXV

List of Tables

1.1. List with numbers of potentially contaminated sites, listed by type in Europe (Prokop and Schamann, 2000). 2
1.2. Compilation of published studies dealing with mobility of nZVI in field experiments. 19
1.3. Particle characteristics of Carbo-Iron colloids (CIC) (Bleyl et al., 2013; Bleyl et al., 2012; Mackenzie et al., 2012). 23

2.1. List of porous media used in column experiments. The list contains abbreviation, type of porous medium, grain size and supplier. Abbreviations: QS = Quartz sand, AS = Aquifer sample, GB = Glass beads 31

4.1. Compilation of studies investigating on the mobility of nZVI in field studies. 76

5.1. Classification of X-ray technologies in terms of scale and resolution according to Ketcham and Carlson (2001). 98

A.1. Zeta potential and standard deviation for c-nZVI colloids in the presence of different amounts of CMC. XXII
A.2. Zeta Potential of c-nZVI in the stock suspension and after passing the porous media. The concentration in the stock suspension was 1000 mg/L c-nZVI and after passing the column 250 - 360 mg/L. XXII

C.1. Soil classification of the extraction well. XXXII

A. Supporting Material to Chapter 2

Supporting material to J. Busch, T. Meißner, A. Potthoff & S.E. Oswald (2014): Transport of carbon colloid supported nanoscale zero-valent iron in saturated porous media. Journal of Contaminant Hydrology 164 p.25-34

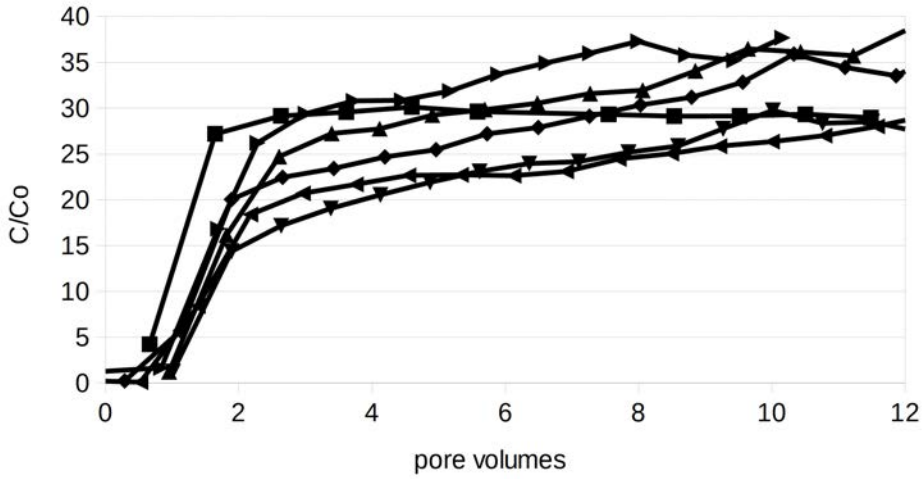

Figure A.1.: Breakthrough curves from a reproducibility experiment. A breakthrough experiment was performed in sand B1 six times under identical conditions (1000 mg/L c-nZVI, 200 mg/L CMC). Mean breakthrough level after ten exchanged pore volumes was 32.5%, standard deviation 4.6 (14%), highest breakthrough value was 37.6%, lowest value 26.4%.

Ma.% CMC	zeta potential [mV]	standard deviation
0	-5,73	5,52
0,25	-23,5	1,33
0,5	-24,1	2,07
0,75	-24,2	0,856
1	-26,8	0,839
1,5	-28,2	0,951
2,5	-29,5	0,759
5	-31,8	1,25
10	-36,7	0,89
20	-43,4	0,502
40	-52,7	0,718

Table A.1.: Zeta potential and standard deviation for c-nZVI colloids in the presence of different amounts of CMC.

sample	zeta potential [mV]
stock susp.	-62.0
1 PV / 22 min	-80.8
2 PV / 35min	-78,4
3 PV / 50min	-77,6
5 PV / 80min	-75,5
7 PV / 100min	-75,9
10 PV / 150min	-75,2

Table A.2.: Zeta Potential of c-nZVI in the stock suspension and after passing the porous media. The concentration in the stock suspension was 1000 mg/L c-nZVI and after passing the column 250 - 360 mg/L.

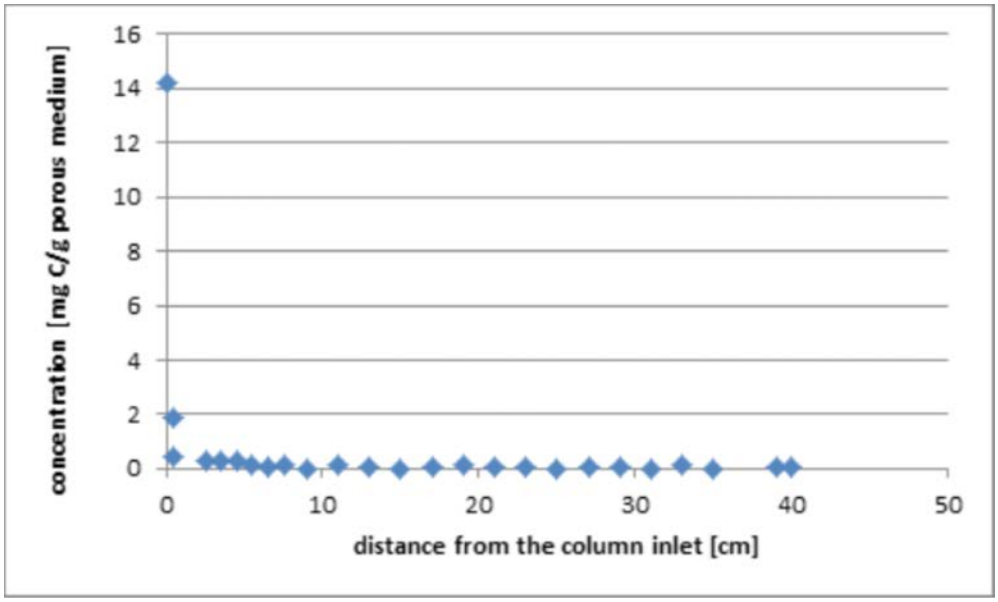

Figure A.2.: Carbon content distribution in the porous medium (sand B1) after ten exchanged pore volumes of a 1000 mg/L c-nZVI suspension with 200 mg/L CMC. After injection of c-nZVI suspension the column was washed with CMC containing solution and deionized water for ten pore volumes. Measurement was with a method for solid samples. Result shows strong attachment of colloids in the first centimeter of the column.

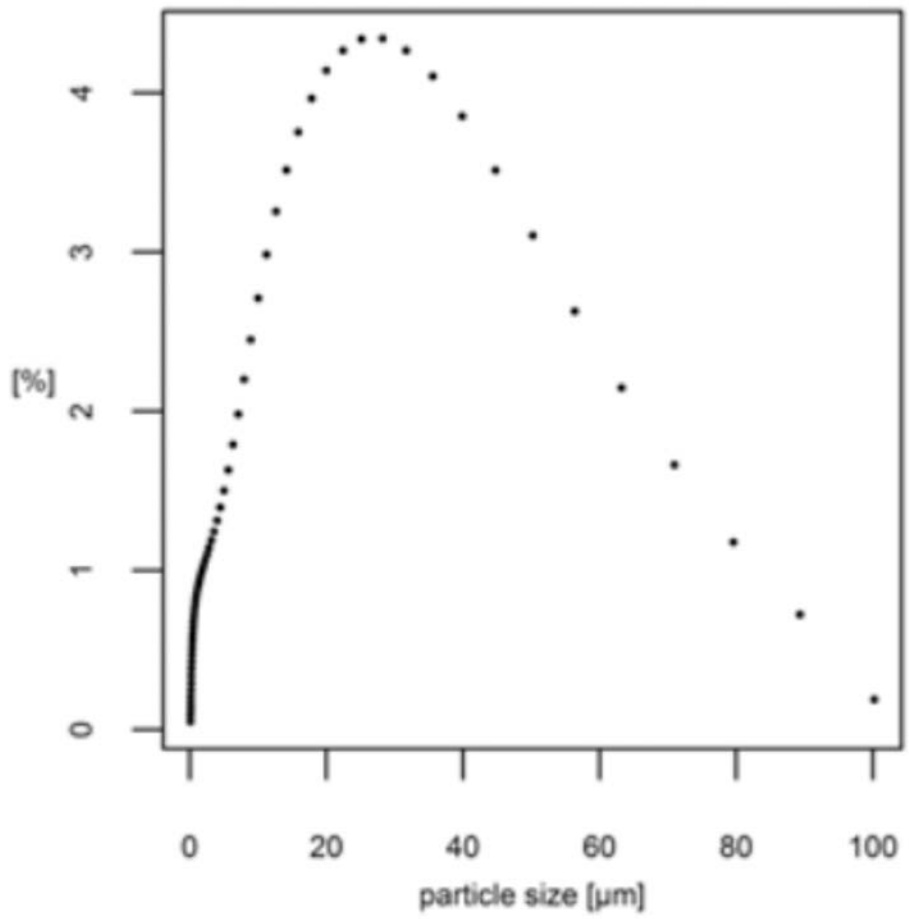

Figure A.3.: Particle size distribution of a sample from the stock suspension. Particle size distribution does not follow a Gaussian distribution. In samples from the column effluent, the distribution follows a Gaussian shape.

B. Supporting Material to Chapter 3

Supporting maaterial to J. Busch, T. Meißner, A. Potthoff & S.E. Oswald (2014): Investigations on mobility of carbon colloid supported nanoscale zero-valent iron (nZVI) in a column experiment and a laboratory 2D-aquifer test system Environmental Science & Pollution Research. (21): 10908-10916

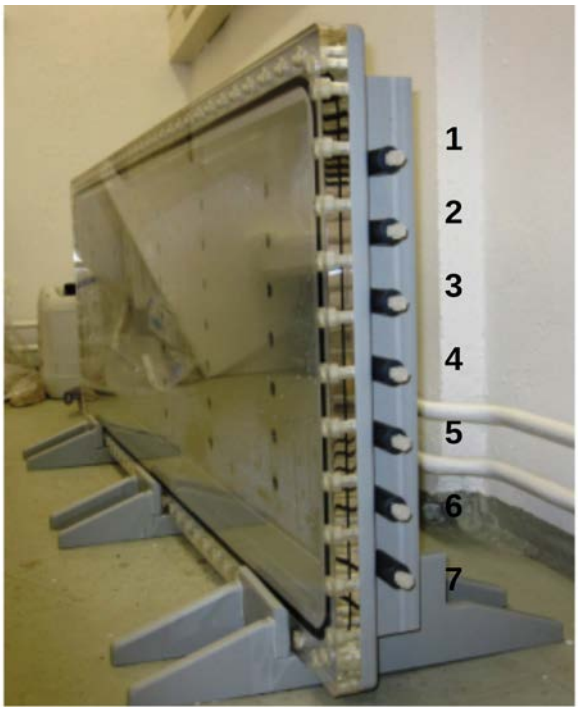

Figure B.1.: Side view on the 2D-aquifer test system. The numbers of the ports are beginning at the highest port at number 1 and ends with the lowest port at number 7.

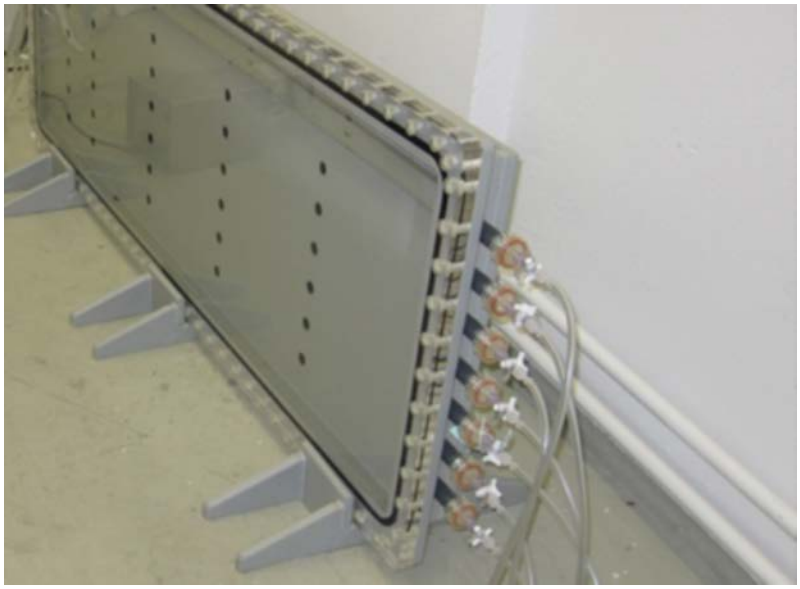

Figure B.2.: Side view on the 2D-aquifer test system with connected tubes.

Figure B.3.: Image of the opened column. On the left side, residues of c-nZVI are visible (black color).

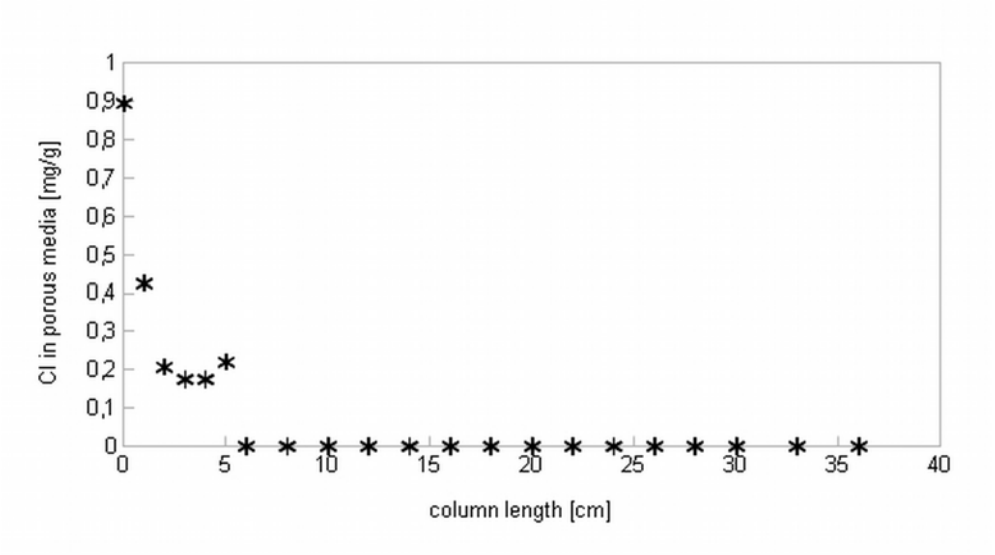

Figure B.4.: Residuals of Carbo-Iron in porous media of the column experiment. The column was opened after the transport experiment and samples of the porous media (Sand 0.1 – 0.5 mm) were taken for analysis of CIC residuals. Results represent loading of CIC on porous media ($m_{CIC}/m_{sediment}$ [g/g]).

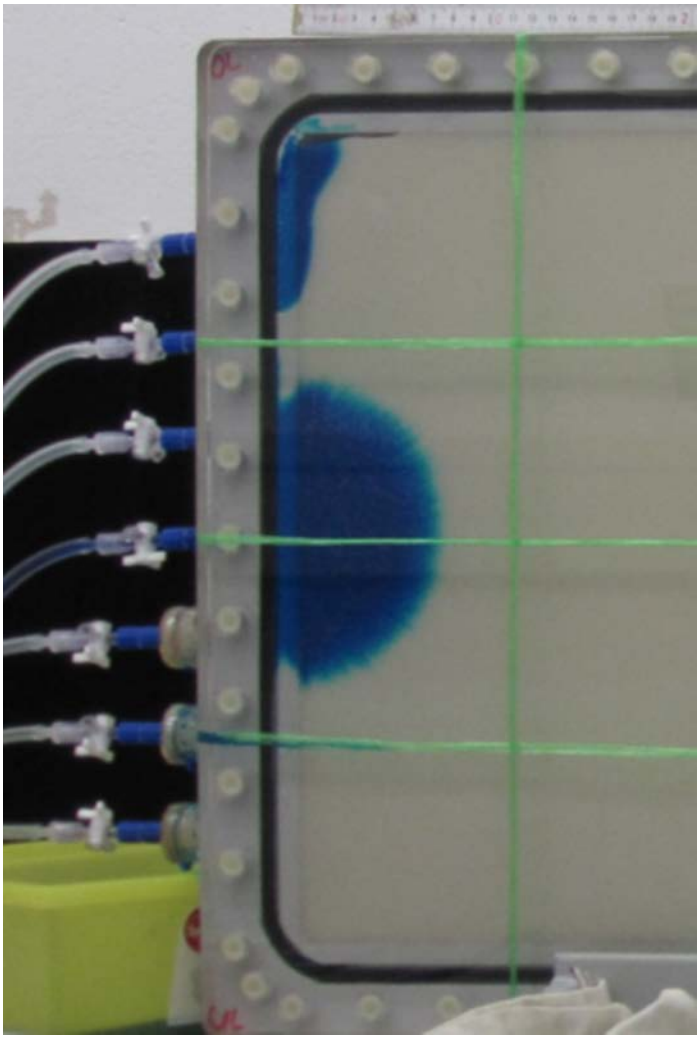

Figure B.5.: Image from a transport experiment of color tracer with a preferential flow path, which does not cross the porous medium. Here the porous medium is glass beads.

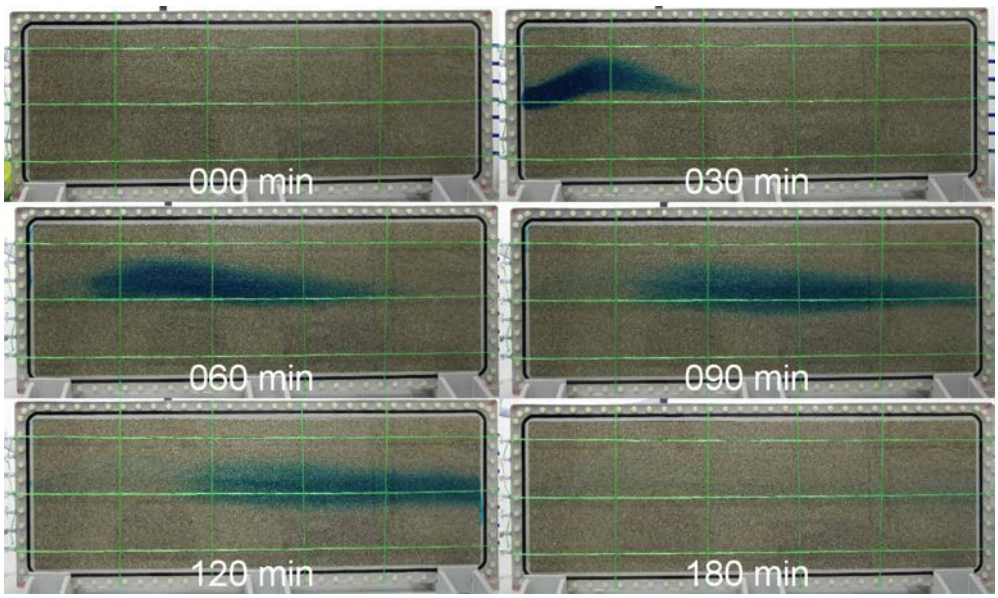

Figure B.6.: Photos of tracer breakthrough in the 2D-aquifer test system at different time steps during the experiment. Color tracer was fed into the middle injection port for thirty minutes and observed for two hours. Horizontal gridlines were placed along between between the ports on the left and right side at ports 1, 4, and 7.

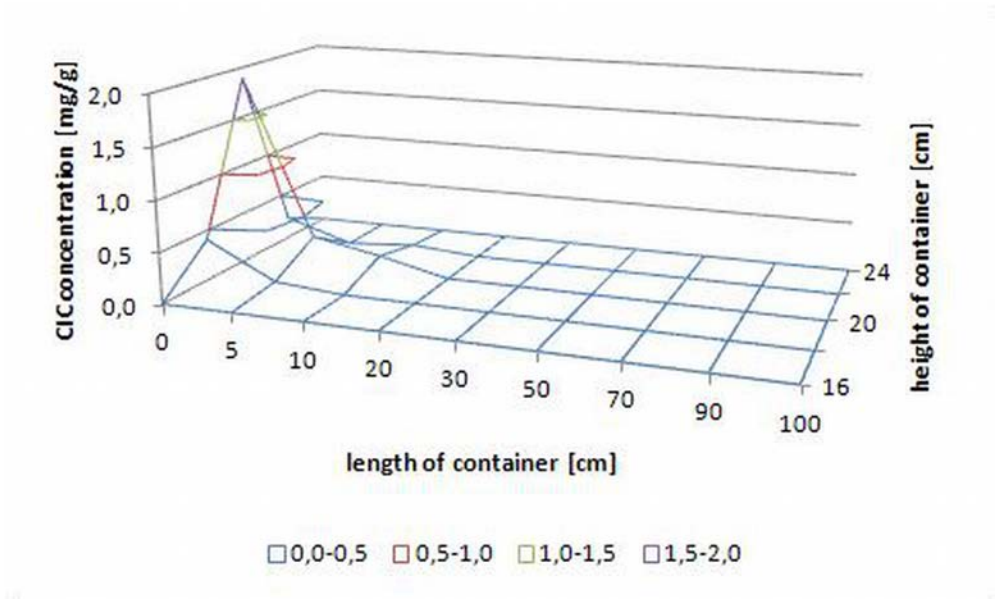

Figure B.7.: Residuals of CIC in porous medium of the 2D-aquifer test system.

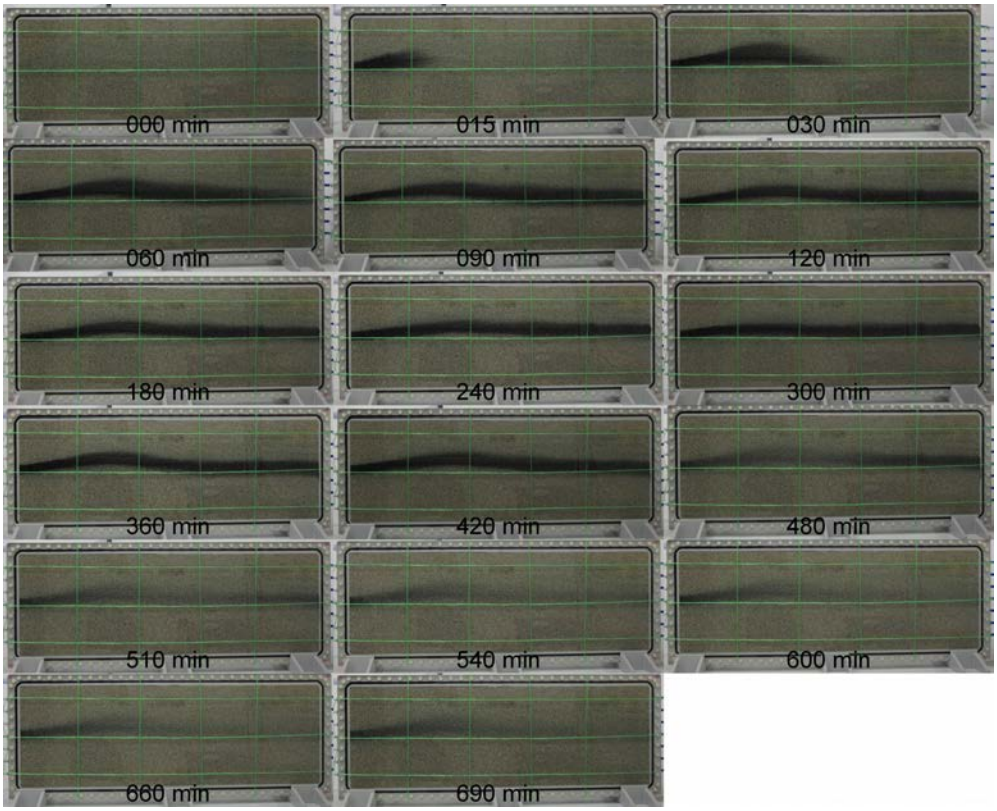

Figure B.8.: Additional photos on CIC breakthrough. This additional figure was shown originally as figure B.6 in the submitted version of this PhD thesis, but replaced then by the appropriate diagram and caption, as remarked by a review comment.

C. Supporting Material to Chapter 4

Supporting material to J. Busch, Meißner, T., Potthoff, Bleyl, S., A, Georgi, A., Mackenzie, K., Trabitzsch, R., Werban, U., Oswald, S. E. (in review since November 30, 2014): A field investigation on the mobility of carbon supported nanoscale zero-valent iron (nZVI) in groundwater. Journal of Contaminant Hydrology

Figure C.1.: Geographical position of Leuna in Germany. Original image taken from http://www.weltkarte.com/uploads/pics/umrisskarte-deutschland.png

Figure C.2.: View on the field site (Foto: Punctum GmbH, 2010).

Layer (m under surface)	Soil type
0.00 – 1.04	Sand (S+A, g, u)
1.04 – 1.34	Silt (U+A, s, g', t')
1.34 – 2.94	Silt (U. fs, t', fg')
2.94 – 3.34	Sand (fS, u-, ms, fg')
3.34 – 3.94	Sand (S,u', fg', mg')
3.94 – 6.04	Gravel (fG+mG, s-, gg)
6.04 – 6.44	Silt (U, t-, fs)

Table C.1.: Soil classification of the extraction well.

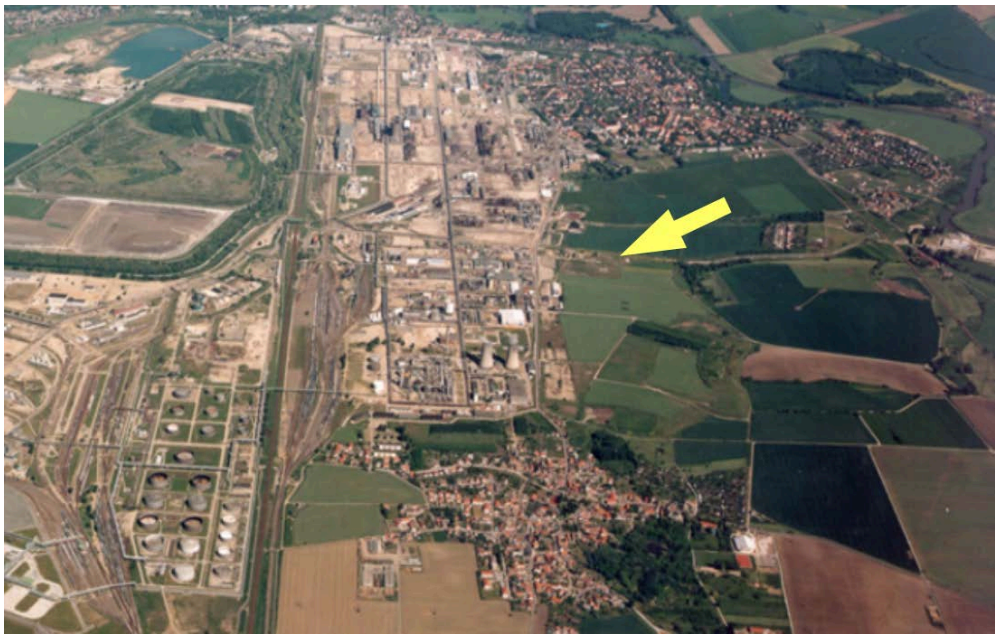

Figure C.3.: View on the field site (Source: UFZ).

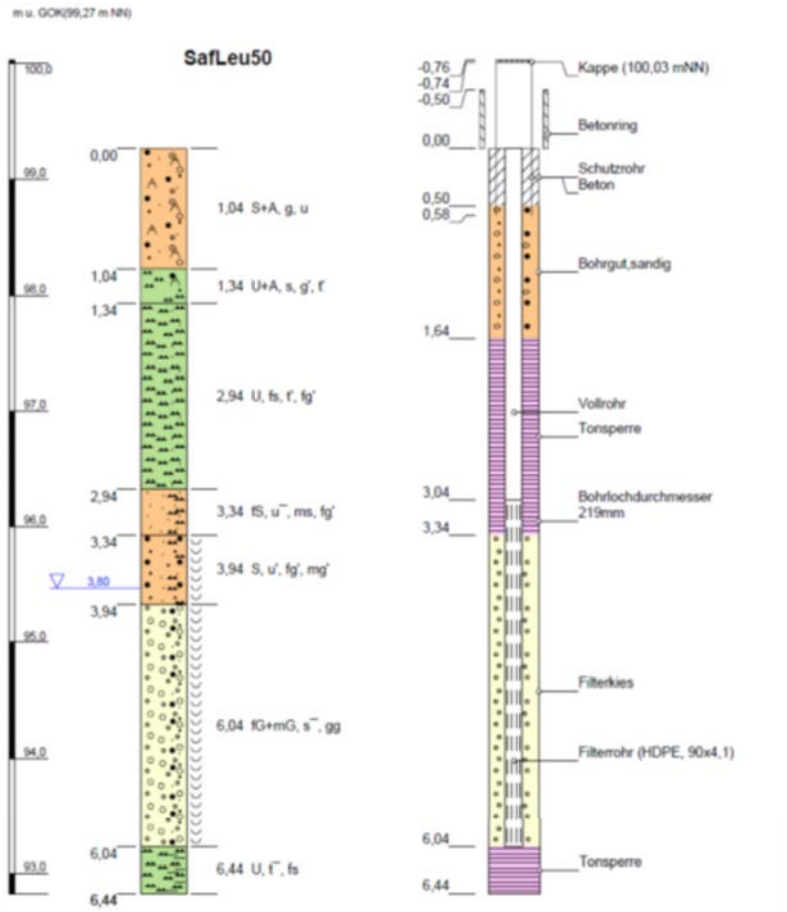

Figure C.4.: Soil classification of the extraction well.

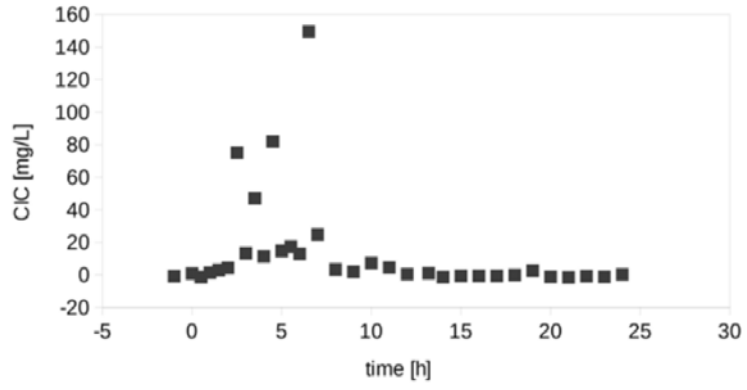

Figure C.5.: Residues in all filters. Here values for all filters are shown. In the manuscript only values from each full hour are presented.

Figure C.6.: An additional image of samples from the extraction well. The tree bottles on the left side represent samples from one hour before the injection to one hour after injection. The samples on the right side represent samples taken after two hours.

Figure C.7.: Image of the extraction well during the experiment.

D. Miscellaneous

Eidesstattliche Erklärung

Hiermit erkläre ich, dass ich die beigefügte Dissertation selbstständig verfasst und keine anderen als die angegebenen Hilfsmittel genutzt habe. Alle wörtlich oder inhaltlich übernommenen Stellen habe ich als solche gekennzeichnet.

Ich versichere außerdem, dass ich die beigefügte Dissertation nur in diesem und keinem anderen Promotionsverfahren eingereicht habe und, dass diesem Promotionsverfahren keine endgültig gescheiterten Promotionsverfahren vorausgegangen sind.

Düsseldorf, im Januar 2015

Unterschrift:

Danksagung

Diese Arbeit entstand im Zeitraum zwischen August 2010 und Dezember 2014 am Institut für Erd- und Umweltwissenschaften an der Universität Potsdam in der Arbeitsgruppe Wasser- und Stofftransport in Landschaften von Prof. Sascha Oswald. Für die Möglichkeit der Anfertigung der Dissertation, Themenüberlassung und Betreuung der Arbeit möchte ich mich ganz herzlich bedanken.
Weiter möchte ich mich ganz herzlich bei den Zweitgutachtern dieser Arbeit bedanken.
Die Finanzierung erfolgte mit Mitteln die durch das BMBF bereitgestellt worden sind. Dafür herzlichen Dank.
Natürlich kann eine solche Arbeit nicht alleine angefertigt werden. Angefangen mit den Mitarbeitern der Arbeitsgruppe Technische Umweltchemie des Helmholtzzentrum Leipzig (UFZ), die mir die Kolloide zur Untersuchung zur Verfügung gestellt haben, dem Projektkonsortium des Projekts Fe-Nanosit, welches durch regelmäßige Projekttreffen wertvollen Input gegeben hat, bis hin zu Annegret Potthoff und Tobias Meißner vom Fraunhofer Institut in Dresden, die viele meiner Proben gemessen haben, waren viele Menschen mit wichtigen Beiträgen am Gelingen dieser Arbeit beteiligt. Weiter sind die Mitarbeiter der externen Einrichtungen zu erwähnen, die durch die Bereitstellung von Materialien und Methoden und vor allem Knowhow wesentlich zum Erfolg des Projektes beigetragen haben. Das sind hoffentlich in vollständiger Aufzählung die Mitarbeiter vom Ernst von Bergmann Klinikum in Potsdam, dem Helmholtzzentrum Berlin (HZB), dem Paul-Scherrer-Institut, verschiedene Projektexternen Arbeitsgruppen des UFZ (Grundwassersanierung, Catchment Hydrology und alle am Standort Leuna eingesetzten Mitarbeiter), Eyk Hasselwander von der G.U.T. Merseburg. Alle hatten einen Anteil am Entstehen dieser Arbeit, dafür ein herzliches Dankeschön.
Weiter möchte ich mich bei allen Mitgliedern der Arbeitsgruppe Stofftrans-

port (Abbas, Benny, Carlos, Gabriele, Hanna, Matthias, Nicole, Peter, Sandip, Theresa, Weishi), den Studierenden, die mir geholfen haben (Jana, Klemens, Theo), den Kollegen aus Gebäude 1, den anderen Doktoranden und Institutsmitgliedern der Geoökologie, für das angenehme Arbeitsklima und die tolle Zusammenarbeit bedanken.
In dieser wohl niemals vollständig werdenden Liste fehlen noch Freunde und Familie, die mehr als einmal meine schlechte Laune ertragen mussten, weil wieder wochen- und monatelang nichts so funktioniert hatte, wie ich mir das vorgestellt hatte. Dafür möchte ich mich ganz besonders bedanken.

Lebenslauf

Die Seiten XLIII und folgende enthielten persönliche Daten und wurden entfernt.